Design, Synthesis and Biological Screening of Potential Anticancer Smac Peptidomimetics to Target XIAP

by

Thashini Chetty

B.Sc. (Hons)

Submitted in fulfilment of the academic requirements for the Degree of Master of Science in the School of Chemistry, University of KwaZulu-Natal, Durban

As the candidates supervisors we have approved this dissertation for submission.

Signed: _____ Name: _____ Date: _____

Signed: _____ Name: _____ Date: _____

December 2009

FACULTY OF SCIENCE AND AGRICULTURE

DECLARATION 1 - PLAGIARISM

I, Thashini Chetty, declare that

1. The research reported in this thesis, except where otherwise indicated, is my original research.
2. This thesis has not been submitted for any degree or examination at any other university.
3. This thesis does not contain other persons' data, pictures, graphs or other information, unless specifically acknowledged as being sourced from other persons.
4. This thesis does not contain other persons' writing, unless specifically acknowledged as being sourced from other researchers. Where other written sources have been quoted, then:
    a. Their words have been re-written but the general information attributed to them has been referenced
    b. Where their exact words have been used, then their writing has been placed in italics and inside quotation marks, and referenced.
5. This thesis does not contain text, graphics or tables copied and pasted from the Internet, unless specifically acknowledged, and the source being detailed in the thesis and in the References sections.

Signed: ……..

FACULTY OF SCIENCE AND AGRICULTURE

DECLARATION 2 - PUBLICATIONS

DETAILS OF CONTRIBUTION TO PUBLICATIONS that form part and/or include research presented in this thesis (include publications in preparation, submitted, *in press* and published and give details of the contributions of each author to the experimental work and writing of each publication)

Publication 1

NOT APPLICABLE

etc.

Signed: ……..

PREFACE

The experimental work described in this dissertation was carried out in the School of Chemistry and the Department of Biochemistry, University of KwaZulu-Natal, Durban, from March 2008 to October 2009, under the supervision of Prof. Hendrik G. Kruger, Dr Thavendran Govender and Dr Patrick Govender.

These studies represent original work by the author and have not otherwise been submitted in any form for any degree or diploma to any tertiary institution. Where use has been made of the work of others it is duly acknowledged in the text.

_____

Thashini Chetty

_____ day of _____ 2009

ABSTRACT

Apoptosis, more commonly referred to as programmed cell death is considered a vital process for the development of multicellular organisms. The disruption of this natural process has been identified as a hallmark of cancer. Apoptosis occurs by both intrinsic and extrinsic pathways. The intrinsic pathway which is regulated through the mitochondria is targeted in this study. More specifically, emphasis is placed on the activation of the effector caspases 3 and 7 and the initiator caspase 9. Suppression of these caspases by inhibitors of apoptosis proteins (IAPs) leads to the inhibition of apoptosis and consequent "wild" growing of cancerous cells.

The aim of this study was to prepare peptides that mimic the natural second mitochondria derived activator of caspase (Smac) protein, which has the amino acid sequence; alanine, valine, proline and isoleucine (AVPI). It was proposed that these compounds will inhibit the IAPs by binding to the BIR 2 and 3 domains present at the amino terminus of XIAP (X-chromosome linked inhibitor of apoptosis protein) and in doing so promote apoptosis in cancer cells. Four synthetic strategies were employed, namely, *N*-methylation, proline substitution by tetrahydroisoquinoline (TIQ) and L-hydroxyproline, incorporation of cage amino acids into the peptide sequence and the use of peptoids. Characterisation of the compounds was carried out by 2-D nuclear magnetic resonance (NMR) and high resolution high performance liquid chromatography-mass spectrometry (HPLC-MS). The novel compounds prepared were thereafter assessed for their anticancer properties/cytotoxic effect by the 3-(4,5-dimethylthiazol-2-yl)-2,5-diphenyltetrazolium bromide (MTT) assay on the MDA-MB-231 and MDBK cell lines. From the testing data obtained it can be concluded that the derivatives containing cage moieties showed a greater efficacy than AVPI and the other designs in this study. In essence, the trishomocubane derivative exhibited the highest cytotoxic effect on the MDA MB 231 cell line (73.969 % ± 3.939) with a reduced effect on the healthy MDBK line (45.614 % ± 2.251) at a concentration of 400 μM. The PCU2 derivative exhibited a maximum cytotoxic effect of 40.553 % ± 1.143 on the MBA MB 231 cell line and 21.176 % ± 1.526 on the MDBK line at a concentration of 200 μM. It was however found to be the most selective drug candidate. This was shown by its relatively low cytotoxic effect on the healthy cell line between 0.001 and 23 μM compared with the cancer line (13.438 % ± 2.711).

TABLE OF CONTENTS

CHAPTER 1: Introduction 1
1.1 General introduction 1
1.2 The Hallmarks of cancer 3
1.2.1 Self-sufficiency in growth signals 4
1.2.2 Sustained angiogenesis 4
1.2.3 Limitless replication potential 4
1.2.4 Tissue invasion and metastasis 5
1.2.5 Insensitivity to antigrowth signals 5
1.3 Apoptosis 6
1.3.1 Apoptosis cascade 6
1.3.2 Apoptosis signalling pathways 8
1.3.2.1 The death receptor pathway (extrinsic) 8
1.3.2.2 Mitochondrial pathway (intrinsic) 9
1.3.3 Architecture of caspases 13
1.3.4 Caspase activation 14
1.4 Inhibitors of apoptosis proteins (IAPs) 15
1.5 Inhibitors of XIAP as putative anti-cancer drugs 18
1.6 Commercial anti-cancer drugs 20
1.7 Scope of this study 21

CHAPTER 2: Peptide chemistry 23

2.1 General background 23
2.2 Resins 30
2.3 Coupling reagents and methods 31
2.4 Tests for complete coupling 32
2.4.1 Kaiser test for primary amines 32
2.4.2 Chloranil test for secondary amines 32
2.5 Protection and deprotection of amino acids 33
2.5.1 Amine protection 33
2.5.2 Side chain protection 35
2.6 Cleavage of peptide from the resin 35
2.7 Incorporation of microwave irradiation in peptide chemistry 35

CHAPTER 3: Design and synthesis of potential anticancer Smac peptidomimetics 37

3.1 Previous drug designs 37
3.1.1 Monovalent Smac mimetics 37
3.1.2 Conformationally constrained Smac mimetics 40
3.1.3 Bivalent Smac mimetics 43
3.2 Results and discussion of peptide synthesis 45
3.2.1 Synthesis of Smac N-terminal tetrapeptide AVPI 47
3.2.2 *N*-methylations 48
3.2.3 Investigation to replace proline in AVPI peptides 52
3.2.4 The use of cage amino acids 54
3.2.5 Peptoids 59
3.3 Conformational analysis of synthesised peptides 61
3.4 Structural elucidation of synthesised peptides by NMR spectroscopy 62

CHAPTER 4: Biological screening of Smac peptidomimetics 77

4.1 Cytotoxicity screening 77
4.1.1 Introduction 77
4.1.2 Cell line selection 79
4.1.3 Results and discussion 80

CHAPTER 5: Conclusion 94

CHAPTER 6: Experimental 96

6.1 Materials and methods 96
6.1.1 Chemistry 96
6.1.2 Biochemistry 96
6.2 General procedure for swelling and deprotecting rink amide resin 97
6.3 The ninhydrin test 97
6.4 The chloranil test 97
6.5 Synthesis of Fmoc-hydroxyproline-OH 98
6.6 General SPPS procedure 98
6.6.1 General procedure for coupling of amino acids to primary amines 99
6.6.2 General procedure for coupling of amino acids to secondary amines 99
6.6.3 General procedure for cleavage of the peptide from resin 99

6.7 Peptoid synthesis 99
6.8 Cleavage of peptoid from the resin 100
6.9 Synthesis of adamantane hydantoin 100
6.10 Synthesis of adamantane amino acid 101
6.11 Synthesis of Fmoc-adamantane amino acid 101
6.12 Synthesis of trishomocubane hydantoin 101
6.13 Synthesis of trishomocubane amino acid 102
6.14 Synthesis of Fmoc-trishomocubane amino acid 102
6.15 Synthesis of peptide 5 (*N*-methylated AVPI) 103
6.16 General procedure for the synthesis of peptides using microwave power (peptides 2, 5, 6, 8 and 9 103
6.17 Cleavage from resin 104
6.18 General procedure for purification of all peptides 104
6.19 Growth and maintenance of cells 105
6.19.1 Preparation of growth media 105
6.19.2 Removal of cells from cryopreservation 105
6.19.3 General procedure for sub-culturing cells 105
6.19.4 Cryopreservation of cells 106
6.20 MTT assay 106

REFERENCES 108

APPENDIX 1 119

APPENDIX 2 170

LIST OF FIGURES

Figure 1: Diagram illustrating the morphological differences in cells undergoing necrosis and apoptosis. 2

Figure 2: The six hallmarks of cancer. 3

Figure 3: The apoptotic process. 7

Figure 4: The extrinsic death receptor pathway and the intrinsic mitochondrial pathway. ... 8

Figure 5: Scanning electron micrograph of epithelial cells undergoing apoptosis. 11

Figure 6: The Cell cycle. 12

Figure 7: Caspase activation 14

Figure 8: Classification of IAPs based on structure and specificity 16

Figure 9: Crystal structure showing the detailed interactions between AVPI and the XIAP BIR3 domain. 19

Figure 10: The amide bond formed between two alanine residues with the loss of water .. 23

Figure 11: Delocalization of the peptide bond 24

Figure 12: Bond lengths and torsion angles in the peptide backbone 24

Figure 13: The primary, secondary and tertiary peptide structures 25

Figure 14: Hydrogen bonding in (A) parallel and (B) antiparallel β-pleated sheets 26

Figure 15: Criteria used to identify β-turn characteristics 27

Figure 16: Oxazolone formation as a result of N→C peptide synthesis. 28

Figure 17: Summarised SPPS procedure 29

Figure 18: Acid forming resins. 30

Figure 19: Amide forming resins. 31

Figure 20: Thermodynamics involved in amide bond formation 31

Figure 21: Chemical reaction between ninhydrin and a primary amine 32

Figure 22: Chemical structure of chloranil. 33

Figure 23: The most commonly used protecting groups in SPPS, Fmoc and *t*-Boc. 33

Figure 24: Fmoc deprotection mechanism using piperidine 34

Figure 25: A summary of the SAR of the Smac based peptides to the BIR3 domain of XIAP..... 38

Figure 26: The four most potent Smac peptidomimetics designed by Oost *et al.* and their respective binding affinities 40

Figure 27: Formation of the bicyclic lactam by fusing the isopropyl side chain of valine with the five-membered proline ring..... 41

Figure 28: Chemical structure of the most potent conformationally constrained Smac mimetic designed by Wang's team with a K_i of 350 nM. 41

Figure 29: Most potent Smac peptidomimetic designed by Sun *et al.* in 2005..... 42

Figure 30: Most potent conformationally constrained compound developed by Zobel *et al.* in 2006. 42

Figure 31: SM-131, the most potent compound developed by Sun *et al.* in 2006. 43

Figure 32: The first bivalent Smac mimetic designed by Wang *et al.* in 2004 43

Figure 33: SM-164 designed by Sun *et al.* in 2007..... 44

Figure 34: BI-75D2 designed by Huang *et al.* in 2008 44

Figure 35: The three most active Smac mimetics based on 4-substituted azabicyclo[5.3.0]alkanes designed by Mastrangelo *et al.* in 2008..... 45

Figure 36: Summary of compounds prepared in this study. 46

Figure 37: Peptide 1; Smac N-terminal tetrapeptide. 47

Figure 38: Structural difference between a traditional amino acid (A) and an *N*-methylated amino acid (B). 48

Figure 39: Peptide 2; *N*-methylated AVPI. 50

Figure 40: Possible product formed from manual synthesis of peptide 2. 50

Figure 41: Chemical structure of TIQ. 52

Figure 42: Peptide 3; Proline substitution with TIQ. 53

Figure 43: Fmoc protection of 4-hydroxyproline..... 53

Figure 44: Peptide 4; Proline substitution in a Smac peptide with 4-hydroxyproline. 54

Figure 45: Well known polycyclic “cage” compounds. 54

Figure 46: Synthesis of adamantane hydantoin. 55

Figure 47: Base hydrolysis of adamantane hydantoin to the amino acid. 55

Figure 48: Peptide 5; Adamantane AVPI. 56

Figure 49: Peptide 6; Trishomocubane AVPI. 57

Figure 50: PCU AVPI. 58

Figure 51: Structural difference between (A) peptide and (B) peptoid. 58

Figure 52: Reaction scheme for synthesis of a peptoid on a solid support; (A) acylation and (B) nucleophilic displacement. 59

Figure 53: DKP formation. 60

Figure 54: Peptide 7; AVPI peptoid. 60

Figure 55: CD spectra for peptides 1 to 7 in MeOH 61

Figure 56: CD spectra obtained for peptides 8 and 9 in MeOH 62

Figure 57: Overlay of the HSQC spectrum of peptide 1 (AVPI) (blue and green) and peptide 2 (*N*-methylated) (red). 66

Figure 58: Overlay of the HSQC spectrum of peptide 1 (AVPI) (blue and green) and peptide 4 (HP) (pink and red) derivative of AVPI. 70

Figure 59: Reduction of MTT to formazan by NADH. 79

Figure 60: Optimisation of the seeding cell number and solubilisation time for MTT assay using the MDA MB 231 cell line 81

Figure 61: Cytotoxic effect of cadmium ($CdCl_2$) on MDA MB 231 cell line.. 82

Figure 62: Cytotoxic effect of cadmium on MCF-7 and MDBK cell lines. 82

Figure 63: Assessment of the cytotoxicity of AVPI on the MCF-7 cell line. 83

Figure 64: Assessment of the cytotoxicity of AVPI on the MDBK cell line 84

Figure 65: Assessment of the cytotoxicity of AVPI on the MDA MB 231 cell line. 84

Figure 66: Assessment of the cytotoxicity of adamantane derivative on the MDBK and MDA MB 231 cell line.....88

Figure 67: Assessment of the cytotoxicity of trishomocubane derivative on the MDBK and MDA MB 231 cell line.....89

Figure 68: Assessment of the cytotoxicity of PCU1 derivative on the MDBK and MDA MB 231 cell line.....90

Figure 69: Assessment of the cytotoxicity of PCU2 derivative on the MDBK and MDA MB 231 cell line.....90

LIST OF TABLES

Table 1: Leading causes of death in humans 2
Table 2: Percentage yields of purified peptides 47
Table 3: ^{1}H and ^{13}C NMR data for peptide 1 (AVPI) 65
Table 4: ^{1}H and ^{13}C NMR data for peptide 2 (*N*-meth) 66
Table 5: ^{1}H and ^{13}C NMR data for peptide 3 (TIQ) 68
Table 6: ^{1}H and ^{13}C NMR data for peptide 4 (HP) 71
Table 7: ^{1}H and ^{13}C NMR data for peptide 5 (Ada) 72
Table 8: ^{1}H and ^{13}C NMR data for peptide 6 (Tris) 75
Table 9: Summary of toxicity to the MDA MB 231 cell line on exposure to novel Smac mimetics as determined by the MTT assay 86
Table 10: Microwave conditions for automated peptide synthesis 103
Table 11: Summary of solvent systems used to purify peptides 104

LIST OF ABBREVIATIONS

A549	Human lung epithelial cells
ACE	Angiotensin-converting enzyme
Ada	Adamantane
Ala	Alanine
$AlCl_3$	Aluminium chloride
ANOVA	One-way analysis of variance
Asp	Aspartic acid
ATCC	American type culture collection
ATP	Adenosine triphosphate
BBB	Blood brain barrier
CAMs	Cell-cell adhesion molecules
$CdCl_2$	Cadmium chloride
$(CD_3)_2SO_2$	Deuterated dimethylsulfoxide
$CDCl_3$	Dueterated chloroform
COSY	Correlation spectroscopy
^{13}C NMR	Carbon-13 nuclear magnetic resonance spectroscopy
Cpp	Cell penetrating peptide
DCM	Dichloromethane
DIABLO	Direct IAP binding protein with low pI
DIC	*N,N'*-diisopropylcarbodiimide
DIEA	Di-isopropyl ethylamine
DIPEA	Di-isopropyl ethylamine
DMEM	Dulbecco's minimal essential medium
DMF	*N,N'*-Dimethylformamide
DMSO	Dimethylsulfoxide
DMSO(d6)	Deuterated dimethyl sulfoxide
EDC	Ethyl(3-diethylaminopropyl)-carbodiimide hydrochloride
FADD	Fas-associated death domain
FCS	Foetal calf serum (heat-inactivated)
Fmoc	9-fluorenylmethoxycarbonyl
Fmoc(-Cl)	9-fluorenylmethyl (chloro)formate
g	Grams

GS	Growth signals
Hsp	Heat shock proteins
IAP	Inhibitor of apoptosis protein
Ile	Isoleucine
HATU	1-[bis-(dimethyl-amino)methyliumyl]-1H-1,2,3-triazolo[4,5-b]pyridine-3-oxide hexaflurophosphate
HBTU	2-(1H-Benzotriazole-1-yl)-1,1,3,3-tetramethyluronium-hexafluorophosphate
HEPES	2-[4-(2-hydroxyethyl)-1-piperazinyl] ethanesulfonic acid
HMBC	Heteronuclear multiple bond coherence
HOBt	1-Hydroxybenzotriazole
HPLC	High performance liquid chromatography
HSQC	Heteronuclear single quantum coherence
LC/MS	Liquid chromatography/Mass spectrometry
LDH	Lactate dehydrogensae
MCF-7	Human adenocarcinoma cells
MDBK	Madin Darby bovine kidney epithelium
mL	Millilitre
Mmol	Millimole
MS	Mass spectra
MTS	(3-(4,5-dimethylthiazol-2-yl)-5-(3-carboxymethoxyphenyl)-2-(4-sulfophenyl)-2H-tetrazolium)
MTT	3-(4,5-dimethylthiazol-2-yl)-2,5-diphenyltetrazolium bromide
m/z	Mass to charge ratio
NAD^+	Nicotinamide adenine dinucleotide
NADH/H	Dihydronicotinamide adenine dinucleotide
NADPH	Dihydronicotinamide adenine dinucleotide phosphate
$NaHCO_3$	Sodium bicarbonate
NMR	Nuclear Magnetic Resonance
NOESY	Nuclear overhauser effect spectroscopy
NRF	National Research Foundation
PBS	Phosphate buffer saline
PCU	Pentacyclo-[5.4.0.02,6.03,10.05,9]-undecane
ppm	Parts per million
pRb	Retinoblastoma protein
PT	Permeability transition
RBF	Round bottom flask

ROESY	Rotational nuclear overhauser effect spectroscopy
SAR	Structure-activity relationship
SD	Standard deviation
Smac	Second mitochondria-derived activator of caspase
SPPS	Solid Phase Peptide Synthesis
TIQ	Tetrahydroisoquinoline
TFA	Trifluoroacetic acid
THF	Tetrahydrofuran
TLC	Thin layer chromatography
TOCSY	Total correlation spectroscopy
TRADD	TNF-associated death domain
Tris	Trishomocubane
UKZN	University of KwaZulu-Natal
UV	Ultra-violet
Val	Valine
WHO	World Health Organisation
XIAP	X-linked Inhibitor of Apoptosis Protein

ACKNOWLEDGMENTS

I would like to express my sincere gratitude to everyone who contributed in any way towards the successful completion of this project. A special mention is given to;

- The founding members of the GGKM research group (Dr T. Govender, Dr P. Govender, Prof. H.G. Kruger and Dr G.E.M. Maguire) for enabling this research to be carried out.
- My supervisors and mentors, Prof. H.G. Kruger and Dr P. Govender for their supervision, guidance and for their continuous encouragement.
- Dr G.E.M. Maguire for his fastidiousness and invaluable contribution.
- Miss Karen Muthusamy for her patience and guidance.
- Mr Dilip Jagjivan for extensive assistance with NMR.
- Mr Oluseye Onajole and Miss Maya Makatini for their assistance with NMR interpretation.
- Mr Byron Peters for his assistance.
- Dr Katharigatta Venugopala for proof reading of this dissertation.
- NRF for financial support.
- My friends and family whose warmth and encouragement fuelled my motivation for completion.

CHAPTER 1

Introduction

This is a multidisciplinary study (Chemistry and Biochemistry) and it is not possible to adhere to the prescribed standards of both disciplines in a masters dissertation. It is also difficult to satisfy the expectation of the expert reader in terms of the depth of discussion of all aspects involved in this study. This dissertation was written from a chemistry perspective. The format of the thesis and the references are based on standard practice for the School of Chemistry. Since the study was performed from a chemistry background, some basic chemical knowledge is assumed. For the convenience of the non-biologists/biochemists, footnotes would be used to explain and define various biochemical concepts that may seem standard knowledge by people in the field.

1.1 General introduction

Initially cancer was described as the process when the rate of cell proliferation overtook the rate of cell death resulting in cells rapidly dividing in an uncontrollable manner.[1] Today however, this definition has been refined and the term cancer now refers to mutated products from alterations in the regulated cell cycle that leads to the unregulated amplification of cell numbers. This includes the proliferation of mutated cells which would ordinarily be killed in the normal cell cycle. Hence leading to an accumulation of mutated cells that grow rapidly.[2] Cell homeostasis[i] is therefore disrupted and potentially leads to tumour development and malignancy.[3,4]

Cancer amongst other diseases such as heart disease and stroke has recently been widely acknowledged as a leading cause of death in the United States (Table 1).[3,5] Statistics released by the World Health Organisation (WHO) revealed that numbers will increase to 16 million new cases *per* year by 2020.[6] In South Africa however, recent statistics reveal the one in six men and one in seven women will develop cancer in their lifetimes.[7]

[i] Homeostasis refers to an equilibrium being maintained, *i.e.* no net change in cell numbers.

Table 1: Leading causes of death in humans[5]

Rank	Cause
1	Heart disease
2	Cancer
3	Stroke
4	Chronic lower respiratory disease
5	Diabetes

Essentially, there are two mechanisms by which a cell can die namely, necrosis and apoptosis (Figure 1).

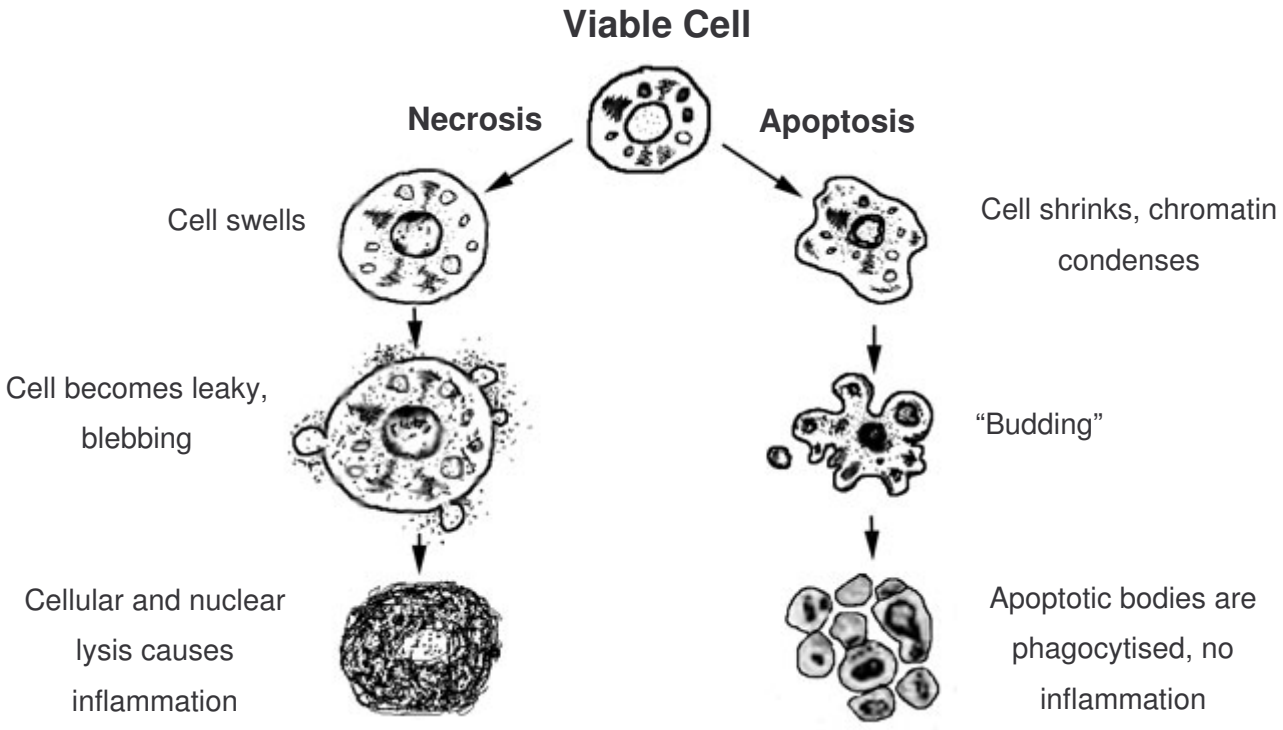

Figure 1: Diagram illustrating the morphological differences in cells undergoing necrosis and apoptosis.[8]

In necrosis, cell death does not isolate the damaged cell but rather lyses[ii] its membrane. The cellular components escape into the extracellular space and consequently invoke an inflammatory response that eventually spreads to surrounding cells leading to cell death.[9] Most important to this study however is programmed cell death *i.e.* apoptosis which is discussed in detail in the rest of the chapter. The morphological changes that cells undergoing apoptosis experience is summarised in Figure 1.[8]

The main alterations in cancer cells that differentiate them from healthy cells are described next.

1.2 The hallmarks of cancer

Although tumours have been found to develop as a result of rapid cell growth, decreases in cell death or some combination of the two,[10] six key physiological alterations in the cells that potentially lead to the formation of malignant tumours exist. These alterations are commonly referred to as the "Hallmarks of Cancer" (Figure 2).[11]

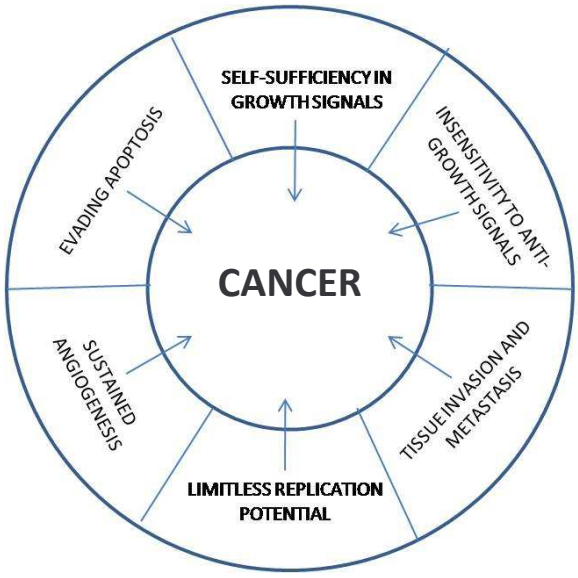

Figure 2: The six hallmarks of cancer. Redrawn from Hanahan and Weinberg (2000).[11]

[ii] Lyses refers to the process of cell destruction through the action of specific lysins. It refers to the complete breakdown of cellular components.

Whilst concise outlines of five of these processes are presented herein, they have been extensively reviewed by Hanahan and co-workers in 2000.[11] This review attempts to provide an up to date understanding of aspects pertaining to the '*evasion of apoptosis'*.

1.2.1 Self-sufficiency in growth signals

In order for healthy cells to proliferate, they require mitogenic[iii] growth signals (GS) that are transmitted into the cell by transmembrane receptors. Tumour cells however, have the capacity to generate their own growth signals which consequently results in the disruption of cellular homeostasis.[11] This is carried out by dominant oncogenes[iv] that mimic normal growth signals. Three main molecular strategies have been identified[11] for cancer cells acquiring GS independence namely:

- Alteration of extracellular growth signals
- Alteration of transcellular transducers
- Alteration of intracellular circuits

1.2.2 Sustained angiogenesis

Cells require oxygen for survival. They also require nutrients such as amino acids and glucose. Without an efficient blood supply to provide these necessities, and to remove metabolic wastes such as urea, water and carbon dioxide, they will die. The cancer cells that make up tumours attract blood vessels to grow into the tumour mass *i.e.* they become angiogenic. These blood vessels serve to nourish the tumour.[12] This induction and new blood vessel growth is termed angiogenesis and is critical for the development of almost all cancers.

1.2.3 Limitless replication potential

Hayflick (1997) has shown that healthy cells being cultured possess a limited replicative potential. Simply stated this means that cells can only divide a certain number of times and

[iii] Mitogenic growth signals are those that cause mitosis or cell division.

[iv] Oncogenes are genes that when mutated or over-expressed, contribute towards making a healthy cell cancerous.

after numerous duplications (60-70) this process ceases. A point is reached where the cells stop growing and this process is termed senescence. Telomeres[v] which are located at the ends of chromosomes are responsible for this control mechanism.[13] As cell growth and division of normal cells occurs, their telomeric DNA decreases in length until it loses the ability to protect the ends of the chromosomal DNA from end-to-end fusions. Once the chromosomes fuse, the cell consequently dies.[14] Malignant cells which are cultured however seem to exhibit an infinitive replication potential. It is therefore believed that tumour cells acquire this phenotype *in vivo*. They have the ability to switch on telomerase which elongates the telomeres and enables further cell growth and replications.

1.2.4 Tissue invasion and metastasis

Cancer progression relies on the primary malignant tumour allowing "pioneer" cells to initially inhabit neighbouring tissue which then travel further to form colonies on healthy tissue. These distant tumour settlements are termed metastases and the new environment supplies enough nutrients and space for them to thrive.[11] Mechanistically both tissue invasion and metastasis alter the physical attachment of cells to their microenvironment and activation of extracellular proteases. In tumour cells various classes of proteins which facilitate the binding of cells to surrounding tissue are affected, including cell-cell adhesion molecules (CAMs) and integrins[vi].[15]

1.2.5 Insensitivity to antigrowth signals

In healthy tissue, homeostasis is regulated by anti-proliferative signals. These signals include soluble growth inhibitors as well as immobilized inhibitors that are fixed in the extracellular matrix. Antigrowth signals potentially stop cell proliferation by either forcing the cells out of their growth phase into the stationary state or by making them enter the post-mitotic stage. Tumour cells however posses the ability to evade these antigrowth signals.[11] The majority of antigrowth signals are channelled through either the retinoblastoma protein (pRb) or p107[vii]

[v] Telomeres are regions of repetitive DNA present at the end of chromosomes. They serve to protect the chromosome from destruction.

[vi] Integrins are receptors that mediate attachment between a cell and the tissues surrounding it, which may be other cells or the extracellular matrix.

[vii] p107 refers to protein (107kD) that is very similar to the retinoblastoma gene product.

and p130[viii]. Disruption of this pathway by malignant cells therefore enables cell proliferation.[16]

1.3 Apoptosis

The term, apoptosis, which refers to the biochemical, molecular and physiological processes that are involved in programmed cell death was initially coined by Kerr and co-workers. The naming of this process is especially apt since the Greek term signifies leaves falling from deciduous trees.[17-20] Apoptosis is required in both controlled-embryonic development; such as in the formation of hands and feet by the removal of the webbing between the digits, and for the maintenance of cellular homeostasis of an organism.[20-22] Problems with the regulation of apoptosis can lead to diseases such as cancer, Parkinson's, Alzheimer's, pre-eclampsia and various auto-immune diseases.[23]

1.3.1 Apoptosis cascade

Apoptosis has been identified as the main route of cell death. A cell may die because it is damaged or old. Once a cell is signalled to die, the cell produces proteases and enzymes that degrade its components. The DNA in the nucleus is fragmented, the cell membrane shrinks, and, eventually, a neighbouring cell engulfs the cellular remains. Wyllie *et al*. described this step-wise process in detail which can be briefly summarized as follows (Figure 3).[23]

[viii] p130 is a member of the retinoblastoma family of pocket proteins.

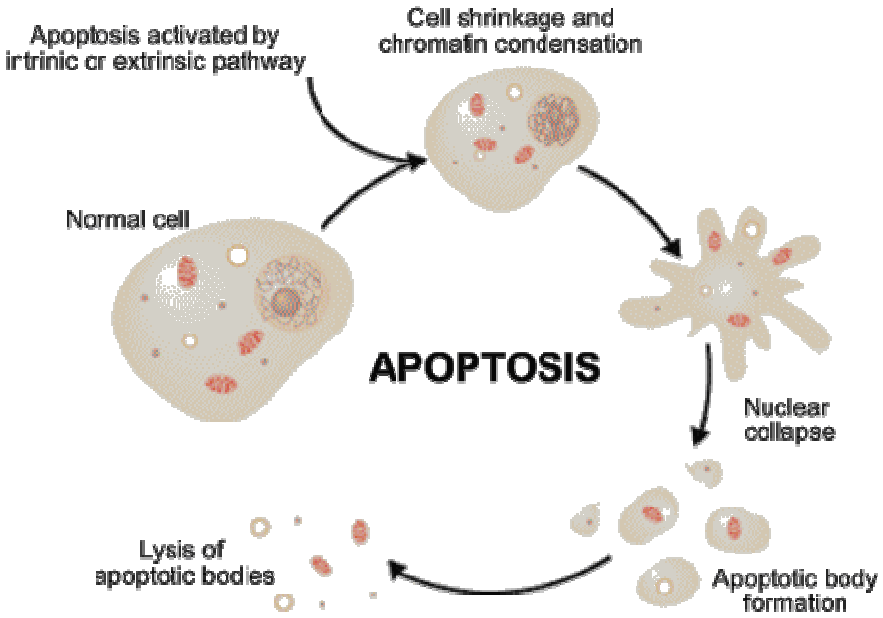

Figure 3: The apoptotic process.[23]

Once apoptosis has been triggered, the cell membrane becomes disrupted which is caused by cleavage of the cytoskeletal proteins (fodrin and gelsolin) which leads to the loss of cell shape and shrinkage. This is followed by the disintegration of the cytoplasmic and nuclear skeletons. Cytochrome C[ix] is then released from the mitochondria[x] which consequently leads to caspase activation and cleavage of PAK2[xi] that plays a role in blebbing of the plasma membrane, phosphatidylserine externalization on the plasma membrane and DNA fragmentation.[9,20,24-26] Fragmentation of the chromosomes and degradation of the nucleus then occurs due to nucleases (DNase) that once activated by nuclear condensation degrade chromosomal DNA into large subunits of 50 to 300 kb and thereafter into smaller 180 base pair fragments thereby yielding apoptotic bodies which are phagocytised[xii] by surrounding

[ix] Cytochrome C is a small heme protein found loosely associated with the inner membrane of the mitochondrion intermediate in apoptosis. The release of cytochrome C activates caspase 9, a cysteine protease. Caspase-9 then activates caspase-3 and caspase-7, which are responsible for destroying the cell from within.

[x] The mitochondria is a structure housing genetic material in cells. It produces enzymes that are required for the metabolic conversion of food to energy.

[xi] PAK2 (p21 activated kinases 2) is a member of a family of serine/threonine protein kinase defined by their interaction with the small GTPases.

[xii] Phagocytosis is the process in which phagocytes engulf and digest microorganisms and cellular debris.

healthy cells (macrophages).[27] This safety mechanism involves removal of damaged cells which may otherwise prove harmful to neighbouring cells.[9] It is important to appreciate the complexity and regulation involved in the sequential action. Protein-protein interaction mediates these regulations and once the cell has "decided to commit suicide", the assignation is carried out swiftly and efficiently.[9]

1.3.2 Apoptosis signalling pathways

A description of the extrinsic or death receptor mediated apoptotic pathway follows.

1.3.2.1 The death receptor pathway (extrinsic)

Apoptosis is initiated upon extracellular binding of a specific ligand (toxins, hormones and cytokines) to its cognate transmembrane receptor [Fas, TNFR1 (Tumour necrosis factor receptor) and TRAIL (Tumour necrosis factor related apoptosis-inducing ligand)] (Figure 4).[26]

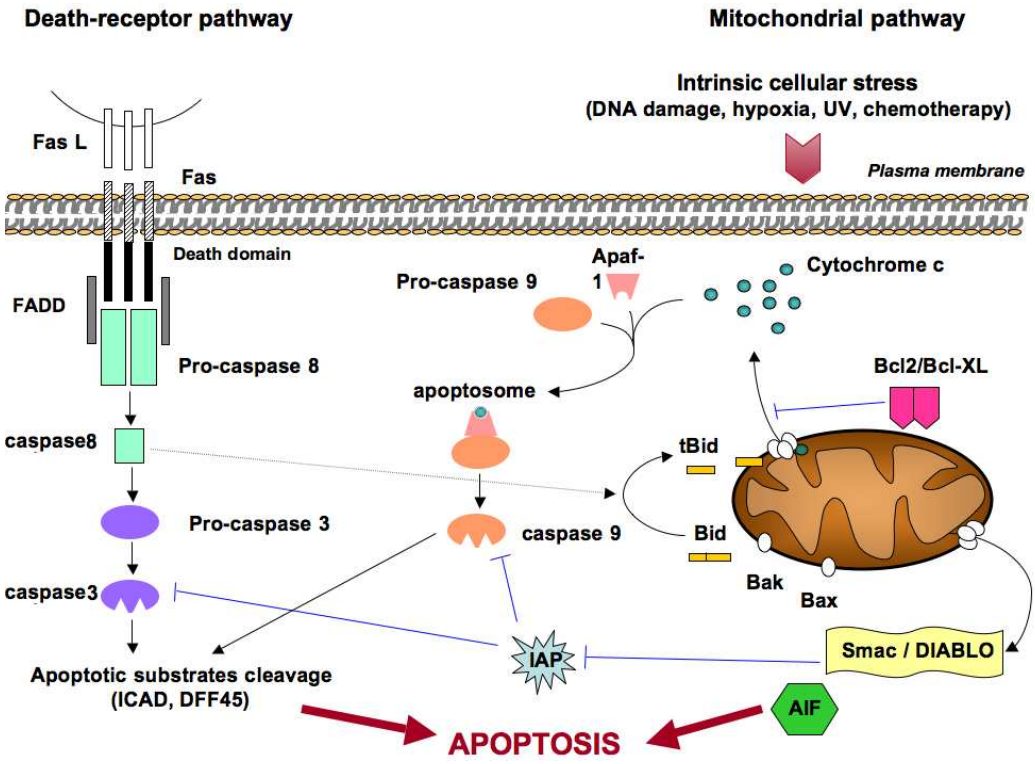

Figure 4: The extrinsic death receptor pathway and the intrinsic mitochondrial pathway.[28]

Formation of the receptor-ligand complex facilitates receptor trimerization which subsequently leads to the clustering of receptor death domain proteins, which in turn facilitates a conformational change by allowing adapter proteins [FADD (Fas-associated death domain) or TRADD (TNF-associated death domain)] to bind to the receptor. This conformational change exposes a death effecter domain that allows pro-caspase-8 to bind and form active caspase 8. This active caspase then cleaves specific substrates and importantly activates the final effector caspase 3.[28]

1.3.2.2 Mitochondrial pathway (intrinsic)

The activation of the mitochondrial pathway is dependent on the release of regulatory factors or proteins from the mitochondria that can be divided into the following categories;

- Pro-apoptotic factors[29]
  - Cytochrome C
  - Apoptosis inducing factor (AIF)
  - Second mitochondria-derived activator of caspases/direct IAP binding protein with low pI (Smac/DIABLO)

- Anti-apoptotic factors [26]
  - Inhibitors of apoptosis proteins (IAPs)
  - Heat shock proteins (Hsp)
  - Regulatory membrane pore protein family (Bcl-2 family: Bax, Bad, Bid, Bcl_2, Bcl_{xL})

An equilibrium exits in favour of the anti-apoptotic pore proteins (*e.g.* Bcl_2, Bcl_{xL}) thus inhibiting release of pro-apoptotic mitochondrial proteins in normal cells. However increased expression of Bax and Bak due to DNA damage favours the release of the mitochondrial pro-apoptotic proteins (Figure 4). Finucane and co-workers have proposed that Bax and Bcl_2 interact with transmembrane channel pumps thereby disturbing mitochondrial membrane potential that results in the pores bursting and cytoplasmic release of mitochondrial proteins.[30]

DNA damage, hypoxia, and chemotherapeutics are examples of apoptotic signals that lead to programmed cell death through the mitochondrial pathway. This intrinsic apoptotic pathway

is initiated by increased permeability of the mitochondrial outer membrane. This membrane permeabilization is thought to occur in either a permeability transition (PT) pore dependent or independent manner.

Permeability transition dependant mechanism

The PT pore is made up of three parts, namely the matrix protein, inner and outer mitochondrial proteins.[31] Opening of this pore results in disruption of the electron transfer across the membrane and hence uncoupling of oxidative phosphorylation. Once opened, water is able to enter the mitochondria.[32] The internal membrane area swells in response and results in damage to the outer membrane. As a result, the apoptogenic proteins *e.g.* cytochrome C or AIF escape into the cytosol.[33] Cytochrome C in conjunction with apoptosis protease activating factor (APAF-1) and pro-caspase-9 form an apoptosome. This apoptosome consequently promotes activation of caspase-9 hence leading to apoptotic cell death.[34] AIF on the other hand, contributes towards the morphological features such as DNA fragmentation and chromatin condensation exhibited by cells undergoing apoptosis.[35] Smac/DIABLO is also released from the mitochondria. Its main role is to antagonize IAPs and hence facilitate apoptosis.[36]

Permeability transition independent mechanism

The Bcl_2 family consists of proteins that regulate PT independent membrane permeabilization. These proteins are characterised by a combination of four Bcl_2 homology (BH) domains and was named after the founding member of the family which was identified as a gene in B-cell lymphoma.[26,32] This family consists of anti-apoptotic members *e.g.* Bcl_2 and Bcl_{xL} as well as pro-apoptotic members. The latter are further divided into multi-domain (Bax, Bak,) and BH_3 proteins (Bad, Bid). The BH_3 proteins activate the multi-domain members while disrupting the anti-apoptotic members.[37,38] It has been suggested that these multi-domain Bcl_2 members form channels in the outer mitochondrial membrane.[39-41] Bax is present in the cytosol of living cells. After an appropriate signal, Bax undergoes a conformational change and consequently moves to the mitochondrial membrane where it results in the release of cytochrome C into the cytosol. Bid however, is cleaved by capsase-8

to yield the fragment (truncated Bid, tBid). tBid then migrates to the outer mitochondrial membrane.[42] This fragment in conjunction with the other propaptotic proteins *e.g.* Bax and Bak, induce the formation of the PT pore which consequently allows the apoptogenic proteins to escape.

There exists cross communication between the intrinsic and extrinsic pathways *via* the Bid protein, thus indicating that extrinsic signals can also promote mitochondrial protein release.[26] The released proteins result in the activation of the apoptosome which is a trimeric complex that is composed of caspase-9, cytochrome C and Apaf-1. The activated apoptosome cleaves specific substrates that also lead to caspase-3 activation. Caspase-3 thereafter cleaves the inhibitor of CAD (ICAD) that releases the caspase activated DNase (CAD). It is this release that triggers the fragmentation of DNA and hence apoptosis (Figure 5).

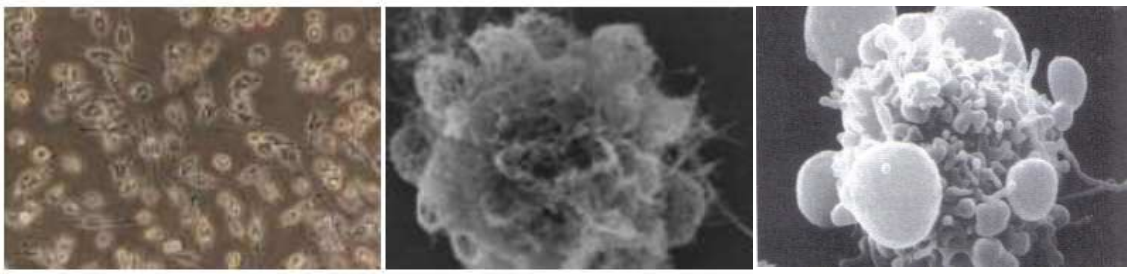

A **B** **C**

Figure 5: Scanning electron micrograph of epithelial cells undergoing apoptosis.[43,17,44,45] (A) Normal cells in culture, in contact with surrounding cells. (B) Induction of apoptosis, cells isolates themselves, remove cytoplasmic connections and begin blebbing. (C) A single apoptotic cell with apoptotic bodies showing externalised phosphatidylserine that facilitates phagocytosis by macrophages.

The cell cycle is crucial in cell homeostasis, either allowing cell growth or prompting cell death (Figure 6).[46] The cell cycle is induced by various mitogenic agents that result in the

progression of the cell cycle. The key regulation features of the cycle are the tumour suppressor proteins, retinoblastoma protein (pRb) at G1/S[xiii] checkpoint and p53 at the

G2/M[xiv] phase. The p53 protein is a transcription factor that detects chromosomal DNA damage. The mechanism for this identification has yet to be identified.[47] In the event of DNA damage being detected, p53 expression levels increase by containing the cell in the G1 phase to attempt DNA repair. If repair is not an option due to severe damage, p53 up-regulates the Bax protein expression thus inducing cell death *via* the intrinsic pathway (Figure 4).

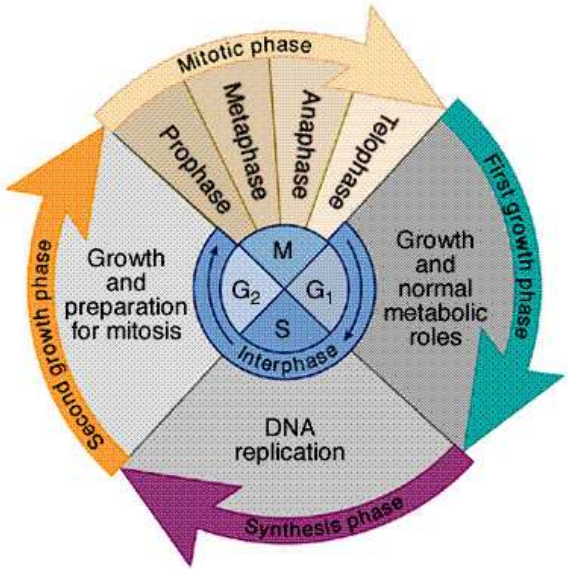

Figure 6: The Cell cycle.[46]

The p53 protein is also able to regulate the phosphorylation state of pRb. This prevents the cell from entering the S phase and thus allows time for repair and prevents the proliferation of cells with damaged DNA. Thus it can be seen that p53 is the "guardian of the genome", since it protects DNA against unwanted changes or mutations that might lead to cancerous cell growth.

[xiii] The G1/S transition is a stage in the cell cycle at the boundary of the G1 and S phases.

[xiv] The G2/M checkpoint refers to the DNA checkpoint that prevents cells from undergoing mitosis if they are damaged.

1.3.3 Architecture of Caspases

One of the most important groups of enzymes involved in promoting the morphological and biochemical changes in cells during apoptosis are the caspases, however the detailed mechanism by which they promote apoptosis is uncertain.[9] Caspases are cytoplasmic cysteine aspartate specific proteases that naturally exist in cells as catalytically inert zymogens[xv]. On the basis of their substrate specificities and the amino acid sequence of their NH_2 terminal pro-domain, caspases can be divided into two classes.[48]

- *Initiator* caspases (*e.g.* caspase-2,-8,-9 and -10)
- *Effector* caspases (*e.g.* caspase-3,-6 and -7)

The *pro*-initiator caspases possess long *N*-terminal *pro*-domains which enable interaction with proteins that can trigger caspase activation and hence initiate the apoptotic cascade. In contrast, the *pro*-effector caspases possess short *N*-terminal *pro*-domains and require activation by the initiator caspases.[25]

The general structure of inactive *pro*-initiator caspases consists of three domains, namely the NH_2 terminal *pro*-domain, the large subunit (~20 kDa) and the small subunit (~10 kDa) domains (Figure 7).[49] Activation to fully functional proteases occurs after cleavage of two aspartate residues at suitable positions. The first proteolytic aspartate cleavage breaks the chain into large and small caspase subunits while the second cleaves off the *N*-terminal *pro*-domain. The activated caspase however is a hetero-tetramer which consists of two large and small subunits and two active sites.[24,48]

[xv] Zymogens are inactive enzyme precursors. They require a biochemical change to become the active enzyme.

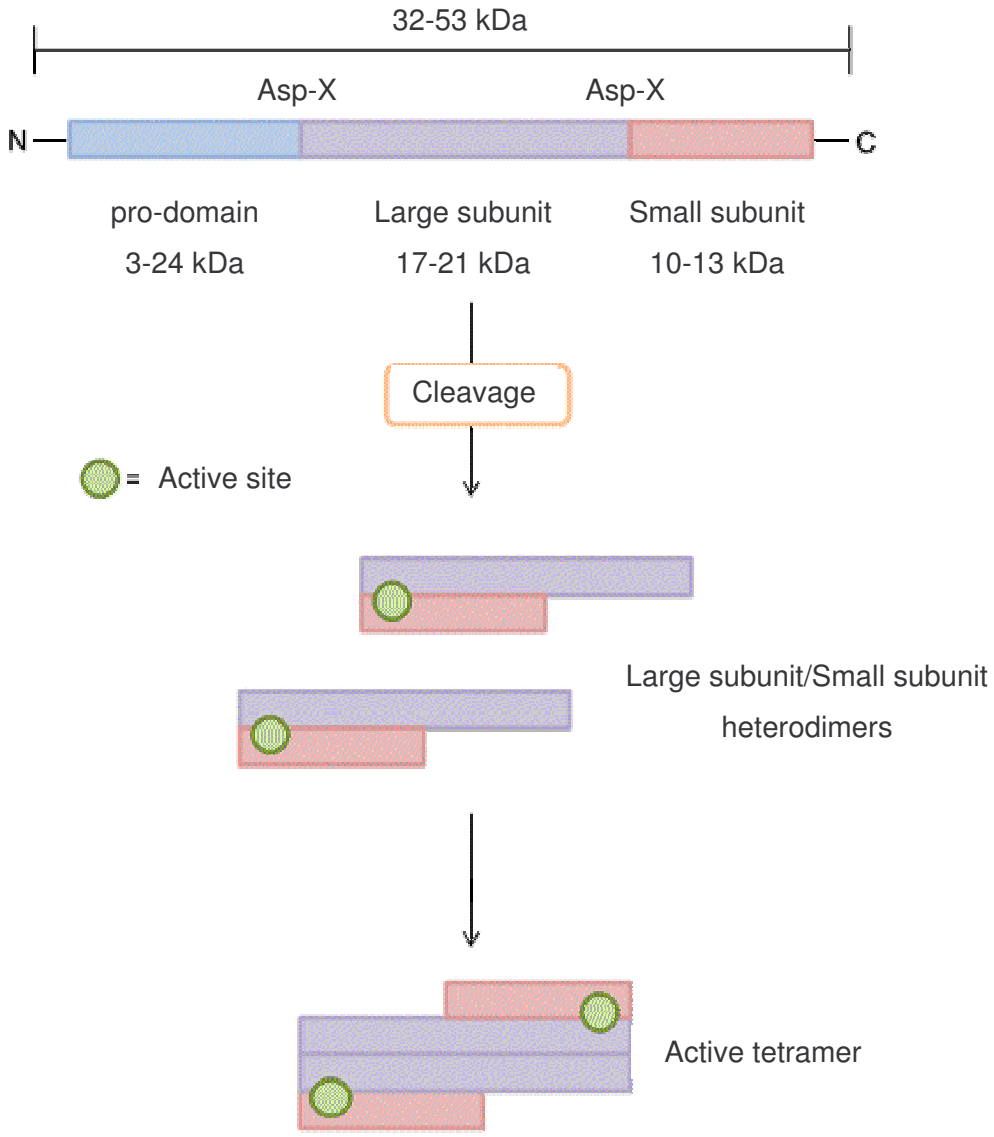

Figure 7: Caspase activation.[49]

1.3.4 Caspase activation

Apoptosis can be initiated by both intrinsic or extrinsic factors that involve the mitochondrial and death receptor pathways respectively. Both pathways, although different are linked in that they are implicated in the activation of initiator upstream caspases thereby promoting apoptosis. This consequently activates a series of sequential positive feed-back activations of downstream effector caspases, a so called "domino effect".[26] Essentially, for caspase activation, the *pro*-caspases require proteolytic cleavage after an aspartic acid residue which separates the *pro*-domain from the large subunit.[20,24,48] Proteolytic cleavage of the zymogen can occur either between the large subunit and small subunit domains or between the *pro*-

domain and the large subunit domain (Figure 7).[49] Caspases cause programmed cell death by cleaving various cellular proteins such as nuclear lamins[xvi] and DNA repair enzymes *e.g.* poly(ADP-ribose) polymerase (PARP) and cytoskeletal proteins such as fordin, gelsolin and actin.[50-54]

1.4 Inhibitors of apoptosis proteins (IAPs)

In the past, researchers focused on determining the molecular mechanisms that controlled cell division.[55] Today however, this interest has deviated somewhat to centre on the cellular machinery that regulates apoptosis.[55] This shift was mainly due to the finding that changes in apoptotic pathways potentially leads to diseases such as cancer.[56,57] Cell death pathways therefore paved the way for drug design since killing a cell was thought easier than sustaining it.[58] Pro-apoptotic therapies which include radiation and chemotherapy are currently employed, however their lack of specificity to cancer cells is limiting.[18,58]

A family of caspase inhibitors termed Inhibitors of Apoptosis Proteins (IAPs) has received a lot of attention.[55] These proteins were initially found in baculoviruses and shown to inhibit virus-induced apoptosis in insect cells.[59,60] Their popularity in the pharmaceutical industry as drug targets is dictated by their specificity to bind and inhibit both initiator caspases -3 and -7 and effector caspase -9.[61] To date eight IAPs have been identified in mammals[62-69] and based on structural differences, they have been divided into three classes (Figure 8).[3] Generally IAP molecules at their amino-terminus contain between one and three Baculovirus IAP repeat (BIR) domains, with each domain being composed of approximately seventy amino acid residues.[10,60,62] In addition IAPs could also contain other domains such as a Really Interesting New Gene (RING) domain at the carboxyl-terminus or a Caspase Activation Recruitment Domain (CARD).[3]

[xvi] Nuclear lamins are intermediate filament-type proteins that comprise the major building blocks of the nuclear lamina, a fibrous proteinaceous meshwork underlying the inner nuclear membrane.

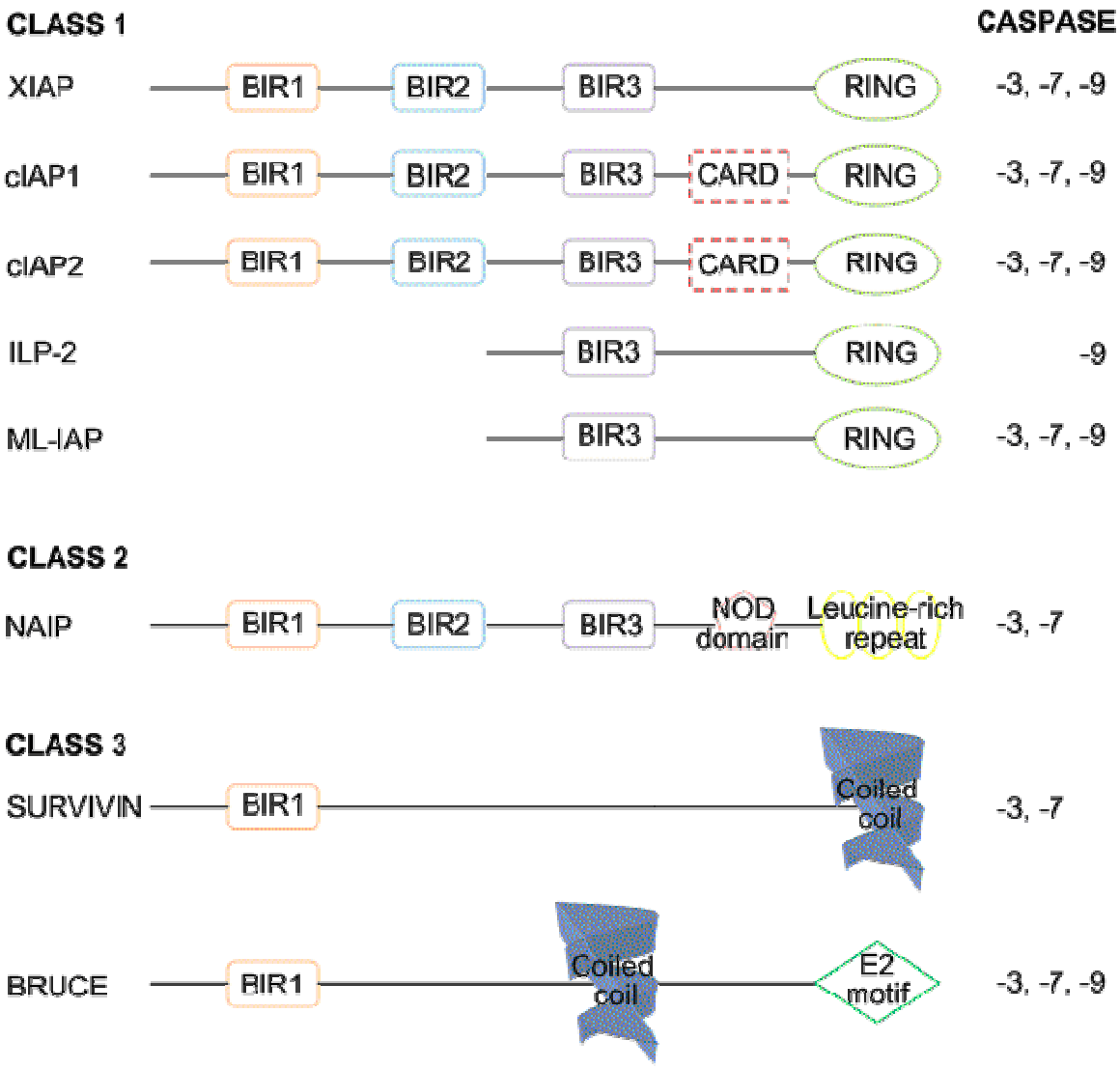

Figure 8: Classification of IAPs based on structure and specificity. Redrawn from Dean *et al.* (2007).[3]

IAPs are present in the cytosol of both normal and malignant cells and generally hinder apoptosis by binding and inhibiting caspases or through caspase-independent mechanisms.[10] Since it is involved in both the intrinsic and extrinsic apoptotic pathways the human X-linked IAP (XIAP)[xvii] in comparison to other IAP molecules has been shown to be the most efficient in inhibiting apoptosis.[70,71] As shown in Figure 8, XIAP consists of a modular organisation

[xvii] X-linked inhibitor of apoptosis protein is a member of the inhibitor of apoptosis family of proteins (IAP). It stops apoptotic cell death induced either by viral infection or by overproduction of caspases, the enzymes primarily responsible for cell death.

that consists of three BIR domains and a C-terminal RING domain. The BIR3 domain has been shown to selectively inhibit initiator caspase-9 by binding to a specific region that is only exposed after cleavage and hence sterically hinders dimerization.[10,72] The BIR2 domain and the linker joining BIR1 and BIR2 domains was found to inhibit both effector caspases -3 and -7.[10,73-75] The C-terminal RING finger domain has been found to contain an E3 ubiquitin ligase and hence has the ability to mediate caspase ubiquitination and proteosomal degradation.[3,10,61,62] This topic has been extensively covered by Nachmias *et al*. in 2004.[10] To date, no specific function in suppressing apoptosis has been associated with the BIR1 domain.[72,76]

Genetic expression levels of IAPs in both normal and malignant cells are strictly regulated at the transcription level.[10] However, XIAP has been shown to be upregulated in many malignant human cell lines and tumour samples.[76,77] It has been shown that over expression of XIAP down-regulates apoptosis in mammalian cells. It should be noted that the extent of XIAP expression did not directly correlate with the rate of apoptosis but it was rather associated with a decrease in cell proliferation.[10] In addition the expression level of XIAP across various malignant cell lines varied significantly. This seems to indicate that different regulations of the respective anti-apoptotic genes occur.[3] It was also observed that mRNA levels of XIAP did not correlate with protein levels in the tumours, possibly indicating post-transcriptional regulation of expression.[3] However, inhibition of IAPs can occur at different biological levels, including down-regulation at the nucleic acid level by antisense[xviii] or small interfering RNA (siRNA). IAPs can also be directly blocked at the protein level by anti-bodies or small synthetic compounds.[10] Targeting IAPs at the nucleic acid level has been described by Nachmias *et al.* in 2004.[10] For this study however, inhibiting XIAP at the protein level is important and is hence discussed in this review.

[xviii] A DNA single strand or sequence is referred to as sense [or positive (+) sense]. If an RNA version of the same sequence is translated or translatable into protein, its complement is referred to as antisense [or negative (-) sense].

1.5 Inhibitors of XIAP as putative anti-cancer drugs

Considering that apoptosis is the main biochemical route to cell death, numerous *in vitro* and *in vivo* studies have centred on the resistance of cells to programmed death. These studies have clearly shown that almost all cell types in the body undergo apoptosis. The idea that induction of apoptosis in cancerous cells could be employed as an effective anti-cancer strategy was initially mooted by Kerr *et al.*[19] Various studies have concluded that the removal or mutation of genes that are involved in cell cycle regulation and that are critical to apoptosis will lead to the progression of cancer.[78-81] The p53 tumour suppressor gene was identified in studies employing transgenic mice as a major regulator of cell cycle events and apoptosis.[82] The functionality of the mutant p53 encoded protein is silenced and thus the ability to elicit apoptosis is unavailable. Studies have shown that p53-induced evasion of apoptosis is responsible for 50% of human cancers.[83] Similarly the genes responsible for the expression of X-chromosome linked inhibitor of apoptosis proteins (XIAP) in normal cells are consequently over-expressed in malignant cells thereby evading apoptosis.[61,77]

The Second Mitochondria-derived Activator of Capsase/Direct IAP Binding protein with Low pI (Smac/DIABLO) is the newly identified natural inhibitor of XIAP.[77,84] Smac/DIABLO is a potent 25 kD proapoptotic protein that is released from the mitochondria into the cytosol. It has been proposed that a dimeric Smac/DIABLO complex binds directly to the BIR2 and BIR3 domains of XIAP or other IAP molecules, consequently inhibiting their anti-apoptotic effect.[84,85]

Designing and developing small molecules that could mimic the metabolic activity of the Smac protein has recently emerged as an attractive target for the development of a new class of potential anticancer drugs. The binding mechanism of Smac/DIABLO that is capable of removing the inhibition of XIAP to caspase-9 was established by Wu and co-researchers.[86,87] From the X-ray crystallographic interpretation of Smac/DIABLO-BIR3 complexes, they were able to conclude that the Smac protein forms an elongated homodimer. Both X-ray crystallographic and NMR solution structural studies concurred that at the *N*-terminal four amino acid residues alanine-valine-proline-isoleucine (AVPI) in Smac/DIABLO inserts itself into a surface groove on BIR3.[86,88] Wu and his research team also reported that the methyl group of the first residue, (NH_2-Ala) inserts itself into a small hydrophobic pocket and that

the free amino group is involved in hydrogen bonding interactions with the neighbouring glutamic acid 314 and glutamine 319 residues on BIR3 (Figure 9).[86] The X-ray structure also shows that the backbone carbonyl group of alanine forms a hydrogen bond with the indole NH group tryptophan 323. Structural evidence proved that the amino and carbonyl groups of the second residue, valine, formed hydrogen bonds with the carbonyl and amino groups of threonine 308 respectively. The iso-propyl side chain of valine was shown to lie in a solvent exposed position and share no interaction with any other protein residues. The third residue in this sequence is proline and its five-membered ring exhibits Van der Waals interactions with the side chains of tryptophan 323 and tyrosine 324. Finally, the amino group of the fourth residue, isoleucine is shown to form a hydrogen bond with the carbonyl group of glycine 306. This structural information on the AVPI tetrapeptide motif has become the building block for the design of potential anticancer drugs.

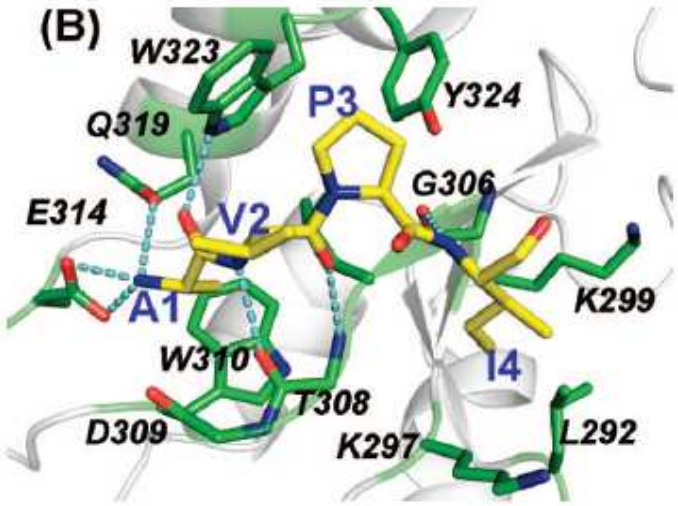

Figure 9: Crystal structure showing the detailed interactions between AVPI and the XIAP BIR3 domain[76] (PDB 1G73 included on CD).

Huang *et al.* [75] have reported the crystal structure of the complex between caspase-7 and XIAP.[75] Contrary to prior assumptions that the BIR2 domain of XIAP was involved in inhibiting caspase-7, crystallographic studies revealed that it was in fact an 18 residue peptide "linker" fragment. This "linker" is located in-between the BIR1 and BIR2 domains of XIAP and is specifically bound to the *N*-terminal side of the BIR2 domain.[77] It interacts and inhibits the substrate groove of the caspase while the BIR2 domain remains invisible.[75] More

recently, Scott *et al.* showed that other interactions occurred between XIAP and caspase-3 and -7.[89] They involve the IAP Binding Motif (IBM) groove in the BIR2 domain that is similar to that of BIR3.[89] It should be highlighted that the exact mechanism by which Smac/DIABLO alleviates the inhibition of caspase-3 and -7 by XIAP has yet to elucidated.[85]

Due to the high levels of XIAP found in cancer cells, the physiological balance between Smac/DIABLO and XIAP is offset. The amount of Smac/DIABLO released from the mitochondria may therefore be insufficient to overcome the inhibitory effect of XIAP on the caspases, thus preventing apoptosis. As such several research groups have designed Smac mimetics that are based on this deficiency. Interestingly some of these mimetics were found to efficiently induce apoptosis in cancerous cell lines *via* two mechanisms. First, Smac mimetics directly target XIAP.[77,84] Second, they have been recently shown to bind to cIAP-1 and cIAP-2 and effect the breakdown of these proteins. Their binding interaction leads to autoubiquination of the cIAP-1 and cIAP-2 proteins which inevitably results in the activation of nuclear factor κB (NF-κB) and the production and secretion of tumour necrosis factor α (TNFα) in sensitive cancer cell lines. After the removal of cIAP-1 and cIAP-2, TNFα induces the formation of a Receptor Interacting Serine-threonine Kinase 1 (RIPK1)-dependent caspase-8-activating complex. As a result, caspase-8 and caspase-3/-7 are activated which consequently induces apoptosis.[90-94]

1.6 Commercial anticancer drugs

Commercially available anticancer drugs function by a variety of mechanisms of action. There are numerous targets for which these drugs are designed. The possibility of scientists discovering a single cure for the disease is therefore highly unlikely which has lead to the marketing of various drugs to treat the many different types of cancer that exist.[95]

Traditional anticancer treatments were designed to kill rapidly dividing cells since cancer cells were found to divide more rapidly than healthy cells. Some healthy cells also have the ability to divide rapidly which has consequently resulted in undesired side effects. A new approach has therefore been adopted and is referred to as “targeted therapy”. By adopting this strategy, scientists hope to gain selectivity in that drugs will attack cancer cells instead of the healthy ones. Exploiting the biochemical differences between cancerous and healthy cells

is therefore crucial. These drugs are therefore designed to disrupt the growth, division, repair or communication of cancer cells.[95,96]

Three target therapy strategies have currently been defined. First, the drugs can act on the internal cellular components and cell function.[95] This usually involves the use of small molecule drugs that enter the cancer cell, disrupt cellular function and result in cell death. The second approach involves targeting specific receptors on the outside of the cell.[96] These drugs have been termed monoclonal antibodies. The last strategy uses angiogenesis inhibitors that prevent oxygen from being supplied to the cells and consequently results in their death.[97]

A good example of a commercially available targeted therapy drug is Velcade®. This compound targets the proteosome within the cell. The main function of the proteosome is to regulate the proteins that control cell division and growth. By disrupting its function, Velcade® potentially leads to selective apoptosis in cancer cells.[98]

There are many other mechanisms of action of cancer drugs. Chemotherapeutic drugs such as Taxol® function by inhibiting the microtubule structures in cells. These microtubules are essential for cell division and replication. Inhibition therefore results in cell death. Etoposide and topotecan are topoisomerase inhibitors that damages the DNA of cancer cells and leads to their death.[98]

1.7 Scope of this study

The discovery of a new drug requires not only its design and synthesis based on a naturally occurring target, but also the development of testing methods and procedures. This investigation was undertaken in order to obtain a holistic insight into the multidisciplinary design and development of potential anticancer peptidomimetics.

It entailed the design, synthesis and characterization of potential drug candidates based on the current mimetics of the target Smac/DIABLO as well as an investigation into proline substitution with either polycyclic “cage” compounds, 1,2,3,4-tetrahydroisoquinoline-3-carboxylic acid (TIQ) or hydroxyproline. The use of *N*-methylated peptides and peptoids

were also investigated. This study included biological screening in which the cytotoxicity of the compounds were determined by the 3-(4,5-dimethylthiazol-2-yl)-2,5-diphenyltetrazolium bromide (MTT) assay on the MDA-MB-231 cell line. Structural analysis of the synthetic products utilizing normal spectroscopic techniques was also performed.

In order to carry out this investigation, an understanding of peptide synthesis is essential and is therefore discussed in the following chapter.

CHAPTER 2

Peptide Chemistry

A detailed description of the underlying concepts behind chemical peptide synthesis is described herein.

2.1 General Background

Since the discovery of synthetic peptide chemistry in 1901 by Emil Fischer, peptides have become important in the design and synthesis of modern drugs. The Greek derived term "peptide" refers to a short chain of amino acids that are held together by peptide or amide linkages. These bonds are formed between the carboxyl group of one amino acid and the amino group of another and result in the loss of water (Figure 10).[99]

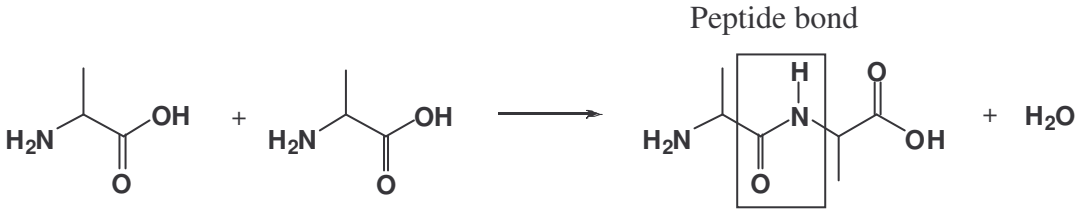

Figure 10: The amide bond formed between two alanine residues with the loss of water.[99]

In 1951 Pauling and Corey used crystallographic information of amino acids, amino acid amides and simple linear peptides to prove that the carbon nitrogen (C-N) bond in peptides are significantly shorter than normal C-N bonds.[99] Accepted explanations for this could include the mesomeric[xix] nature of the amide bond which would restrict the free rotation about the C-N bond. The delocalization of the nitrogen lone pair of electrons to the carbonyl group then confers a partial double bond character to the bond hence reducing its length (Figure 11).[100]

[xix] Mesomeric refers to the electron withdrawing or releasing properties of substituents based on relevant resonance structures.

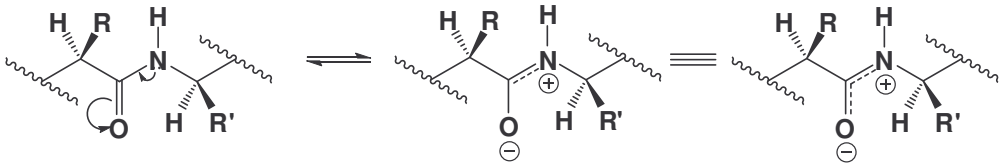

Figure 11: Delocalization of the peptide bond.[100]

The peptide backbone conformation is generally described by three torsion angles, φ (phi), ψ (psi) and ω (omega), (Figure 12).[99] The partial double bond character ensures that the atoms involved in the amide bond lie in a plane with ω = 180° with the exception of proline where ω = 0°. This difference is due to the *cis*-orientation of prolines' side chain group (R) to the adjacent amino acids R group whereas it is usually *trans* across the amide bond due to the reduction in steric hindrance between large groups.[99]

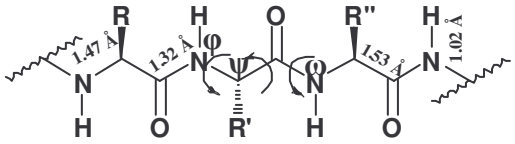

Figure 12: Bond lengths and torsion angles in the peptide backbone.[99]

Peptide architecture can be described by three main types of structures, namely, the primary, secondary and tertiary structures. A primary structure is the simplest and is defined by the number and sequence of amino acid residues in the peptide chain. The secondary structure is more complex and includes repetitive conformations such as α-helices and β-sheets as well as non-repetitive conformations such as tight turns. The tertiary structure comprises the 3-D arrangement of the secondary structure (Figure 13).[99,101,102]

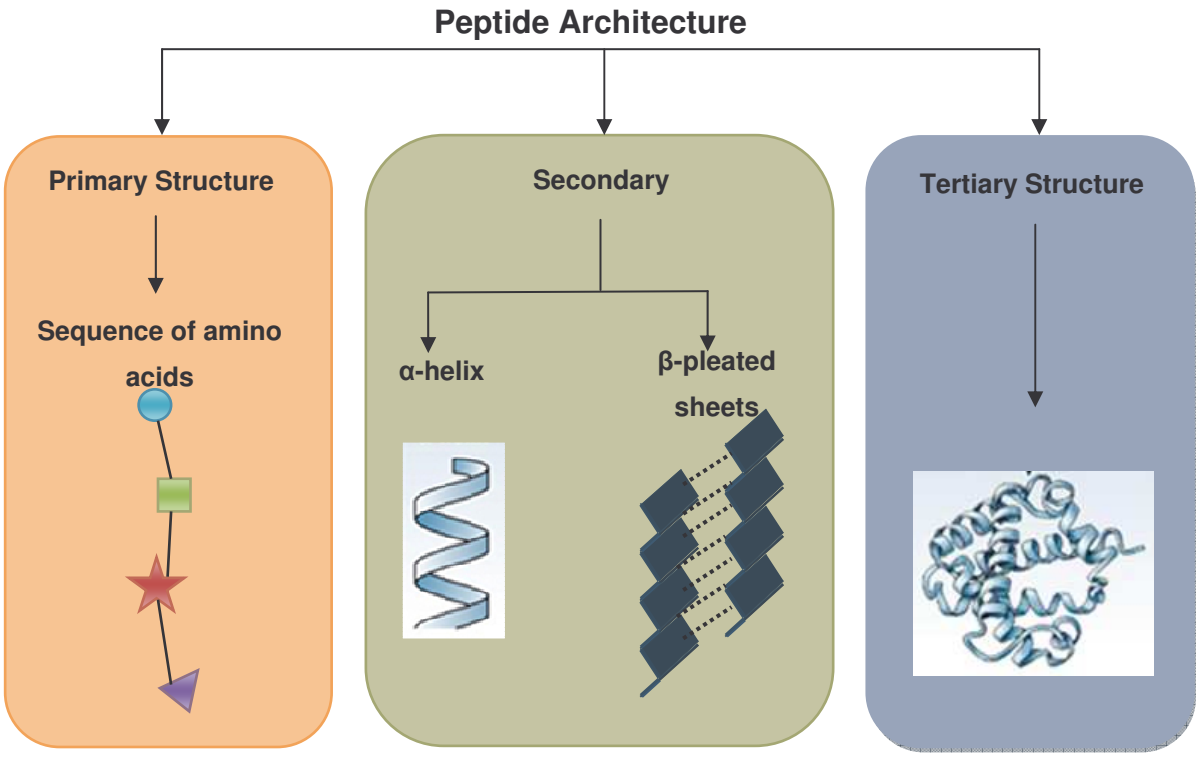

Figure 13: The primary, secondary and tertiary peptide structures. Redrawn from Sewald and Jakubke (2002).[99]

Due to the importance of α-helices and β-sheets in describing peptide structures, emphasis will be placed on the secondary peptide structure. Substituents at the amide bond can be either *cis* or *trans* orientated with ω = 0° and 180° respectively. The number of possible structures is however limited by the constricted partial double bond character exhibited by the amide bond. Generally, these structures are stabilized by hydrogen bonds between the NH group (hydrogen bond donors) and carbonyl oxygen atom (hydrogen bond acceptors). The energy of a single H-bond (20 kJ mol^{-1}) is much lower than that of a covalent bond (200-400 kJ mol^{-1}) however a cumulative effect of multiple H-bonds stabilizes the secondary peptide structure.[99] Molecules at room temperature have enough inherent energy (kinetic, vibrational, rotational *etc.*) to overcome processes requiring up to about 63-84 kJ mol^{-1}.[103] Stabilization of a peptide helix at room temperature therefore requires about six intramolecular hydrogen bonds.

The α-helices are the most common form of helix and were initially proposed by Pauling and Corey who based this discovery on the X-ray diffraction pattern of α-keratins. Generally, this

is a spiral arrangement of amino acids whose stability is determined by the steric and electrostatic characteristics of the amino acids side chain. Amino acids such as proline and hydroxyproline are unable to facilitate hydrogen bonding required for α-helix stabilization and hence result in breakage of the helix.[99]

The formation of β-sheets results from hydrogen bonding that occurs between two neighbouring polypeptide chains. Depending on the orientation of the polypeptides, either parallel or antiparallel β-sheets can form (Figure 14).[99] Parallel β-sheets form from interaction between either two C-terminal or two *N*-terminal peptides whereas antiparallel β-sheets form due to interaction of a C-terminal and *N*-terminal peptide. Ideally β-sheets exhibit torsion angles of φ and ψ = 180°.[101]

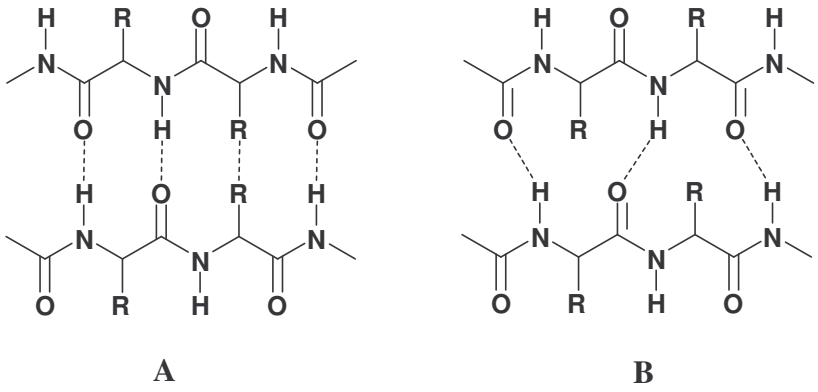

Figure 14: Hydrogen bonding in (A) parallel and (B) antiparallel β-pleated sheets. Redrawn from Sewald and Jakubke (2002).[99]

Aside from the α–helix and β-sheets, tight peptide turns has been recognized as one of the three most important structural peptide features. Tight turns commonly occur in small peptide fragments (two to six amino acid residues) within a large protein.[101] They are classified according to the number of amino acids involved. The smallest turn, a δ-turn involves two amino acids with γ, β, α and π-turns representing three to six amino acids respectively. Since this investigation involves potential anticancer drugs based on a tetrapeptide motif, it is most important to understand the nature of β-turns which is therefore discussed in detail.[99,101,102]

The β-turn was initially discovered by Venkatachalam in 1968. His studies showed that this turn was stabilized by a hydrogen bond that forms between the backbone carbonyl and amine groups in the same peptide.[104] Lewis *et al.* in 1973 however furthered the study and discovered that 25 percent of β-turns exhibit no hydrogen bonding and were termed "open". Since open turns cannot be classified by dihedral angles, β-turns have been defined as four consecutive residues where the distance between $C^{\alpha}(i)$ and C^{α} $(i+3)$ is less than 7Å.[99,101,105,106] It is also important that the tetrapeptide chain should not form a helical conformation.[99,101,102,105,106] The most common characteristics of β-turns have been illustrated in Figure 15.

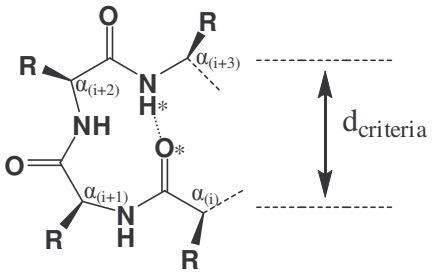

Figure 15: The criteria used to identify β-turn characteristics. Redrawn from Albericio *et al.* (2008).[102]

Three criteria for β-turns are currently accepted. First, is the presence of a hydrogen bond between the NH group of the second amino acid (i+2) and the CO group of the first amino acid (i). This H-bond interaction results in a critical distance of less than 7 Å between atoms $C_{\alpha(i)}$ and $C_{\alpha(i+2)}$.[99] A further requirement is that the virtual torsion angle (τ) created by $C_{\alpha(i)}$, $C_{\alpha(i+1)}$, $C_{\alpha(i+2)}$ and $C_{\alpha(i+3)}$ needs to lie within a range of $-90\,^{\circ} \leq \tau \geq 90\,^{\circ}$.[101,105,106] The last requirement is that the distance between the carbonyl oxygen of residue (i) and the amide hydrogen of residue (i+3) be less than 4 Å.[99,107]

Various types of β-turns exist with some being stabilized intrinsically by certain amino acids. Proline has been found to exhibit the greatest tendency to promote reverse turns which are of biological and hence pharmaceutical importance.[104,108,109]

Initially, the main goal in peptide chemistry was to synthesize naturally occurring peptides or proteins that were composed of various sequences of the 20 natural α-amino acids[xx]. Two main types of peptide synthesis have to date been developed. The first being the classical "solution" phase peptide synthesis and second, the more modern solid phase peptide synthesis (SPPS) approach. The solution phase approach has been somewhat replaced by SPPS due to problems associated with solubility and purification as the number of amino acid residues increase.[110] SPPS was first described by Merrifield in the 1960's which earned him a Nobel Prize in 1984.

Essentially SPPS involves the covalent attachment of a N^{α}-derivatized amino acid to a commercially available solid support.[110,111] In this "step-wise" approach, the peptide is synthesized by the addition of one amino acid at a time in a predetermined sequence. Traditionally, the peptide is built up in a C→N direction by anchoring the C-terminal amino acid to the solid support. This is in order to limit racemization and side reactions that could reduce yields or purity of the final peptide if formed in the N→C direction.[112] If SPPS was carried out by elongation from the N-terminus (N→C), then activated carboxyl groups could acylate peptide bonds preceding them, resulting in the undesirable formation of oxazolones (Figure 16).[113] Peptide esters are also prone to quick diketopiperazine formation in solution.[114]

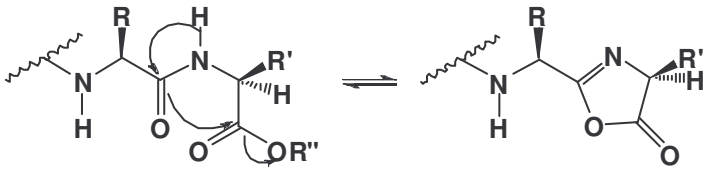

Figure 16: Oxazolone formation as a result of N→C peptide synthesis. Redrawn from Atherton (1989).[113]

Another advantage of the C→N synthetic strategy is the fact that efficient monitoring of the coupling reaction can be achieved.[99] A simple ninhydrin or chloranil test can be used.[113]

[xx] α-amino acids refers to a carboxylic group and amino group bonded to the same carbon atom.

The general SPPS procedure involves 4 steps, namely covalently anchoring of the first amino acid to the resin, N^{α}-deprotection, sequential coupling of amino acids and cleavage of the peptide from the resin once the desired sequence has been obtained. This procedure has been concisely summarised in Figure 17. This method provides a procedure where excess reagents and by-products could be removed after each coupling step by simple filtration and successive washing procedures. The main advantage of this method is that one can drive the coupling reaction to completion with the aid of coupling agents, excess reagent (the Le Chatelier principle) and even by adding fresh reagents if coupling was not 100% efficient. This not only reduces the time and intensity of labour required for peptide synthesis but also leads to greater efficiency and the production of purer compounds.[112]

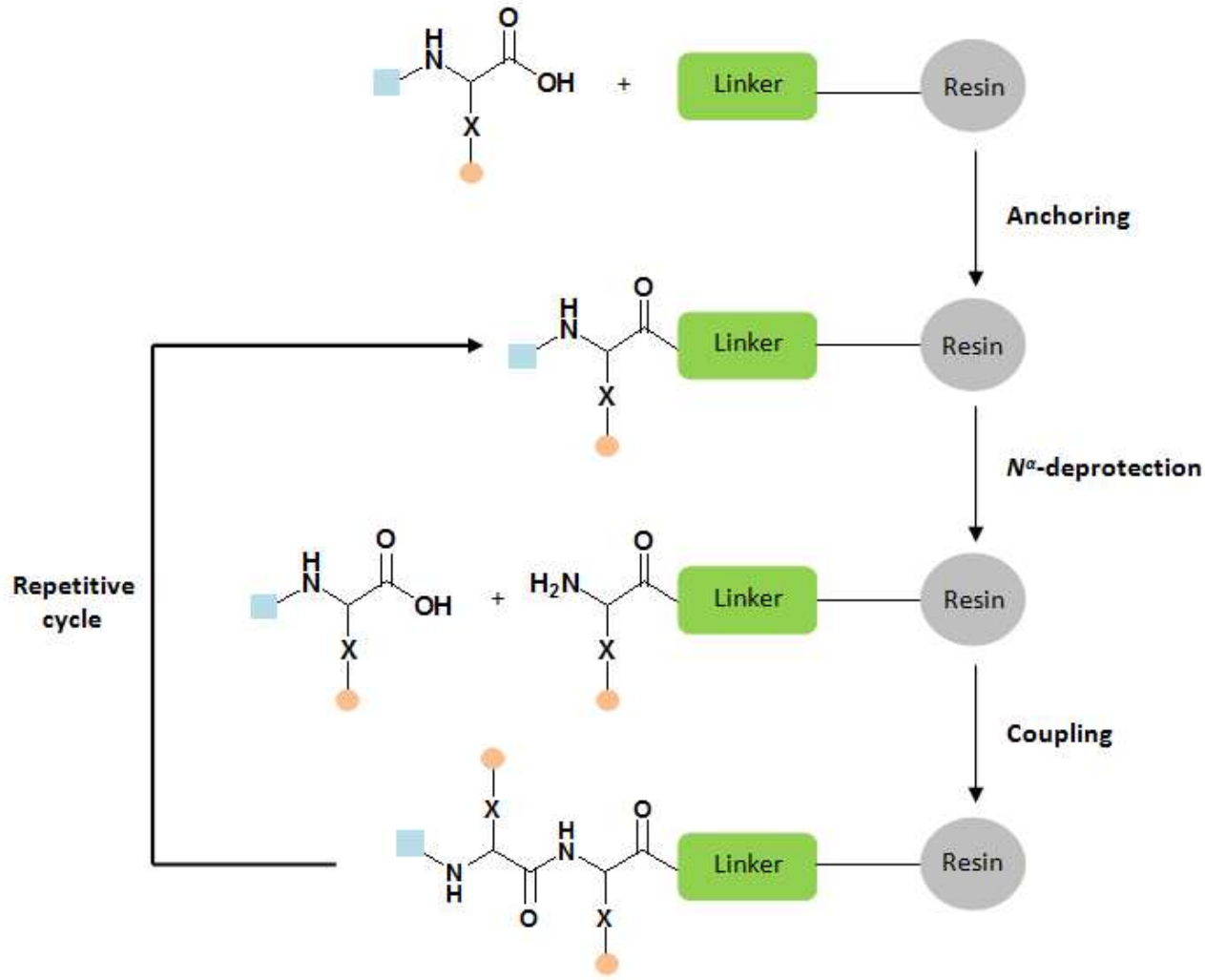

Figure 17: Summarised SPPS procedure. Redrawn from Sewald and Jakubke (2002).[99]

2.2 Resins

There is currently a wide selection of chemically inert resins that are commercially available for SPPS. For efficient SPPS these solid polymer supports need to exhibit certain properties including high surface area or loading capacity. They should also be insoluble in all solvents required for the synthesis, have a stable physical form to facilitate filtration and possess a suitable functional group for the formation of a covalent bond with the first protected amino acid. These can be divided very broadly into two groups based on the terminal functional groups they yield upon cleavage from the resin. Some of the more commonly used resins that yield acids upon cleavage are illustrated in Figure 18.

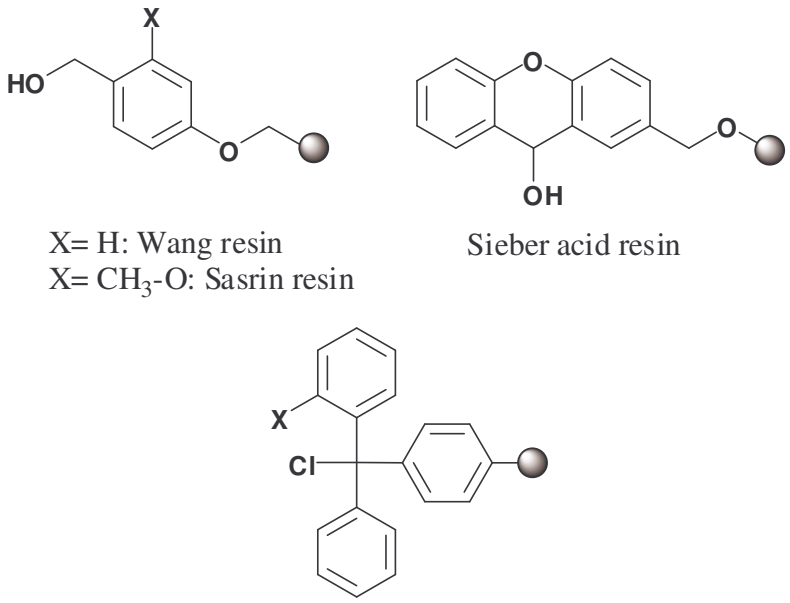

Figure 18: Acid forming resins where the ball represents the resin.

Certain cleavage mixtures are required to remove the desired peptide sequence from the resin. These mixtures vary according to the type of resin used. This enables selection of suitable resins based on the acid-sensitivity of amino acid residues in the desired peptide sequence.

Examples of resins that yield amides upon peptide cleavage are illustrated in Figure 19.

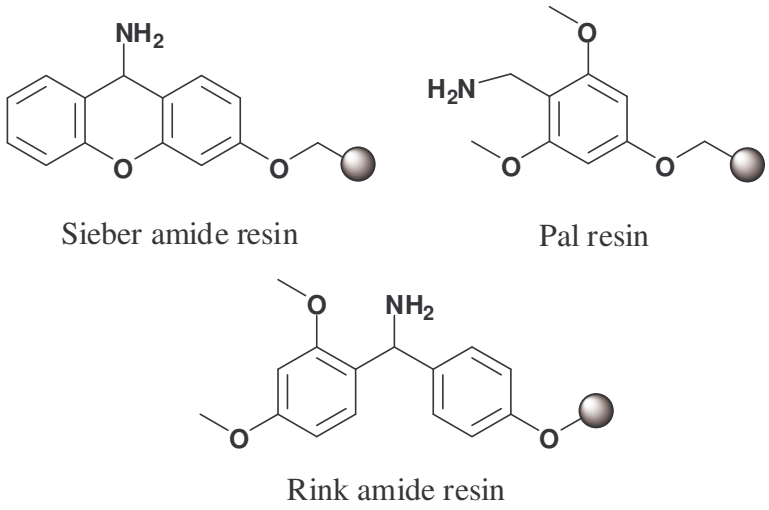

Figure 19: Amide forming resins where the ball represents the resin.

2.3 Coupling reagents and methods

The coupling of amino acids in SPPS generally refers to the formation of the amide bond between amino acids as described in Figure 20. This formally is an acid base reaction that results in the formation of a stable salt. In order for the amide bond to form, it is necessary to overcome the adverse thermodynamics shown in Figure 20 where the equilibrium is unfavourable for amide formation.[115]

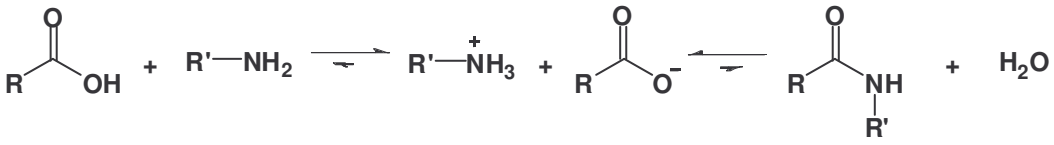

Figure 20: Thermodynamics involved in amide bond formation.[115]

In order to overcome this hindrance, researchers have made use of coupling reagents that activate the carboxyl group to facilitate coupling to the free amino group attached to the resin. There are many coupling reagents currently being used with the most widely used being the carbodiimides and phosphonium and aminium salts.[116]

Previously, carbodiimides such as diisopropylcarbodiimide (DIC) and carbodiimide ethyl(3-diethylaminopropyl)-carbodiimide hydrochloride (EDC) were frequently used to induce amide bond formation. The carbodiimide reacts with the carboxyl group and forms an o-

acylisourea mixed anhydride. This intermediate is then able to directly react with the amine to yield the desired amide and insoluble urea by-product. Due to this and the "weak" coupling efficiency when using (*N,N'*-dimethylformamide) DMF as a solvent, the method has been largely replaced by the use of "aminium" salts such as HBTU and HATU for sterically hindered couplings.[112]

2.4 Tests for complete coupling

To ensure efficient coupling of amino acids and deprotection, simple colour tests can be carried out.

2.4.1. Kaiser test for primary amines

This is a very sensitive test that is commonly used to detect primary amines. It is based on the reaction between ninhydrin and primary amines which produces a vibrant blue/purple colour by the following reaction (Figure 21).[113]

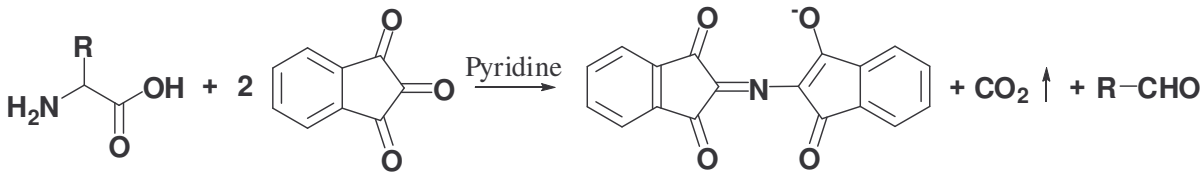

Figure 21: Chemical reaction between ninhydrin and a primary amine.[113]

In the presence of secondary amines however, a brownish-red colour develops. This method then enables determination of whether complete coupling or deprotection of amino acids has occurred.[117]

2.4.2. Chloranil test for secondary amines

The chloranil test is primarily used for the detection of secondary amines but can however also be used to detect primary amines (Figure 22). This is a quantitative test which produces dark blue to green coloured beads in the presence of secondary amines and yellowish beads in the presence of primary amines.[113]

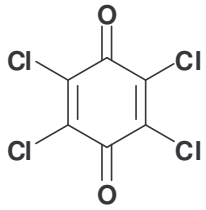

Figure 22: Chemical structure of chloranil.

An important aspect of peptide synthesis involves the protection and deprotection of the amine functionality and side chains of amino acids.

2.5 Protection and deprotection of amino acids

2.5.1 Amine protection

Amino acids contain a number of reactive functional groups, namely the carboxyl terminus, the amino terminus and possibly a reactive side chain. In order to achieve high efficiency in the desired coupling reaction, it becomes necessary to protect the reactive functionalities other than those directly involved in the peptide linkage. Urethanes are the most commonly used protecting groups for amines. They are both readily formed and removed using appropriate conditions. Two of the most commonly used urethanes are illustrated in Figure 23, namely 9-fluorenylmethoxycarbonyl (Fmoc) and *tert*-butyloxycarbonyl (t-Boc).[99,113]

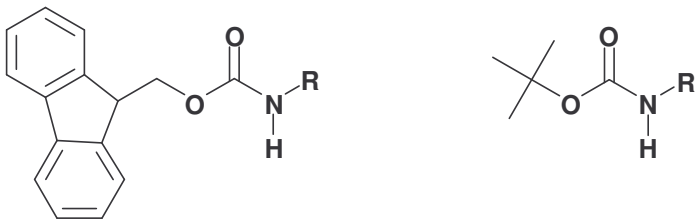

Fmoc protected amine t-Boc protected amine

Figure 23: The most commonly used protecting groups in SPPS, Fmoc and *t*-Boc.

Removal conditions of these protecting groups are relatively mild. Fmoc is a base-labile group and hence requires the use of a mild base such as 20 – 50 % piperidine in DMF. It is also stable toward acids unlike t-Boc which is usually removed in the presence of

trifluoroacetic acid (TFA). In this investigation Fmoc SPPS has been used therefore detail is provided on the Fmoc deprotection mechanism (Figure 24).

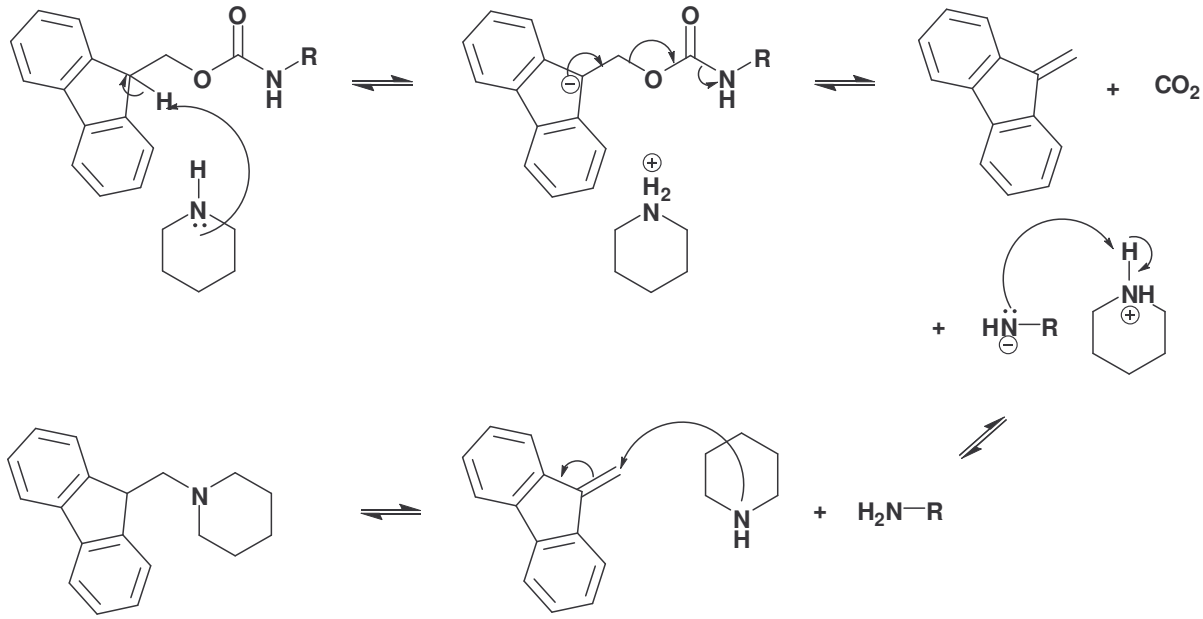

Figure 24: Fmoc deprotection mechanism using piperidine. Redrawn from Sewald and Jakubke (2002).[99]

The Fmoc is removed by a base induced β-elimination. The piperidine acts to remove the dibenzofulvene and thereby prevents irreversible attachment to the free amino group.[99] Dibenzofulvene and CO_2 are produced.

Fmoc deprotection with piperidine is effective for deprotecting most peptides however very long peptide chains could experiences incomplete Fmoc deprotection even when using up to 50% piperidine. This might occur due to the shielding of certain amino acids from the solvent as a result of unique turns. It would then require longer deprotection time or alternatively, a stronger base such as 1,8-diazabicyclo[5.4.0]undec-7-ene (DBU) can be used. It is however recommended that 2 % piperidine be used in conjunction with DBU to scavenge the dibenzofulvene produced and thus preventing alkylation of amino groups.[99]

2.5.2 Side chain protection

Amino acids such as arginine and lysine contain reactive side chains possessing terminal amines. It therefore becomes necessary to protect the amines of these side chains to prevent undesired reactions during peptide bond formation. Side-chain protecting groups that are orthogonal with N^{α}-Fmoc protection include ether, ester and urethane derivatives based on *t*-butanol. These protecting groups are stable during Fmoc deprotection with piperidine and are removed during cleavage of the complete peptide sequence from the resin with TFA.[99,111]

2.6 Cleavage of the peptide from the resin

The penultimate and probably most crucial step in SPPS involves cleavage of the built up peptide chain from the solid support. This involves breaking the covalent bond formed between the resin/linker and the peptide chain. The general method used involves acidolysis with concentrated TFA which also enables deprotection of side chain protecting groups *e.g.* t-Boc.[99] Exposure to the cleavage solution should be minimised to avoid undesired effects on the final product such as decreased yields by the formation of byproducts. Some amino acids contain potentially reactive side chains that generate carbonium ions and other reactive species during cleavage with TFA. This then requires the use of carbocation scavengers in order to minimize destruction of sensitive amino acids. Various resins require different cleavage conditions.

2.7 Incorporation of microwave irradiation in peptide chemistry

The first automated peptide synthesizer was developed by Merrifield in the mid 1960's. To date there have been many improvements on his initial design with the most recent being the incorporation of microwave irradiation. Microwave energy has been associated with organic chemistry since 1984. The first attempt at peptide synthesis incorporating a domestic microwave took place in 1992 when Yu *et al.* reported improved coupling efficiency by up to 4-fold.[118] Their observations also included no detectable racemisation and consistent reduced reaction times even with sterically hindered amino acids containing bulky side chain groups.[119]

Improvements were therefore made in 2002 with the development of the Smith Synthesizer that was specifically designed for organic synthesis.[119] Since then microwave irradiation has been shown to be effective in both the coupling and deprotection steps of Fmoc SPPS. The most recent development in automated microwave assisted SPPS has been the CEM Odyssey system which enables deprotection, coupling and cleavage. The microwave irradiation enables difficult reactions to be driven to completion more efficiently than conventional manual synthesis.

CHAPTER 3

Design and Synthesis of Potential Anticancer Smac Peptidomimetics

The synthesis of the Smac peptidomimetics was performed at the School of Chemistry, University of KwaZulu-Natal. The experimental details are described in Chapter 6.

3.1 Previous drug designs

Two main classes of Smac mimetics have been identified to date, namely monovalent and bivalent models.[76] They are named in accordance with the number of AVPI binding motif mimetics that each contains *i.e.* monovalent mimetics contain one AVPI binding motif whereas bivalent mimetics consists of two motifs joined by a suitable linker. It has been well documented by many researchers, (Kipp *et al.* 2002[60], Arnt *et al.* 2002[62], Fulda *et al.* 2002[120] and Yang *et al.* 2003[121]) that both classes of drugs improve the anticancer activity of other antitumor agents when used together. They were also found to induce apoptosis independently in human cell lines *in vitro* while exhibiting the ability to potentially regress tumours in animal models of human cancers.[76] Both classes possess advantages and disadvantages as potential anticancer agents. While the bivalent mimetics were shown to be between 100 and 1000 times more potent than the monovalent mimetics, they also have much higher molecular masses in comparison. This can lead to lower oral bioavailability as demonstrated by Lipinski in his revolutionary rule of five which describes the physicochemical and structural properties required for bioavaiability.[76,122-124]

3.1.1 Monovalent Smac Mimetics

Having taken all the structural insight gained by Wu *et al.*[87] and Liu *et al.*[88] in 2000, McLendon's research team undertook a study to obtain a structure-activity relationship (SAR) of Smac based peptides that inhibit XIAP *via* its BIR3 domain in 2002.[60] They did this by modifying the AVPI template. A summary of their findings is illustrated in Figure 25.[76]

More specifically, the outcome from their study showed that AVPI bound to the BIR3 domain of XIAP with a binding constant[xxi] (K_d) of 480 nM. They also reported that replacing the first residue, alanine by either glycine or serine results in a 20 fold decrease in the binding affinity. The valine residue was able to tolerate replacement by many different amino acids without a large change in the binding affinity. This confirmed the experimental data obtained from the X-ray crystal structure by Wu *et al.*[87] in 2000, namely, that the isopropyl side chain of valine is solvent exposed and exhibits no interactions with the XIAP BIR3 domain. A significant decrease in the binding affinity was however observed when valine was replaced by aspartate, glycine or proline. Lastly, they demonstrated that modifying isoleucine with more hydrophobic residues for example, valine, phenylalanine or tryptophan has a positive influence while more polar or charged residues exhibit a decrease in binding affinity. McLendon and his team also investigated the effect of *N*-methylations. The result of that study is shown in Figure 25. The SAR results gained from their investigation became the starting point for the development of both peptide and nonpeptidic mimetics of Smac.

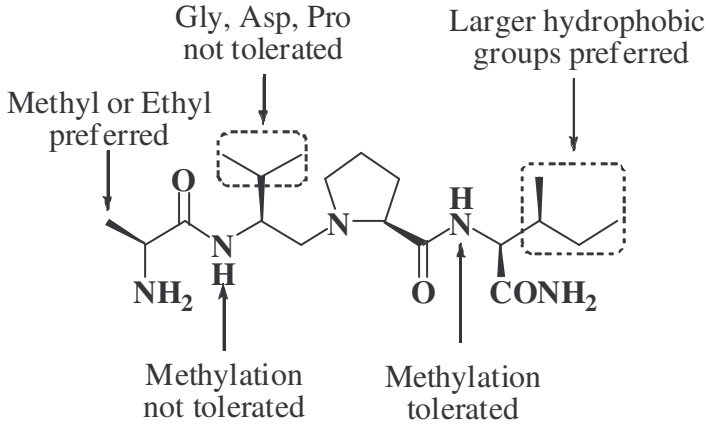

Figure 25: A summary of the SAR of the Smac based peptides to the BIR3 domain of XIAP. Redrawn from Sun *et al.* (2008).[76]

[xxi] The binding constant of a compound refers to the balance between the binding and dissociation processes of the drug with its target. It measures the affinity of a drug for its target. These values are normally expressed as drug concentrations. The lower this value, the more potent the drug.

The next area of concern for researchers was the fact that the Smac-based peptides designed were not very cell permeable even though they exhibited strong binding affinities to the BIR3 domain of XIAP.[76] Yang *et al.* 2003[121] devised a method to facilitate intracellular delivery of these peptides. This involved attaching cell permeable "carrier" peptides to the active mimetics. They investigated the conjugation of polyarginine residues to the cell impermeable Smac mimetics.[121] By attaching fluorescent tags to these compounds they were able to estimate the internalization of each peptide into the cell by fluorescence microscopy. However, the *in vivo* studies of these molecules were not very accurate, due to the potential drugs being injected directly into the tumour cells. This defeats the purpose of their strategy since the compounds do not cross the cell membrane.

In 2004, Oost *et al.*[125] set out to synthesize potent Smac peptidomimetics. Following McLendon's[60] lead, they too carried out modifications on the AVPI tetrapeptide motif. The results obtained only confirmed those found by McLendon and his team. In addition, they concluded that mono-methylation of the free terminal amino group does not alter the binding affinity of the compound significantly whereas di-methylation did. Replacement of proline which contains a five-membered ring by either a four- or six-membered ring had a negative effect on the binding affinity. In contrast, substitution by a hydrophobic residue into the proline ring leads to a slight increase. From their investigation, four Smac peptidomimetics with binding affinities in the nanomolar (nM) ranges were identified (Figure 26).[76,125]

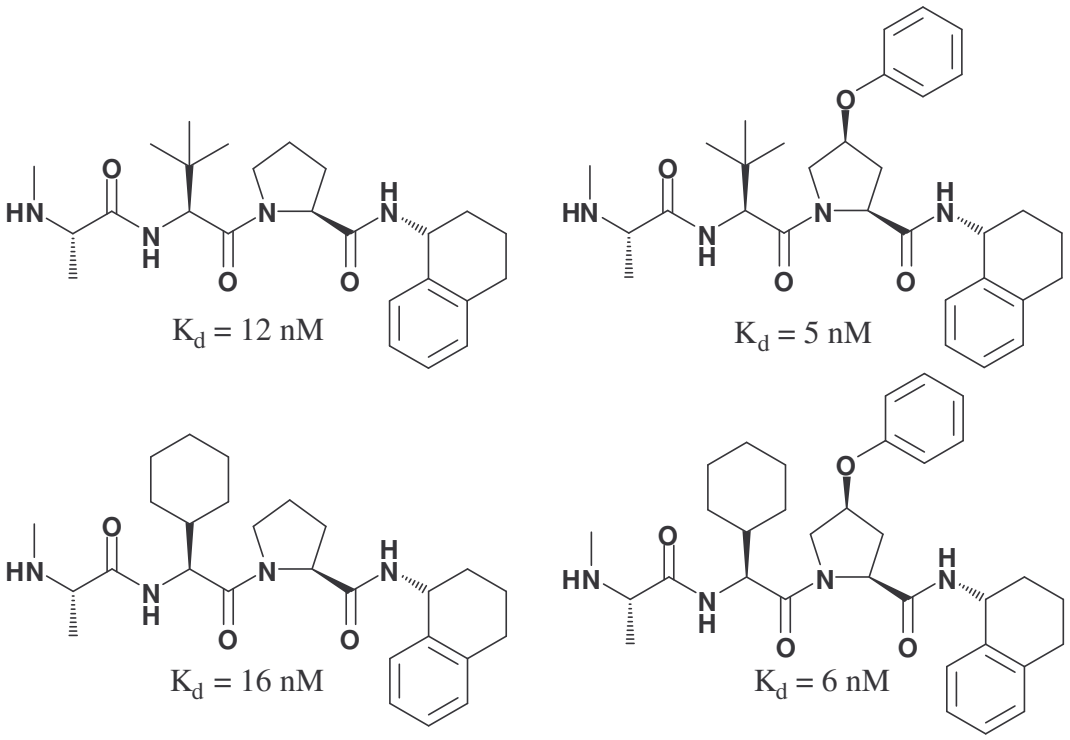

Figure 26: The four most potent Smac peptidomimetics designed by Oost *et al.* and their respective binding affinities. Redrawn from Oost *et al.* (2004).[125]

3.1.2 Conformationally constrained Smac mimetics

This class of potential anticancer agents was initially introduced by Wang's research team at the University of Michigan in 2004. They developed a series of conformationally constrained bicyclic Smac mimetics.[76] by utilising the structural data obtained by Wu *et al.*[87] and Liu *et al.*[88] in 2000. The concept behind their design was simple yet elegant. Since the isopropyl side chain of the valine residue in the tetrapeptide motif was solvent exposed and had no interactions with the protein and the proline had hydrophobic interactions with Trp 323, the idea that the two residues could be fused together to create a bicyclic lactam without altering the basic structural conformation was conceived (Figure 27).[126]

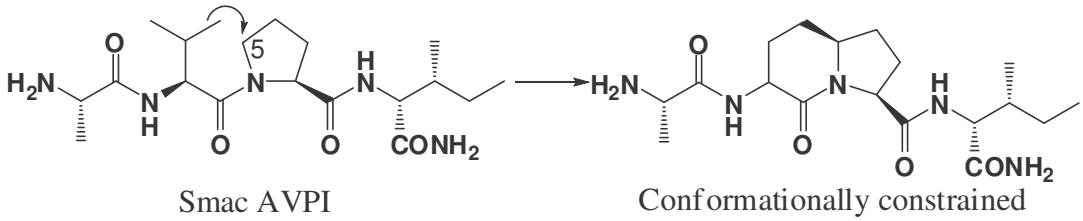

Figure 27: Formation of the bicyclic lactam by fusing the isopropyl side chain of valine with the five-membered proline ring. Redrawn from Sun *et al.* (2004).[126]

This structure was used as the template for further potential drug designs and optimization. After synthesising many structures, the most potent compound included an ethyl group replacing the methyl on the alanine and a diphenylmethyl group replacing the isoleucine residue (Figure 28).[126]

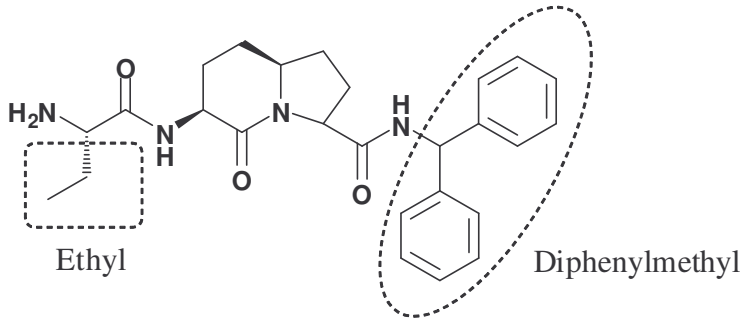

Figure 28: Chemical structure of the most potent conformationally constrained Smac mimetic designed by Wang's team with a K_i of 350 nM. Redrawn from Sun *et al.* (2004).[126]

Sun *et al.*[127] and Park *et al.*[128] made their mark on the Smac AVPI mimetic scene in 2005. Sun and his research team opted for designing Smac peptidomimetics as potential inhibitors of XIAP. Their study involved substitution of the methyl group on the alanine residue and the entire isoleucine residue of the AVPI tetrapeptide motif by various functional groups.[127] From their study they came to similar conclusions to that of Wang and his team. They also found that substitution of the methyl group of alanine by an ethyl group has a positive effect on the potency of the compound as does substitution of isoleucine by diphenylmethyl (Figure 29).[127] This compound was found to be 24 times more active than the Smac AVPI tetrapeptide with a K_i of 24 nM.

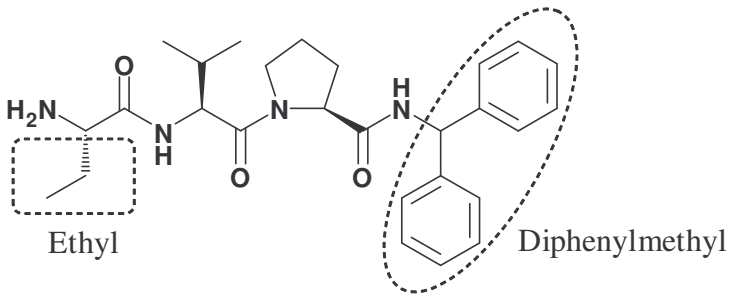

Figure 29: Most potent Smac peptidomimetic designed by Sun *et al.* in 2005. Redrawn from Sun *et al.* (2005).[127]

Park's approach involved the synthesis of non-peptidic small molecule inhibitors of XIAP. Their design was based on the replacement of selected AVPI residues with substituted five-membered heterocylces such as thiazoles and imidazoles. From the study it was concluded that nitrogen containing heterocylces were more potent than other heteroatoms.

In 2006, Zobel et al.[129] designed conformationally constrained Smac mimetics based on a [7,5] bicyclic lactam structure to target the BIR3 domain of XIAP. This saw the evolvement of a simple peptide into a more drug-like molecule or peptide isostere. The most potent of their series of analogues exhibited a K_i of 270 nM and is illustrated in Figure 30.[129]

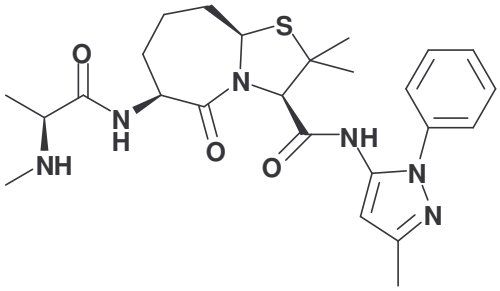

Figure 30: Most potent conformationally constrained compound developed by Zobel *et al*. in 2006. Redrawn from Zobel *et al.* (2006).[129]

Sun[84] and his research group then proposed a potent, cell-permeable, conformationally constrained Smac mimetic, SM-131 (Figure 31)[84] which was found to possess a K_i of 61 nM in a competitive binding assay and an IC_{50} value of 100 nM when tested on the MDA-MB-231 human breast cancer cell line.

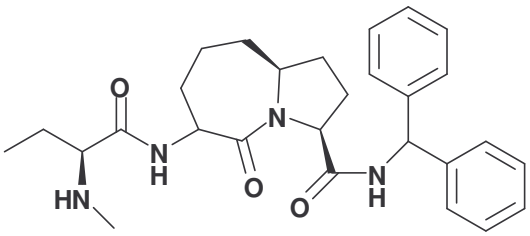

Figure 31: SM-131, the most potent compound developed by Sun *et al.* in 2006. Redrawn from Sun *et al.* (2006).[84]

3.1.3 Bivalent Smac Mimetics

Wang and Harran in 2004 investigated the efficacy of a bivalent Smac mimetic aimed at simultaneously targeting the BIR2 and BIR3 domains of XIAP. This idea was conceived following reports that the natural Smac protein forms a dimer *in vivo* and consequently exhibits a higher binding affinity to XIAP than the monovalent Smac AVPI motif.[130] The most potent bivalent compound (Figure 32) was recently shown to exhibit a binding constant of less than 0.7 nM by Nikolovska-Coleska *et al*. using a fluorescence-polarization assay.[131]

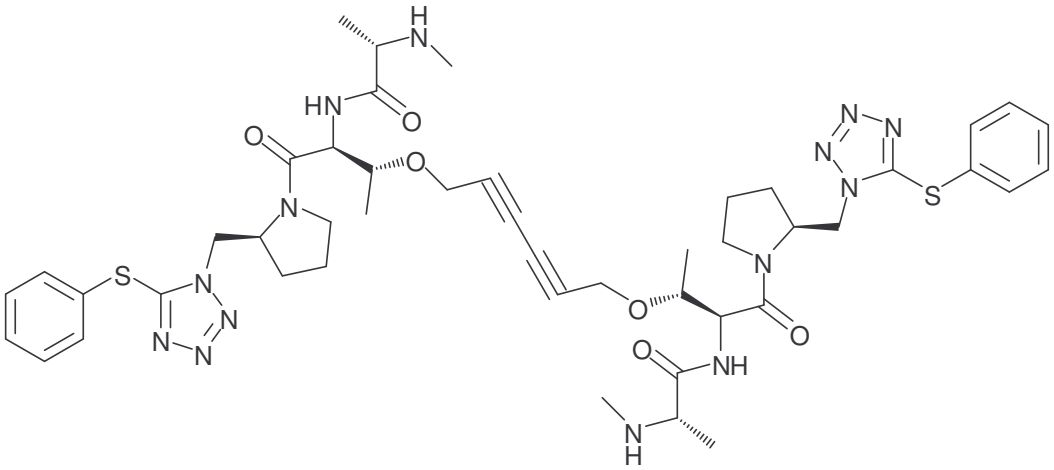

Figure 32: The first bivalent Smac mimetic designed by Wang *et al.* in 2004. Redrawn from Wang *et al.* (2004).[132]

More recently Sun *et al.*[85] collaborated the ideas proposed regarding the efficacy of conformationally constrained and bivalent Smac mimetics and designed potent, nonpeptidic bivalent Smac mimetics based on conformationally constrained monovalent Smac mimetics. SM-164 (Figure 33)[85] was found to possess an IC_{50} concentration of 1.39 nM which is 300

and 7000 times more potent than the monovalent equivalent and natural Smac AVPI peptide motif respectively. This investigation took into consideration that the distance between the BIR2 and BIR3 domains of XIAP was approximately 23 amino acids. Hence they designed a suitable linker inducing the same distance between the active sites. The flexible linker was found to separate the two triazole rings of the monomers by a distance of 15 Å which would provide sufficient length and flexibility to concurrently bind both domains.

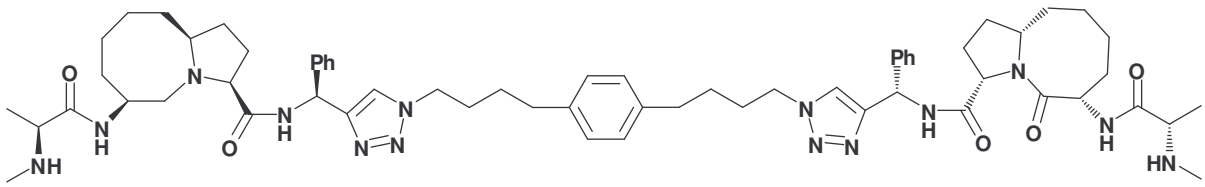

Figure 33: SM-164 designed by Sun *et al.* in 2007. Redrawn from Sun *et al.* (2007).[85]

2008 brought with it further developments in the design of potent, Smac mimetics designed to inhibit XIAP. The main focus was to now synthesize peptide mimetics with more drug-like characteristics. Huang *et al.*[133] proposed a strategy of combining *in silico* docking, fragment-based drug design and NMR spectroscopy and consequently designed BI-75D2 (Figure 34).[133]

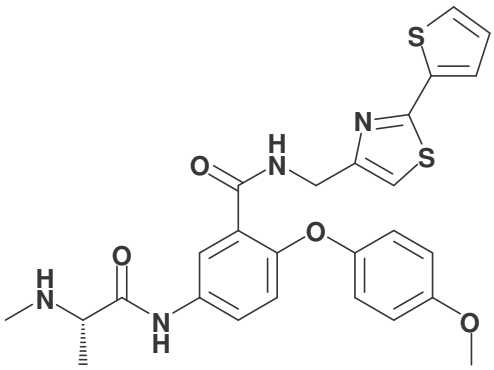

Figure 34: BI-75D2 designed by Huang *et al.* in 2008. Redrawn from Huang *et al.* (2008).[133]

The more drug-like structure of this compound compared to traditional peptides lead to advantages including good metabolic stability and increased cell permeability which are essential for potential drug candidates. BI-75D2 also exhibited an IC_{50} concentration of 16.4

μM compared to 50 μM of the AVPI peptide. This compound was also found to induce apoptosis in MDA-MB-231 breast cancer cells at this low concentration.[133]

4-Substituted azabicyclo[5.3.0]alkane Smac mimetics were evaluated by Mastrangelo *et al*. in 2008.[77] These potentially proapoptotic compounds were found to bind to the BIR3 domain of XIAP in micro to nanomolar concentrations and hence provided a good scaffold for drug lead optimization. Mastrangelo *et al.* studied the complexes formed between the mimetics and the BIR3 domain of XIAP by X-ray crystallography as well as molecular modelling and docking simulations. From this study it was concluded that substitution at the 4-position of the azabicyclo[5.3.0]alkane structure leads to greater activity. The structures of the three most active compounds are shown in Figure 35.[77]

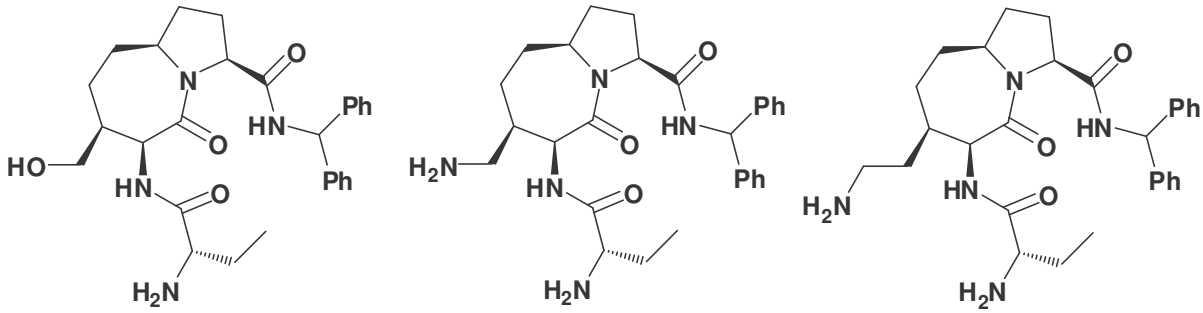

Smac005 Smac010 Smac037

Figure 35: The three most active Smac mimetics based on 4-substituted azabicyclo[5.3.0]alkanes designed by Mastrangelo *et al.* in 2008. Redrawn from Mastrangelo *et al.* (2008).[77]

3.2 Results and discussion of peptide synthesis

Looking at the previous drug designs of Smac mimetics, our synthetic drug design involved four strategies, namely;

- *N*-methylation
- Proline substitution
- The incorporation of "cage" amino acids into the peptide sequence
- The use of peptoids

A summary of the compounds prepared has been included in Figure 36. Each of these synthetic strategies has been discussed in detail thereafter.

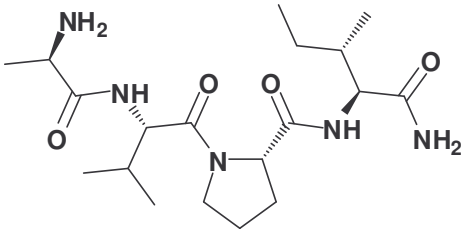

Peptide 1-AVPI

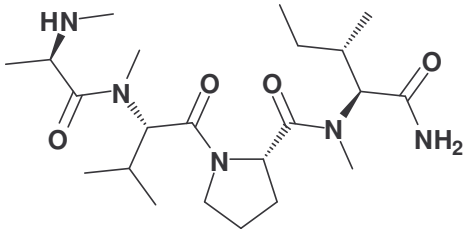

Peptide 2-N-meth

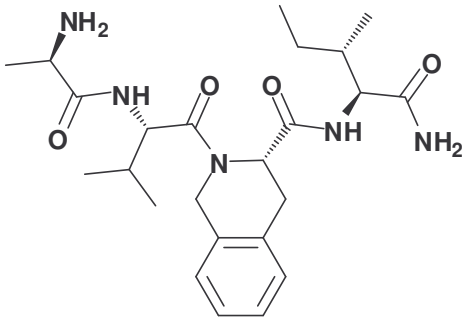

Peptide 3-TIQ

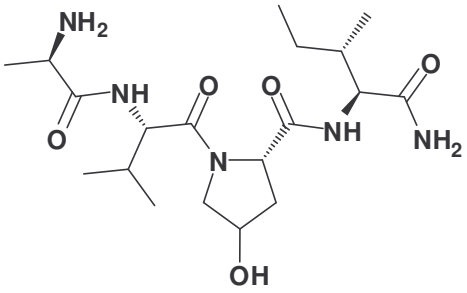

Peptide 4-HP

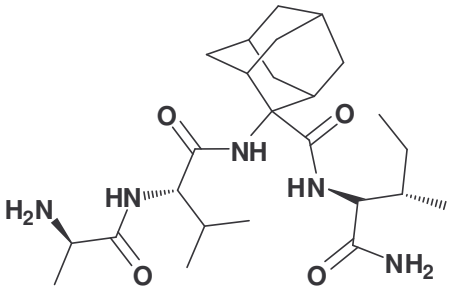

Peptide 5-Ada

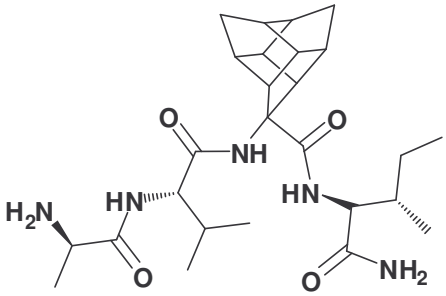

Peptide 6-Tris

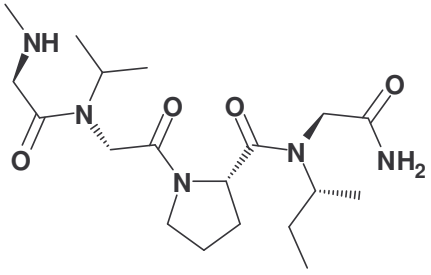

Peptide 7-Peptoid

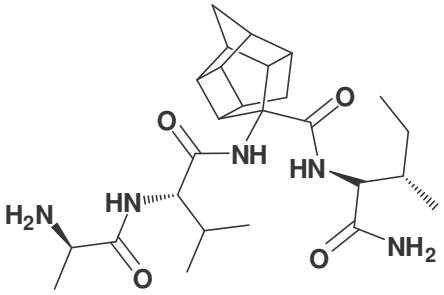

Peptide 8 and 9-PCU1 and PCU2

Figure 36: Summary of compounds prepared in this study.

3.2.1 Synthesis of Smac N-terminal tetrapeptide AVPI

The active Smac N-terminal tetrapeptide NH_2-AVPI (Figure 37) was synthesized using both manual and automated SPPS techniques. This compound was to be used as a control with which biological data obtained for the novel Smac mimetics would be compared.

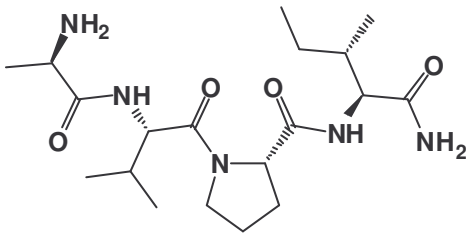

Figure 37: Peptide 1; Smac N-terminal tetrapeptide.[126]

The Rink amide resin was chosen for the synthesis. This resin was selected in order to yield an amino terminal alanine upon cleavage from the resin. Fmoc-Ile-OH was the first amino acid coupled to the resin, followed by Fmoc-Pro-OH, Fmoc-Val-OH and Fmoc-Ala-OH. HBTU and DIPEA were used as the coupling agent and base respectively and cleavage from the resin was carried out with 95 % TFA in water. No synthetic challenges arose during this preparation and the pure compound was obtained in good yield (Table 2).

Table 2: Percentage yields of purified peptides

Peptide	Calculated Mass + H (g mol^{-1})	Observed Mass + H (g mol^{-1})	Yield (%)
1-AVPI	398.2762	398.2753	84
2-*N*-meth	440.3231	440.3224	35
3-TIQ	460.2918	460.2904	60
4-HP	414.2711	414.2696	70
5-Ada	478.3388	478.3381	35
6-Tris	488.3231	488.3224	55
7-Peptoid	398.2762	398.2751	75
8-PCU1	488.3231	488.3213	30
9-PCU2	488.3272	488.3260	24

3.2.2 *N*-methylations

The application of peptides as potential drugs is limited by their weak pharmacokinetic properties including poor oral bioavailability and short half life *in vivo*.[134] These are a few of the reasons for increased interest in studying peptides containing *N*-methylated amino acids. Compounds for example *cyclosporine A*, a multiple *N*-methylated cyclic peptide are commonly found in nature. They are known to exhibit interesting biological properties such as improved metabolic stability and increased hydrophobicity and therefore inspired the *N*-methylation of lead compounds as a promising method to improve their poor pharmacokinetic properties.[135] *N*-methylation could therefore potentially contribute to increased bioavailability thus increasing the therapeutic potential of lead compounds.

N-methylated amino acids differ from traditional amino acids in that the proton of the amide nitrogen is replaced by a methyl group (Figure 38). Conformationally, this substitution results in peptides with fewer hydrogen bonds and hence compounds that are less likely to exist in *trans* conformations leading to enhanced bioavailability.[135,136]

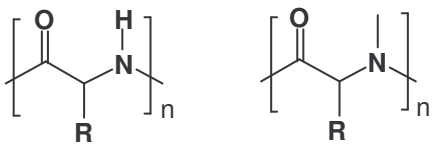

Figure 38: Structural difference between a traditional amino acid (A) and an *N*-methylated amino acid (B).

The demand for optically pure *N*-methylated amino acids for peptide synthesis is extremely high due to the improved biological properties its presence exhibits. The synthesis of *N*-methylated amino acids has therefore come a long way since the early synthetic route established by Ben-Ishai in 1957. This method requires the synthesis of 5-oxazolidinone intermediates in benzene by reacting acylamino acids with paraformaldehyde in the presence of catalytic quantities of para-toluenesulfonic acid.[137] The main disadvantage being low yields.

Freidinger *et al.* in 1983 incorporated the earlier findings of Ben-Ishai with those of Carpino *et al.* in 1972. [137,138,139] They were therefore able to increase the range of substrates that could be converted to 5-oxazolidinones through the use of 9-fluorenylmethoxycarbonyl (Fmoc) protected amino acids and paraformaldehyde. Their process however involves the use of excess triethylsilane (Et_3SiH) in trifluoroacetic acid (TFA) and chloroform 1:1.[139] The large amounts of Et_3SiH (> 3 equivalents) and TFA that is required are undesirable due to high cost. TFA is also extremely corrosive and problematic to remove.

In 2005, Zhang *et al.* reported the replacement of TFA in the procedure by Lewis acids such as aluminium chloride ($AlCl_3$). Advantages include reduced reaction times and smaller quantities of Et_3SiH required to open the 5-oxazolidinone ring to the corresponding *N*-methylated amino acid.[140]

The choice of resin for the synthesis of *N*-methylated peptides was important since *N*-methylated amino acids have been shown to be acid sensitive.[135] For this reason, the Rink amide resin used for the AVPI tetrapeptide synthesis would be unsuitable. Cleavage of the peptide from this resin requires a minimum of 95 % TFA and will lead to hydrolysis of the *N*-methyl groups.[141] A Sieber amide resin was therefore selected since cleavage would only require a maximum of 1 % TFA. It has been established that the coupling of *N*-methylated amino acids are difficult and selecting the correct coupling agents would be imperative for this synthesis. The aza-onium derivative HATU was chosen ahead of HBTU used previously. This was due to the greater activity of the active OAt ester over OBt during coupling.[142]

The manual SPPS of *N*-methylated AVPI containing *N*-methylations at the alanine, valine and isoleucine residues was unsuccessful. The synthesis was attempted a number of times with varying synthetic strategies such as coupling reagents and coupling times, deprotection and cleavage methods. Unfortunately the desired compound with m/z = 439.3 g mol^{-1} could not be obtained (Figure 39).

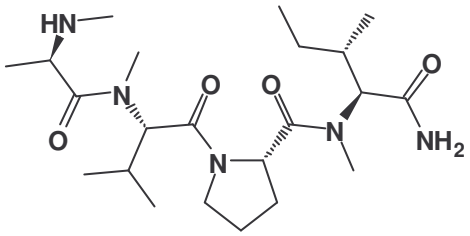

Figure 39: Peptide 2; *N*-methylated AVPI.

Initially, two hour coupling times for each amino acid was carried out and the complete peptide was cleaved with 1 % TFA in DCM for 20 min. A product with molecular mass of 340.2 g mol^{-1} was obtained. The possible product obtained is illustrated in Figure 40.

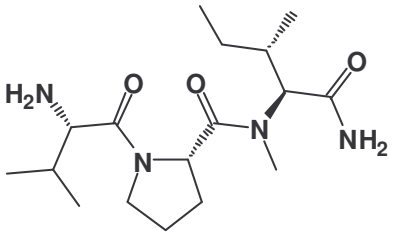

Figure 40: Possible product formed from manual synthesis of peptide 2.

As can be seen, the terminal *N*-methyl alanine residue is absent and removal of the methyl group from the nitrogen of valine has occurred. Three possible causes for this occurrence were identified, the first being that the *N*-methyl alanine did not couple. Second, the *N*-methylated alanine may have been removed during cleavage of the complete sequence from the resin or lastly, it could have been removed during deprotection.

To test the cleavage method, the peptide was synthesized in the same manner as previously. Various cleavage methods were then applied, including a mixture of acetic acid, trifluoroaceticethanol (TFE) and DCM (1: 1: 2), 2 % TFA in DCM, 1 % TFA in DCM and a combination of TFA, water and triisopropylsilane (95: 2.5: 2.5). The desired product was still not obtained.

The next attempt involved coupling of the *N*-methyl alanine over 24 hours. The deprotection method was then tested by cleavage of the peptide in the fully deprotected and not the fully deprotected form. Both forms resulted in an observed molecular weight of 355 g mol^{-1}

indicating the absence of the *N*-methylated alanine. From these results it was concluded that the *N*-methylated alanine was simply unable to couple to the *N*-methylated valine. We therefore attempted to couple Fmoc-Ala-OH to the *N*-methylated valine. This reaction was successful and a molecular mass of 448 g mol^{-1} was observed. An attempt was then carried out to methylate the free NH_2 of the terminal alanine residue. This was done prior to cleavage using 1 molar equivalent of MeI and 2 equivalents of K_2CO_3 in dry THF. Unfortunately, due to the similar retention times, the mixture of unreacted, mono-methylated and di-methylated products could not be separated.

A final attempt was made using a miniature "convergent" SPPS strategy.[112] The first dipeptide was successfully synthesised on Sieber amide resin and it contained *N*-methylated isoleucine and proline residues. For the second dipeptide, 2-chlorotrityl resin was used and valine followed by alanine was coupled in order to yield the free acid group upon cleavage. This dipeptide was then to be coupled to that on the Sieber amide resin. Unfortunately, the *N*-methylated alanine was unable to couple to the *N*-methylated valine with the most likely cause being steric hindrance.

Microwave synthesis was therefore resorted to due to its ability to aid difficult couplings. Upon cleavage from the resin, three products with molecular weights of 340, 355 and 440 g mol^{-1} were obtained. The desired product with molecular mass 440 g mol^{-1} was obtained as the major product. The two by-products obtained both excluded the terminal *N*-methylated alanine. One however maintained the *N*-methylation of the valine residue and the other did not. The required product was separated by semi-preparative HPLC using a water/ acetonitrile solvent system.

3.2.3 Investigation to replace proline in AVPI peptides

The investigation into proline substitution first involved the use of 1,2,3,4-tetrahydroisoquinoline-3-carboxylic acid (TIQ) since they are structurally similar. The tetrahydroisoquinoline family has been under medical investigation for anticancer properties since the late 1960's with the isolation of napthyridinomycin which exhibits potent cytotoxic properties.[143] TIQ is an unnatural amino acid associated with this family and possesses a bicyclic structure. It is a phenylalanine analogue that is composed of two fused six-membered rings with a dihedral torsion angle similar to proline (Figure 41).

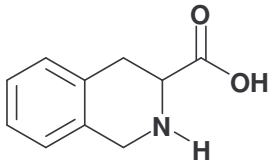

Figure 41: Chemical structure of TIQ.

Due to its rigid structure, TIQ was previously incorporated into the design of conformationally constrained peptidomimetics used to study effector/receptor interactions. There has been growing interest in pharmaceutical applications of this compound since its association with various biological properties including; antibacterial, antiplasmodial, cardiovascular and neuromodulating effects.[144] This compound has previously been shown to be effective as bradykinin agonists[xxii], angiotensin-converting enzyme (ACE) inhibitors[xxiii] and hypotensive drugs.[145]

TIQ was therefore incorporated into the NH_2-AVPI sequence thereby replacing the proline residue (Figure 42). This compound was also synthesized both manually and by using the automated microwave assisted peptide synthesizer. During manual synthesis, the desired product was obtained as the major product although a by-product with m/z = 361.3 g mol^{-1} was also obtained. The molecular mass of this by-product differed from the desired product by 99.1 g mol^{-1} and was therefore identified as A-TIQ-I. It was found that the valine residue had not coupled completely to the TIQ amino acid due to steric hindrance. Automated microwave synthesis was then attempted in order to resolve formation of this by-product but interestingly the same products were obtained using both techniques. Nevertheless the desired product was obtained in good yield however there is room for improvement by the use of different coupling reagents and increased microwave coupling times.

[xxii] Bradykinin agonists refer to the compound having the ability to cross the blood brain barrier and blood brain-tumor barrier (BTB).

[xxiii] ACE inhibitors are a group of drugs that are used primarily in treatment of hypertension and congestive heart failure.

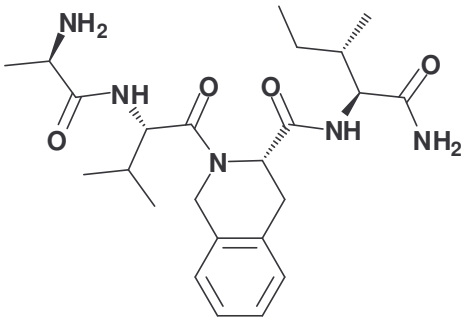

Figure 42: Peptide 3; Proline substitution with TIQ.

The use of 4-hydroxyproline to replace proline in the NH_2-AVPI sequence was also investigated. Prior to use in the peptide synthesis, it was necessary to protect the amino group of the purchased 4-hydroxyproline with an Fmoc protecting group. This reaction was carried out by firstly adjusting the pH of an aqueous solution of the amino acid to pH = 9 with sodium hydrogen carbonate (Figure 43). This was confirmed with universal indicator paper. Fmoc-Cl in 1,4 dioxane was added dropwise with stirring and allowed to react overnight. The reaction mixture was then worked up and the resulting product was purified by recrystallisation from ethyl acetate. The purified product was obtained as a white powder in 75 % yield (Figure 44).

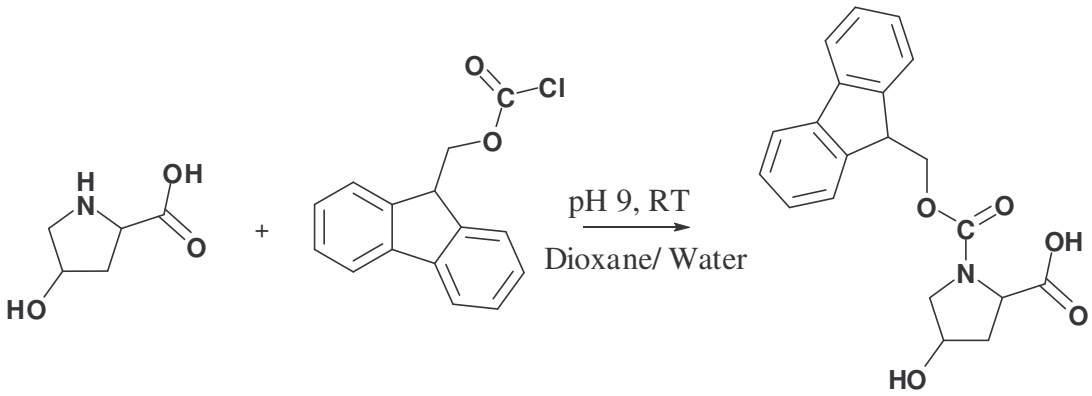

Figure 43: Fmoc protection of 4-hydroxyproline

The manual synthesis of this compound provided no synthetic difficulties and no undesired by-products were obtained.

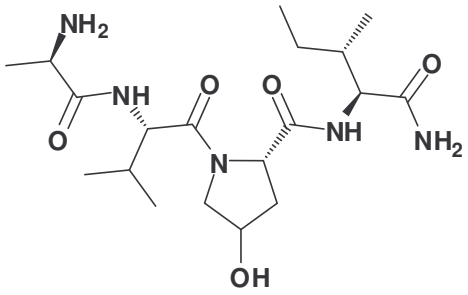

Figure 44: Peptide 4; Proline substitution in a Smac peptide with 4-hydroxyproline.

3.2.4 The use of cage amino acids

Researchers in the pharmaceutical sector have investigated the benefits of incorporating polycyclic "cage" compounds into potential drug leads for over ten years. To date the main focus has been concentrated on the four most well characterised "cage" compounds (Figure 45). These include adamantane, cubane, pentacyclo-[5.4.0.02,6.03,10.05,9]-undecane (PCU) and trishomocubane.

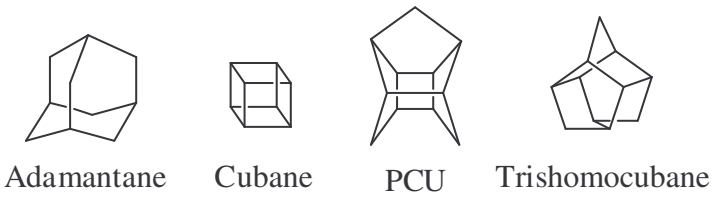

Figure 45: Well known polycyclic "cage" compounds.

These studies involved incorporating cage amino acids into various peptide sequences.[146-149] Conclusions from these investigations have shown that incorporation of these "cages" into potential drug candidates has a number of advantages with regard to drug activity and pharmacokinetics. First, the structural benefits include; improvements in cell permeability and hence enhances drug transport across the blood brain barrier (BBB) and into the central nervous system (CNS).[150,151] Second, due to the hydrophobic nature of the hydrocarbon cage moiety, drugs including the cage reportedly increased the affinity of the drug for lipophilic regions in receptor molecules.[152] Last due to their bulky structure an increase of drug resistance to metabolic degradation was observed, hence increasing the half-life of the drug *in vivo*. This therefore reduces the frequency of drug dosage.[153-155]

The first cage α–amino acid under investigation in this study was 2-aminoadamantane-2-carboxylic acid which was shown to exhibit good antitumor activity.[152,153] Its main drawback was relatively poor solubility at physiological pH (1.5 x 10^{-3} M). Since the adamantane amino acid does not have a chiral centre it can be incorporated into peptide sequences without forming diastereoisomers which is advantageous for pharmaceutical applications.[153]

2-Adamantanone is a commercially available compound that was used to synthesize 2-aminoadamantane-2-carboxylic acid. This involves a multistep route that first requires the preparation of the adamantane hydantoin followed by conversion to the amino acid by base hydrolysis and finally Fmoc protection of the amino group in order to be incorporated into the peptide sequence. 2-Adamantanone was reacted with sodium cyanide, ammonium carbonate, ammonium hydroxide and ethanol *via* the Bucherer-Lieb method to produce the adamantane hydantoin in 89% yield (Figure 46).[153,156,157]

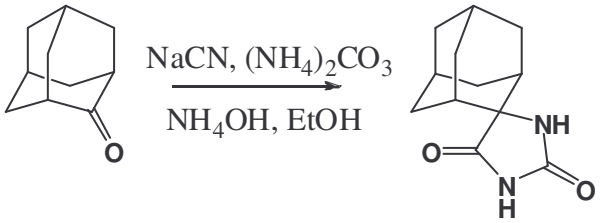

Figure 46: Synthesis of adamantane hydantoin.

The hydantoin was then hydrolysed under pressure[153] to yield the adamantane amino acid in 85 % yield (Figure 47).

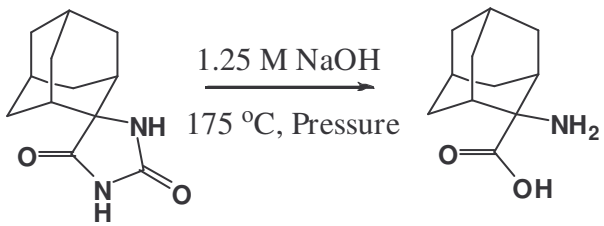

Figure 47: Base hydrolysis of adamantane hydantoin to the amino acid.

The adamantane amino acid was not soluble in any available NMR solvents and therefore had to be further characterised by first preparing the Fmoc protected amino acid. An ESI mass spectrum with molecular mass of 195 g mol^{-1} was however obtained by the addition of a few

drops of formic acid to the sample indicating its successful synthesis. Fmoc protection of the amino acid was carried out in a similar fashion as previously described and a pure white powder was obtained in a 75 % yield after recrystallisation from ethyl acetate.

This amino acid was used as a substitute for proline in the synthesis of the AVPI tetrapeptide. To overcome synthetic challenges experienced previously by researchers to incorporate the adamantane cage structure into a peptide sequence, automated microwave SPPS was employed. The desired sequence was prepared on a Rink amide resin and cleavage from the resin with 95 % TFA in DCM yielded three products. The major product had a molecular mass of 379.1 g mol^{-1} which represents the absence of valine from the sequence. The second by-product with molecular mass 308.0 g mol^{-1} consisted of only isoleucine and the adamantane amino acid. The desired compound with molecular weight 478.2 g mol^{-1} was also obtained (Figure 48). The desired product ratio to minor and major by-product was found to be 20:25:55 respectively. Semi-prep HPLC was therefore carried out on the crude sample in order to isolate the desired product. A solvent gradient of 25 – 60 % CH_3CN in water for 40 minutes was used for the purification and the desired product eluted after approximately 8.4 minutes.

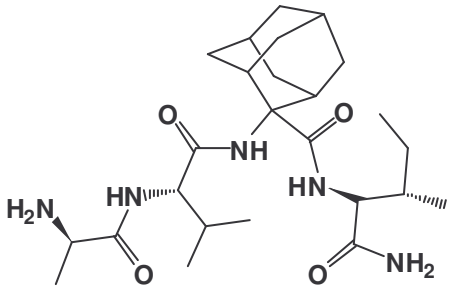

Figure 48: Peptide 5; Adamantane AVPI.

An improvement in the synthesis of peptide 5 was observed when HATU replaced HBTU as the coupling reagent used. Upon cleavage from the rink amide resin with TFA: H_2O: TIS (95:2.5:2.5), only two products were observed. The major product exhibiting a m/z value of 478.2 g mol^{-1} corresponding to the desired sequence and the minor product with a m/z value of 379.1 g mol^{-1} corresponding to the absence of the valine residue from the sequence.

The next cage amino acid used was Fmoc-trishomocubane[142] which was first synthesized by Govender *et al.* in 2005 and has been shown to yield sharp β-turns when incorporated into a peptide chain.[102,156] Unlike the adamantane amino acid, this molecule is intrinsically chiral and therefore when incorporated into the peptide chain results in the formation of diastereoisomers. Prior to incorporation into the peptide sequence, the monoketone was converted to the hydantoin using the same procedure as for the adamantane version. The amino acid was then Fmoc protected. The target peptide sequence was once again synthesized on a Rink amide resin using automated microwave SPPS. Upon cleavage from the resin, two products were obtained. The first had a molecular mass of 488 g mol^{-1} which was the desired product (Figure 49). The second has a molecular weight of 358 g mol^{-1} and corresponds to the absence of valine from the desired sequence. A desired product to by-product ratio of 35:65 was obtained. Unfortunately, the diastereoisomers could not be separated by semi-prep HPLC even when a very shallow solvent gradient was used. This was perhaps not expected to have large effect on the potential bioactivity of the two diastereomeric peptides, since the 3D structure of the peptide backbone of trishomocubane containing diastereomeric peptides are virtually identical.[102] Separation might have been afforded if the peptide sequence had not been completely deprotected. The crude product was purified using a solvent gradient of 10 – 60 % CH3CN in water over 30 minutes and the desired product eluted after approximately 13 minutes.

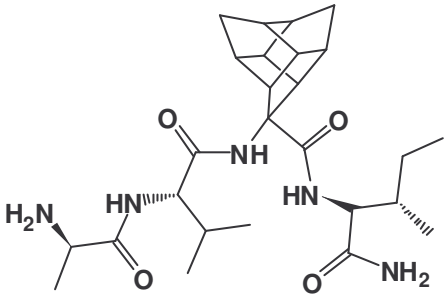

Figure 49: Peptide 6; Trishomocubane AVPI.

The PCU version of the AVPI amino acid sequence (Figure 50) has already been synthesised using microwave assisted SPPS by Saadaldin in 2008.[158] He was able to separate the diastereoisomers and this compound will be tested for its cytotoxic effect on the MDA MB 231 cell line along with the compounds prepared in this study. Microwave assisted SPPS was used for this synthesis and upon cleavage from the resin with TFA: H_2O: TIS (95:2.5:2.5),

only the desired product was observed. Separation of the diasteroisomers was achieved using a solvent system of 5 – 60 % acetonitrile in 60 minutes. The products eluted at 27.7 min and 29.2 min respectively and were named PCU1 and PCU2 peptides.

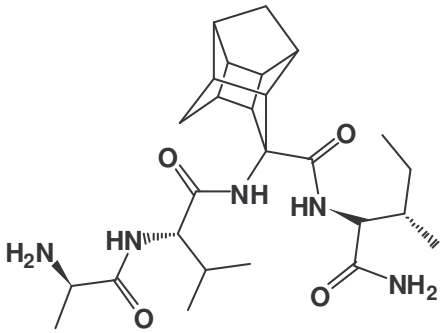

Figure 50: PCU AVPI.

3.2.5 Peptoids

Oligomers of *N*-substituted glycine (NSG) monomers are synthetic polymers that have exhibited good biological activity and proteolytic stability.[159] They are part of an important class of biomimetic oligomers that have recently found use in combinatorial drug discovery, drug delivery, gene therapy and biopolymer folding.[160] Shortfalls of conventional peptides include metabolic instability and poor absorption both of which are overcome by the characteristics of peptoids. Hence peptoids are considered potential mimetics of bioactive polypeptides due to their protease resistance and biocompatibility. Other advantages include the ability to form stable secondary structures and hence result in biomedical applications including protein-protein interactions.

Peptoids differ from peptides in that each appropriate side chain is attached to the amide nitrogen rather than the α-carbon (Figure 51).[161]

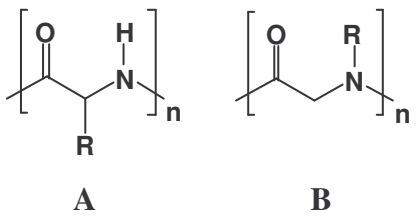

Figure 51: Structural difference between (A) peptide and (B) peptoid.

Peptoids are simply prepared by a solid-phase "submonomer" route established by Zuckermann *et al.* in 1992.[159] This synthetic route involves two steps (Figure 52). The first of which is an acylation carried out with a haloacetic acid, in this case bromoacetic acid and *N,N'*-diisopropylcarbodiimide (DIC) were uses as a suitable activators. The second step is a nucleophilic displacement of bromine by a primary amine. Repetition of these two steps results in the formation of a growing chain and various amine solutions can be used to obtain the desired sequence.

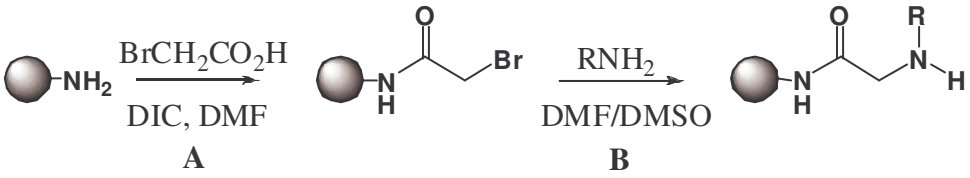

Figure 52: Reaction scheme for synthesis of a peptoid on a solid support; (A) acylation and (B) nucleophilic displacement.

The first attempt to synthesise the AVPI peptoid analogue involved using the "submonomer" method proposed by Maayan *et al.*[162] Upon cleavage from the resin however, the major product formed had a molecular mass of 301.2 g mol^{-1} determined by LC/MS. The desired product with m/z = 398.4 g mol^{-1} was present but as a very minor component. Initially it was thought that the difference in mass of 97.2 g mol^{-1} could be attributed to the absence of proline from the sequence. The coupling of proline was therefore confirmed by cleavage from the resin after coupling. A m/z of 472.3 g mol^{-1} was obtained indicating the presence of proline (449 g mol^{-1} + 23). Further investigations involving varying reagent equivalents, coupling times *etc.* proved that neither the coupling times or cleavage methods posed the problem. It was then decided to investigate the deprotection strategy used and it was found that deprotection with 20% piperidine for 20 minutes after coupling of the proline residue resulted in undesired diketopiperazine (dkp) formation (Figure 53).

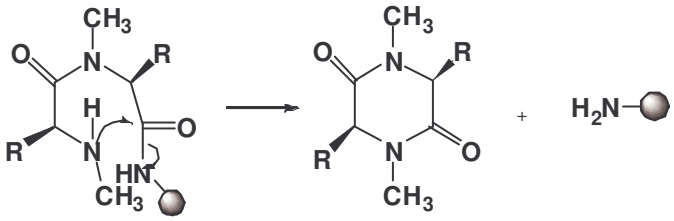

Figure 53: DKP formation.

Peptides containing proline or *N*-alkylated amino acids in the *C*-terminal dipeptide sequence present synthetic difficulties because of the ease with which they cyclise to yield the corresponding diketopiperazine. Diketopiperazine formation is favoured by the presence of *N*-alkylated amino acids, because of their tendency to form *Z*-amides. This consequently results in a reduction in yield of the desired product.[163] Diketopiperazine formation takes place in both solution and solid phase when a dipeptide ester is formed and is both acid and base catalyzed.[114]

Literature was then consulted and alteration of the deprotection strategy to 50 % piperidine for only 5 minutes solved this synthetic difficulty to a degree.[160] The synthetic scheme proposed by Holub *et al*. in 2006 was then used due to its reduced bromoacetylation and monomer amine displacement reaction times.[164] The desired product with m/z = 397.2 g mol^{-1} was obtained as the major product (Figure 54) although some undesired product excluding valine from the sequence was also present. A product to by-product ratio of 67:33 was obtained.

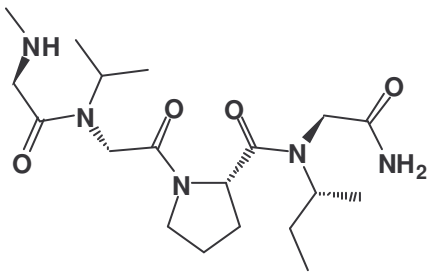

Figure 54: Peptide 7; AVPI peptoid.

3.3 Conformational analysis of synthesised peptides

Plane polarised light consists of 2 equal circularly polarised components, namely, clockwise (right-handed) and counter-clockwise (left-handed).[165] Circular dichroism (CD) spectroscopy is based on the principle that optically active molecules have the ability to preferentially absorb this left or right-handed circulatory polarised light. A CD spectra will only be obtained if radiation is absorbed and this technique has been increasingly used to examine the secondary structure of proteins. In proteins, the peptide bond acts as a choromophore with α-helices, β-sheets, and random coil structures each giving rise to characteristic spectra in the far UV region (190-250 nm). *α*-Helices exhibits its maximum differential absorbance between 190-195 nm and minimum between 208-222 nm. *β*-sheets exhibits its maximum between 195-200 nm and minimum between 215-220 nm while random coils have a maximum at 220 nm and minimum at 200 nm.[166] The CD spectra obatined for each of the compounds prepared in this study is illustrated in Figure 55.

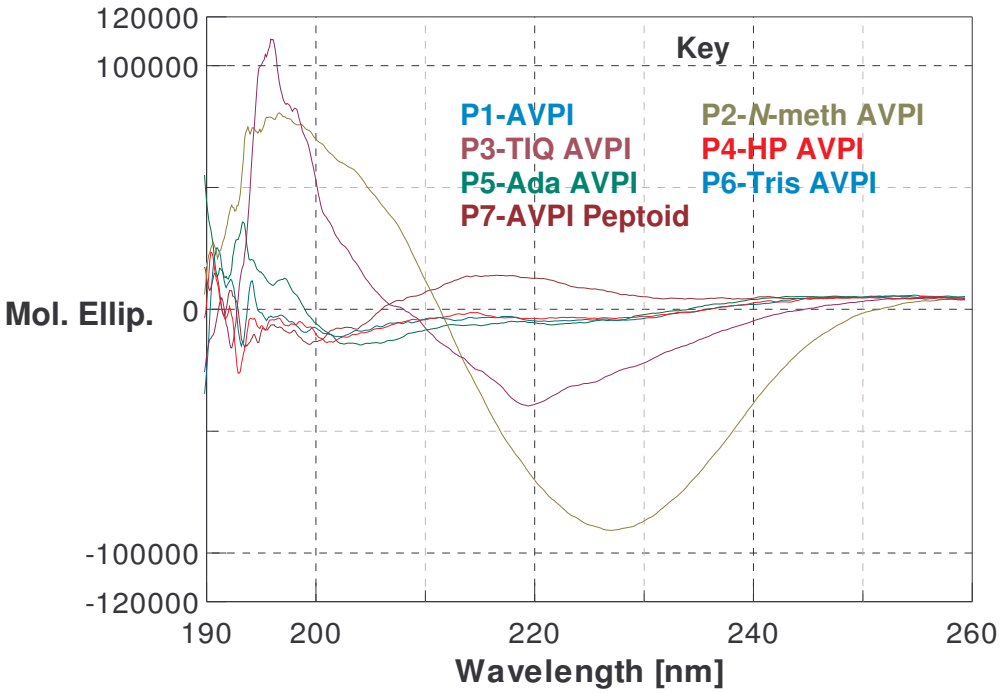

Figure 55: CD spectra for peptides 1 to 7 in MeOH where Mol. Ellip. is the molecule ellipticity measured in deg cm^2 dmol^{-1}.

The data obtained revealed that peptides 2 and 3 could exhibit partial *β*-sheet conformation in solution while peptide 7 might adopt an *α*-helix conformation. Peptides 1 and 6 were

indistinguishable since they exhibited very similar CD spectra. No real secondary structures could be assigned by structural analysis of peptides using CD for peptides 1, 4 and 5 since they all exhibited very flat CD spectra. From Figure 56 it is observed that the two diastereoisomers of the PCU AVPI derivative exhibit different conformations.

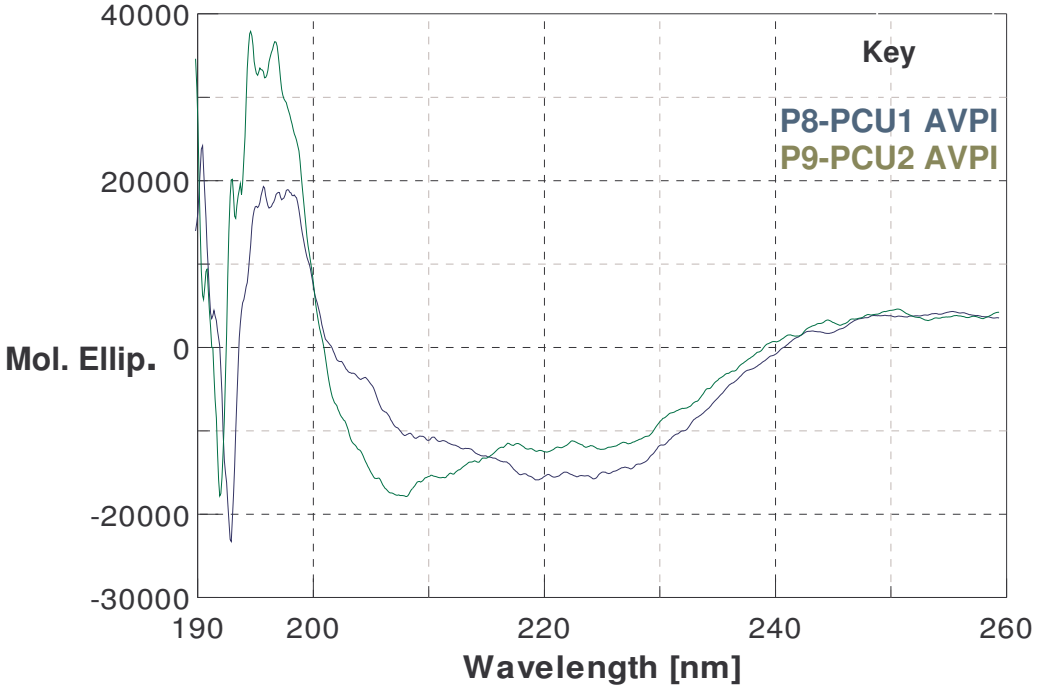

Figure 56: CD spectra obtained for peptides 8 and 9 in MeOH where Mol. Ellip. is the molecule ellipticity measured in deg cm^2 dmol^{-1}.

PCU1 peptide possibly adopts a β-sheet conformation, corresponding to a maximum between 195-200 nm and a minimum between 215-220 nm while PCU2 peptide might adopt an α-helical conformations with its maximum differential absorbance between 190-195 nm and minimum between 208-222 nm.

3.4 Structural elucidation of synthesised peptides by NMR spectroscopy

Structural elucidations of peptides prepared in this study were carried out using 2-D NMR techniques. This information in combination with the data obtained from high resolution mass spectrometry serves to confirm the successful synthesis of the target peptides. Peptides 8 and 9 (PCU1 and 2) were previously elucidated by Saadaldin and the paper is currently "in print" at Magnetic Resonance in Chemistry.

Heteronuclear multiple bond coherence (HMBC) and nuclear overhauser effect spectroscopy (NOESY) or rotational nuclear overhauser effect spectroscopy (ROESY) are valuable techniques to cross link the various amino acid residues to elucidate the peptide structures. There are at least four useful points of entry for the elucidation of the NMR spectra of peptide 1 (AVPI). The HMBC interaction of the alanine methyl protons (H-1) with the carbonyl carbon (C-3), the characteristic methyl protons (H-22/23) of the valine fork, the proline α-hydrogen (H-11) which is the only one that should register as a triplet and the characteristic ethyl group on isoleucine. For the convenience of the reader, the assignment of the NMR signals will start from alanine (H-1) and then move towards the other end of the molecule all along the peptide back bone to isoleucine (H-20).

The methyl proton signal of H-1 is the only methyl group in the structure that can display an HMBC correlation to a carbonyl carbon (Spectrum 15). The carbonyl resonance at 169.8 ppm shows an HMBC correlation to a methyl proton resonance at 1.30 ppm. These signals are therefore assigned to C-3 and H-1 of the alanine residue respectively. The protons of H-1 display a correlation spectroscopy (COSY) correlation (Spectrum 13) with a proton at 3.92 ppm which is assigned to H-2. H-2 shows a COSY correlation to an amide resonance at 8.05 ppm which was assigned to H-24. C-3 exhibits a HMBC resonance to an amide proton at 8.53 ppm which was assigned to H-4.

Moving onto the valine residue, the signals at 0.90 ppm and 0.93 ppm are characteristic of the methyl groups associated with the valine fork. These are therefore assigned to H-22 and H-23 of the valine residue respectively.[158] The corresponding carbon resonances were observed at 18.5 and 18.1 ppm respectively from the heteronuclear single quantum coherence (HSQC) spectrum (Spectrum 14). H-22 and H-23 both show COSY correlations with a proton at 1.99 ppm which from the structure can only be assigned to H-21. H-21 displays a COSY correlation with a proton at 4.37 ppm, this was assigned to H-5. An HMBC correlation is observed between H-5 and a carbonyl at 169.7 ppm, which is assigned to C-6. This assignment was confirmed by the absence of a corresponding proton signal for C-6 (169.7 ppm) on the HSQC spectrum. H-5 (4.37 ppm) shows a HMBC correlation with C-3 (169.8 ppm) which confirms the connection between the alanine and valine residues.

The proline residue contains three methylene protons (H-8, H-9 and H-10). Each of these protons will exhibit a split signal sharing a single carbon. The difference in frequency

between the two H-10 protons will be the largest because it is located adjacent to a chiral carbon (C-11). From the HSQC spectrum, four carbons are observed to have split proton signals (24.7, 25.0, 29.9 and 47.7 ppm). The corresponding proton signals for the carbon at 24.7 ppm was found to be 1.10 and 1.45 ppm. Since these protons show COSY correlations to a methyl proton, they were assigned to H-19a and H-19b of the isoleucine residue. The only other methine proton that can show a COSY correlation to a CH_2 is H-11. H-11 is therefore assigned to 4.42 ppm since it displays a COSY correlation with methylene protons at 1.81 and 1.99 ppm. This methylene signal is therefore assigned to C-10. This is further confirmed by the distance between these two splitting protons (0.18 ppm) which is the largest from the remaining methylene signals. The methylene carbon signals at 25.0 and 47.7 ppm correspond to protons at (1.81 and 1.99 ppm) and (3.60 and 3.68 ppm) respectively from the HSQC spectrum. A COSY correlation is observed between these sets of protons and they can either be assigned to H-8 or H-9. H-8 is expected to appear at a higher frequency due to its position adjacent to a deshielding N atom. The protons at 3.60 and 3.68 ppm were therefore assigned to H-8 while those at 1.81 and 1.92 ppm were assigned to H-9. From the ROESY spectrum (Spectrum 17), H-8 (3.60 and 3.68 ppm) correlates to H-5 (4.37 ppm) from the valine residue. This correlation confirms the connection between proline and valine.

From the isoleucine residue, H-19a and H-19b (1.10 and 1.45 ppm) show a COSY correlation to the methyl protons at 0.81 ppm which was assigned to H-20. Both the protons H-19a and H-19b show a COSY correlation with a signal at 1.68 ppm, this was assigned to the methine proton H-17. A COSY correlation was observed between H-17 and a methyl proton at 0.84 ppm which was assigned to H-18. H-17 (1.68 ppm) displays a COSY correlation to 4.10 ppm which was assigned to H-14. H-14 (4.38 ppm) also shows a HMBC correlation to a carbonyl signal at 173.3 ppm which was consequently assigned to C-15.

H-11 shows a HMBC correlation to a carbonyl carbon at 171.7 ppm. This signal is assigned to C-12. C-12 (171.7ppm) exhibits an HMBC correlation to the proton registering at 7.70 ppm which was assigned to H-13. This assignment was confirmed by a COSY interaction existing between H-14 (4.10 ppm) and the proton at 7.70 ppm (H-13). Finally, C-14 (57.1 ppm) displays a HMBC correlation to a signal at 7.00 ppm which was assigned to H-16. No HMBC or TOCSY correlations could be observed to confirm the connection of the proline residue to isoleucine. ROESY interactions between H-11 (4.42 ppm) and H-13 (7.77 ppm) do confirm this connection. The NMR data for peptide 1 is presented in Table 3.

Table 3: ^{1}H and ^{13}C NMR data for peptide 1 (AVPI)

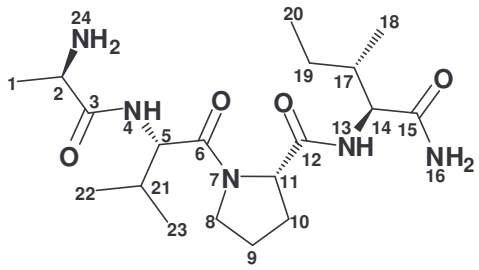

Peptide 1: AVPI			
Atom	**$\delta^{1}H^{a,b}$**	***J*(Hz)**	**$\delta^{13}C^{a,b}$**
1	1.30		17.8
2	3.92		48.4
3	-		169.8
4	8.54		-
5	4.37		56.4
6	-		169.7
7	-	-	-
8a	3.60	[c]	47.7
8b	3.68	[c]	47.7
9a	1.81	[c]	25.0
9b	1.92	[c]	25.0
10a	1.81	[c]	29.3
10b	1.99	[c]	29.3
11	4.42		59.6
12	-		171.7
13	7.70		-
14	4.10		57.1
15	-		173.3
16	7.00		-
17	1.68		37.4
18	0.84		15.9
19a	1.10	7.20	24.7
19b	1.45	7.20	24.7
20	0.81		11.6
21	1.99		30.9
22	0.90		18.5
23	0.93		18.1
24	8.05		-

[a] 600 MHz for ^{1}H and 150 MHz for ^{13}C

[b] Solvent $(CD_3)_2SO_2$

[c] Due to overlapping signals the respective coupling constants could not be determined

The compounds designed for this study involved the substitution of the proline residue in the *N*-terminal Smac tetrapeptide sequence. The remaining residues of AVPI, namely alanine, valine and isoleucine were kept the same for subsequent compounds. Therefore for brevity, these assignments will not be discussed in detail for elucidations of the other compounds. Focus will be placed on assigning the new residues replacing the proline moiety.

The assignment for peptide 2 (*N*-methylated) sequence was carried out in a similar fashion as described for peptide 1. Upon comparison of the HSQC spectrum of peptide 1 (blue and green) and 2 (red) (Figure 57), three distinct methyl signals at 3.02, 2.94 and 2.67 ppm were observed. These signals can be assigned to the *N*-methyl groups present.

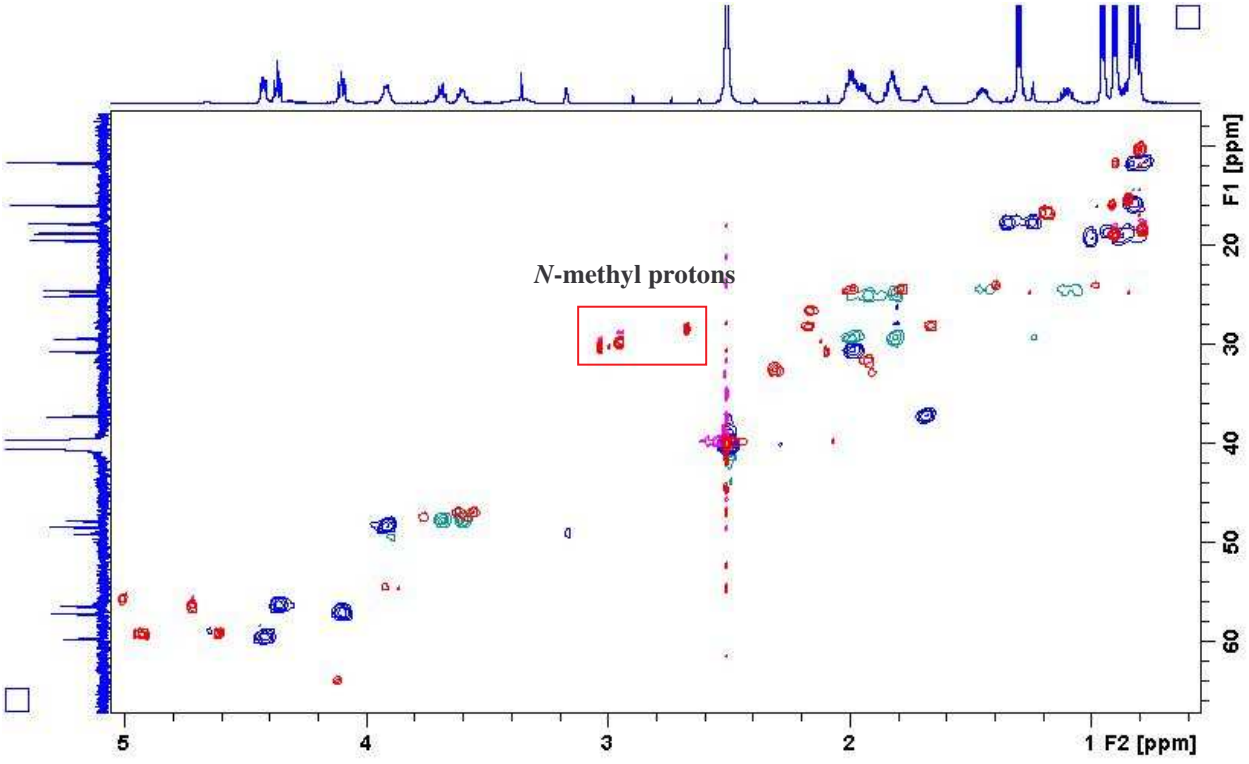

Figure 57: Overlay of the HSQC spectrum of peptide 1 (AVPI) (blue and green) and peptide 2

The *N*-methyl protons at 3.03 and 2.67 ppm show TOCSY correlations to one another. By examination of the structure of the compound, these signals could therefore be assigned to either methyl H-25 or H-26. One would expect H-26 to be slightly more deshielded than H-25 due to the close proximity of the carbonyl group, C-3. The signal at 3.03 ppm is therefore assigned to H-26, while that at 2.67 ppm is assigned to H-25. The NMR data for peptide 2 is presented in Table 4.

Table 4: ^{1}H and ^{13}C NMR data for peptide 2 (*N*-methylated)

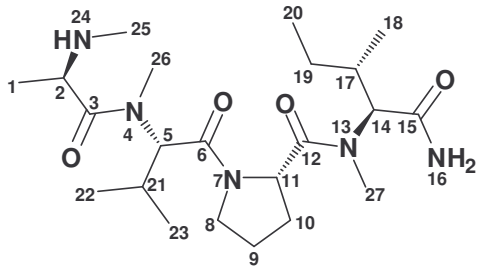

Peptide 2: *N*-meth			
Atom	**$\delta^{1}H^{a,b}$**	***J*(Hz)**	**$\delta^{13}C^{a,b}$**
1	1.18		16.0
2	5.01		55.6
3	-		167.0
4	7.22		-
5	4.92		59.2
6	-		171.7
7	-		-
8a	3.55	[c]	46.9
8b	3.61	[c]	46.9
9a	1.98	[c]	24.4
9b	1.78	[c]	24.4
10a	1.66	[c]	28.1
10b	2.18	[c]	28.1
11	4.71		56.4
12	-		171.8
13	7.29		-
14	4.61		59.0
15	-		170.8
16	6.91		-
17	1.92		31.5
18	0.84		15.2
19a	1.39	[c]	24.0
19b	0.99	[c]	24.0
20	0.79		10.1
21	2.16		26.4
22	0.78		18.4
23	0.90		19.9
24	7.64		-
25	2.67		28.3
26	3.03		30.1
27	2.94		29.6

[a] 600 MHz for ^{1}H and 150 MHz for ^{13}C

[b] Solvent $(CD_3)_2SO_2$

[c] Due to overlapping signals the respective coupling constants could not be determined

By elimination, the third *N*-methyl resonance at 2.94 ppm can be assigned to H-27. From the HSQC spectrum, the corresponding carbons were found to be 28.3, 30.1 and 29.6 ppm for C-25, C-26 and C-27 respectively.

The starting point for elucidation of peptide 3 (TIQ) was the two fully substituted carbons on the aromatic ring. The carbon spectrum of the compound shows six aromatic carbons between 125.0 and 135.0 ppm (Spectrum 25). Of these, the two resonances at 134.5 and 134.7 ppm corresponds to the quaternary carbons C-26 and C-31. These carbons show HMBC correlations (Spectrum 28) to 4.92 ppm and 4.64 ppm (attached to the same carbon atom). The splitting pattern of these protons is characteristic of methylene protons adjacent to a chiral carbon. These signals were therefore assigned to H-32. The aromatic carbon at 134.5 ppm displays a HMBC correlation to a proton at 4.83 ppm which was assigned to H-11, hence 134.5 ppm was assigned to C-31. By elimination, C-26 (no hydrogens attached) was assigned to 134.7 ppm. C-26 and C-31 display a HMBC correlation to a methylene proton at 3.02 ppm which was assigned to H-25. The HMBC spectrum shows a correlation between H-25 and an aromatic carbon at 127.9 ppm, this was assigned to C-27. An HMBC correlation between H-32 and an aromatic carbon at 126.3 ppm was also observed and hence assigned to C-30. The corresponding proton for C-30 was observed at 7.28 ppm from the HSQC spectrum (Spectrum 27). By elimination, the remaining methine protons H-28 and H-29 on the TIQ residue should be 7.15 and/or 7.22 ppm. All assignments for the peptide "arms" were once again made in a similar fashion as described for peptide 1. The corresponding carbon signals of all assigned protons of the TIQ AVPI derivative was assigned using the HSQC spectrum and are presented in Table 5.

Table 5: ^{1}H and ^{13}C NMR data for peptide 3 (TIQ)

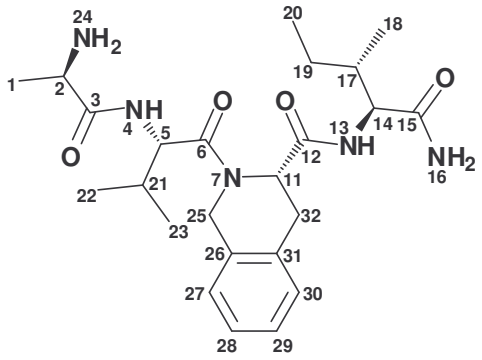

Peptide 3: TIQ			
Atom	**$\delta^{1}H^{a,b}$**	***J*(Hz)**	**$\delta^{13}C^{a,b}$**
1	1.16		20.5
2	3.48		49.8
3	-		173.22
4	7.31		-
5	4.06		57.08
6	-		171.0
7	-		-
11	4.38		54.1
12	-		170.3
13	7.53		-
14	4.81		54.1
15	-		170.8
16	7.51		-
17	2.09		31.3
18	0.97		19.7
19a	0.92	[c]	24.2
19b	1.29	[c]	24.2
20	0.72		15.8
21	1.60		37.4
22	0.90		18.3
23	0.74		11.6
24	7.02		-
25	3.02		31.7
26	-		134.7
27	7.20		127.9
28	7.15/7.22		126.9/127.7
29	7.15/7.22		126.9/127.7
30	7.28		126.3
31	-		134.5
32a	4.92	15.06	46.2
32b	4.64	15.06	46.2

[a] 600 MHz for ^{1}H and 150 MHz for ^{13}C

[b] Solvent $(CD_3)_2SO_2$

[c] Due to overlapping signals the respective coupling constants could not be determined

The next structure to be elucidated was the peptide 4 (HP). The only variation to the original structure is the replacement of one of the H-9 protons on proline with a hydroxyl group. The proline methylene protons (H-9) were observed at 1.81 and 1.92 ppm (^{1}H spectrum) and 25.0 ppm (^{13}C spectrum). By overlaying the HSQC spectrum of AVPI (blue and green) with that of the HP (red and pink) derivative, it is observed that the methylene proton signals for H-9 have in fact been removed (Figure 58).

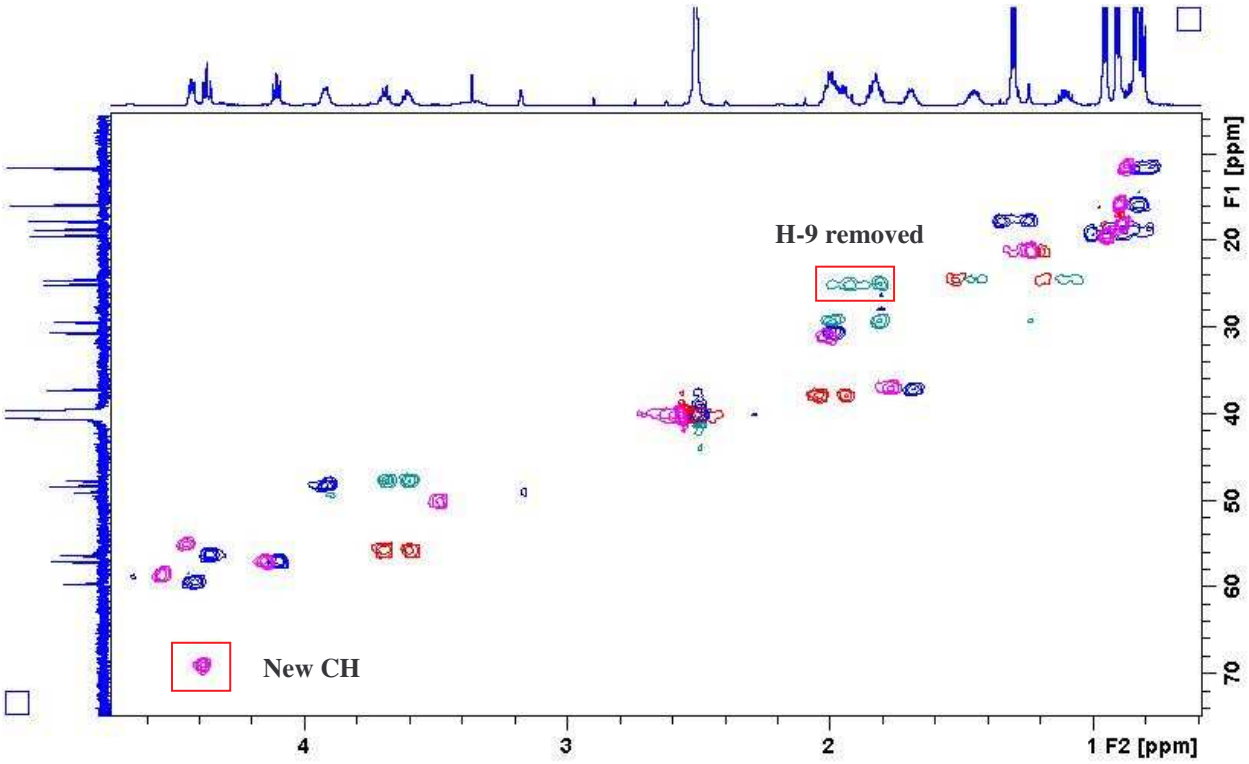

Figure 58: Overlay of the HSQC spectrum of peptide 1 (AVPI) (blue and green) and peptide 4 (HP) (pink and red) derivative of AVPI.

An additional signal at 4.39 ppm is observed which corresponds to a carbon at 69.1 ppm. This proton shows a COSY correlation with H-8a, H-8b and H-10 (methylene protons) of the proline ring at 3.58 ppm, 3.70 ppm and 1.95, 2.05 ppm respectively. This signal was therefore assigned to H-9. H-9 (4.39 ppm) shows a COSY correlation with 8.09 ppm which was assigned to the hydroxyl group (H-25). This was confirmed by the exclusion of a corresponding carbon signal in the HMBC spectrum. All the other signals corresponding to the alanine, valine and isoleucine residues that comprise the peptide "arms" are present although some slight shifts are observed. These assignments and corresponding carbon signals of all assigned protons of peptide 4 using the HSQC spectrum are presented in Table 6.

Table 6: ^{1}H and ^{13}C NMR data for peptide 4 (HP)

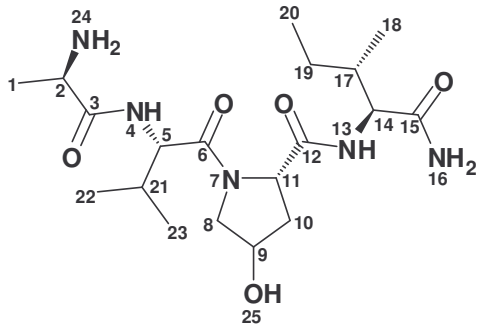

Peptide 4: HP			
Atom	**$\delta^{1}H^{a,b}$**	***J*(Hz)**	**$\delta^{13}C^{a,b}$**
1	1.23		21.2
2	3.48		50.2
3	-		171.5
4	8.10		-
5	4.45		55.1
6	-		173.4
7	-		-
8a	3.58	10.74	55.7
8b	3.70	10.50	55.7
9	4.39		69.1
10a	1.95	[c]	37.8
10b	2.05	[c]	37.8
11	4.55		58.8
12	-		174.5
13	7.81		-
14	4.15		57.1
15	-		170.2
16	6.98		-
17	1.77		37
18	0.89		15.9
19a	1.18	[c]	24.6
19b	1.52	[c]	24.6
20	0.88		11.7
21	2.01		31.0
22	0.95		19.3
23	0.88		17.9
24	7,32		-
25	8.09		-

[a] 600 MHz for ^{1}H and 150 MHz for ^{13}C

[b] Solvent $(CD_3)_2SO_2$

[c] Due to overlapping signals the respective coupling constants could not be determined

The ^{13}C APT spectrum was very useful in elucidating peptide 5, the adamantane AVPI derivative (Spectrum 38). The numbering system used for the adamantane cage is the same as that used by Hickmott *et al.* in 1985.[167] Only one quaternary carbon appears at 63.6 ppm and it was assigned to C-2'. A fairly large shift in the proton signal of H-1 is observed and it resonates at 0.87 ppm. The signal is found to overlap with H-20 which was indicated by the broad proton signal in the HSQC (Spectrum 40). The corresponding carbon signals of these methyl groups also overlap at 11.3 ppm which is indicated by higher intensity of the carbon signal. This assignment is confirmed by the COSY correlation of H-1 with H-2 at 1.78 ppm (Spectrum 39). The amide proton, H-13 (7.56 ppm), exhibits a NOESY interaction with a remaining methine signal which could either be H-1' H-3' or H5' of the adamantane cage (Spectrum 43). After the assignment of H-19a and H-19b (1.10 ppm and 1.45 ppm), the remaining methylene carbon resonances at 32.2 and 33.3 ppm were assigned to the methylene protons of the cage (H-4', H-6', H-8', H-9' and H-10'). Peak overlapping made it impossible to further assign these protons. The assumed signal of H-1'/H-3' and H-5'/H-7' displayed both TOSCY (Spectrum 42) and COSY interactions with all methylene protons appearing between 1.52-1.71 ppm and 1.89-2.74 ppm: thus confirming the assignment of H-1'/H-3' and H-5'/H-7'. A split signal is observed on the ^{13}C APT spectrum, *i.e.* two methine peaks overlap at 31.2 ppm which is indicative of the overlapping of the H-1'/3' and H-5'/7' resonances. Unfortunately, further assignment cannot be carried out due to the extensive peak overlapping occurring from 1.52 to 1.71 ppm and from 1.89 to 2.07 ppm (Spectrum 37). Molecular dynamics (MD) and a conformational search[xxiv] were carried out using MacroModel 9.5 to determine any possible intra-molecular interactions. The MM3 force field was used. It was hoped that the lowest energy structure[xxv] of peptide 5 may contain some heavy atom (oxygen) in close proximity of the adamantane frame work. This would cause a through space deshielding effect to the cage protons as previously reported for cage structures.[101,152,164,165] If that was observed, it would have been very useful to help confirm the complete NMR structure elucidation of the adamantane skeleton. Unfortunately no useful information was obtained from the ten lowest energy conformations. The calculated Cartesian

[xxiv] The MD optimization was performed at 400 K and the duration of the calculation was 20 ps. A total of 100 snapshots were taken and arranged according to energy. The conformational search included a random change of all the back bone torsion angles.

[xxv] The ten lowest energy structures for both the MD and conformational search calculations were again optimized with MM3 and then rank ordered according to energy.

coordinates of the lowest energy structure (conformational search) is provided in the Appendix as well as on the CD accompanying this dissertation.

Table 7: ^{1}H and ^{13}C NMR data for peptide 5 (Ada)

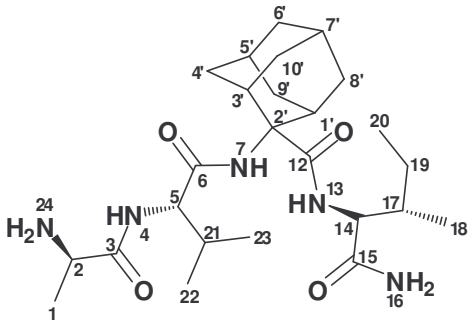

Peptide 5: Ada			
Atom	**$\delta^{1}H^{a,b}$**	***J*(Hz)**	**$\delta^{13}C^{a,b}$**
1	0.87		11.3
2	1.78		26.3
3	-		171.3
4	8.30		-
5	4.31		57.6
6	-		173.6
7	7.32		-
12	-		172.9
13	7.56		-
14	4.19		56.7
15	-		171.6
16	8.00		-
17	1.77		37.0
18	0.88		15.5
19a	1.10	[c]	24.2
19b	1.45	[c]	24.2
20	0.86		11.3
21	2.01		30.7
22	0.91		17.9
23	0.92		19.4
24	7.00		-
2’	-		63.6
1’ 3’ 5’ 7’	2.66-2.74		31.2
4’ 6’ 8’ 9’ 10’	1.52-1.71		33.3
4’ 6’ 8’ 9’ 10’	1.89-2.74		32.2

[a] 400 MHz for ^{1}H and 100 MHz for ^{13}C

[b] Solvent $(CD_3)_2SO_2$

[c] Due to overlapping signals the respective coupling constants could not be determined

The elucidation of peptide 6, the trishomocubane derivative of AVPI is described. The trishomocubane skeleton has previously been elucidated by this research group.[156,168,169] The only quaternary carbon in the structure of the trishomocubane derivative is C-4'. This signal is therefore assigned to the carbon at 69.7 ppm since the other fully substituted carbon signals were present in the carbonyl region of the spectrum (Spectrum 45). From the ^{13}C APT spectrum, other CH_2 signals observed appear at 32.7, 31.9 and 24.1 ppm. The signal at 24.1 ppm was already assigned to C-19 from the isoleucine residue, therefore the remaining signals were assigned to C-7' and/or C-11' from the trishomocubane cage moiety. These carbon signals correspond to methylene protons at 1.35 ppm and 1.31 ppm in the HSQC spectrum (Spectrum 47). Splitting of these signals is observed with the other protons at 1.26 ppm and 1.23 ppm respectively.

The overlapping signals of H-7' and H-11' shows HMBC correlations with a carbon signals at 53.4 and 52.2 ppm (Spectrum 48). Looking at the structure, only two methine proton signals can appear at a high frequency due to their chemical environment, namely H-3' and H-5'. One would expect H-3' to appear at a higher frequency due to the through-space deshielding effect contributed by the C-12 carbonyl while H-5' experiences a smaller deshielding effect from the C-6 carbonyl. Based on this, the resonance at 2.58 ppm was assigned to H-3' and the other at 2.36 ppm to H-5'. Further confirmation of these assignments was obtained from the ROESY spectrum (Spectrum 50). The H-7' doublets display a ROESY correlation to two overlapping methine protons at 2.01 ppm and 2.03 ppm which could be assigned to either H-6' or H-8'. The proton resonances at 2.01 ppm show a ROESY interaction to H-5' and another signal at 2.08 ppm while the second resonance at 2.03 ppm shows a ROESY correlation to a signal at 2.40 ppm and another at 2.48 ppm. The resonance at 2.01 ppm was assigned to H-6' while that at 2.08 ppm was assigned to H-2'. Therefore, the signal at 2.03 ppm was assigned to H-8' by elimination. H-8' displays a ROESY interaction with 2.09 ppm and 2.48 ppm which could be either H-1' or H-9'. H-3' shows a ROESY correlation with a signal at 2.07 ppm which was assigned to H-10' while a signal at 2.48 ppm mentioned earlier shows ROESY to H-8', H-11' and another signal at 2.09 ppm. Therefore 2.48 ppm was assigned to H-9', while that at 2.09 ppm was assigned to H-1'. H-1' shows ROESY correlations with the overlapping signals of H-7' and H-11' between 1.20 ppm and 1.38 ppm. H-6' and H-8' shows ROESY correlations to a proton at 1.35 ppm which was assigned to H-7'. By elimination, H-11' was assigned to 1.31 ppm. As mentioned

earlier, these protons exhibits splitting patterns and hence the second proton signal of H-11' was observed at 1.23 ppm using the HSQC spectrum. Similarly, the second proton of H-7' was assigned to 1.25 ppm. The methine proton at 2.28 ppm was assigned to H-2 by elimination. The relative trend observed for the trishomocubane carbon and proton chemical shifts are similar to previous studies.[156,168,169] The corresponding carbon signals of all assigned protons of the trishomocubane AVPI derivative was assigned using the HSQC spectrum and are presented in Table 8.

Table 8: ^{1}H and ^{13}C NMR data for peptide 6 (Tris)

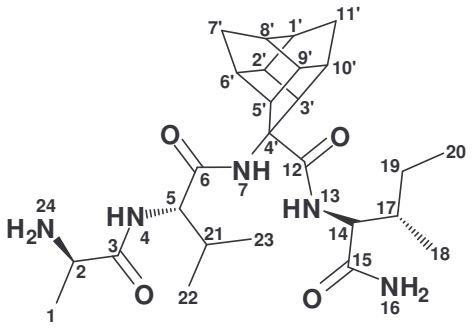

Peptide 6: Tris			
Atom	**$\delta^{1}H^{a,b}$**	***J*(Hz)**	**$\delta^{13}C^{a,b}$**
1	0.93		19.4
2	2.28		43.9
3	-		171.2
4	8.13/8.15		-
5	4.20		57.8
6	-		172.8
7	7.36		-
12	-		172.9
13	7.36		-
14	4.10		56.7
15	-		171.6
16	7.00		-
17	1.80		36.9
18	0.88		15.6
19a	1.10	[c]	24.2
19b	1.40	[c]	24.2
20	0.88		11.2
21	1.98-2.05		30.5
22	0.90		17.9
23	0.91		18.3
24	7.86/7.88		-

Table 8 continued

1'	2.09		41.8
2'	2.08		42.7
3'	2.58		52.2
4'	-		69.7
5'	2.36		53.4
6'	2.01		43.0
7'a	1.35	9.24	32.7
7'b	1.25	9.84	32.7
8'	2.03		42.1
9'	2.48		53.1
10'	2.07		42.7
11'a	1.31	10.26	32.0
11'b	1.23	10.38	32.0

[a] 600 MHz for ^{1}H and 150 MHz for ^{13}C

[b] Solvent $(CD_3)_2SO_2$

[c] Due to overlapping signals the respective coupling constants could not be determined

CHAPTER 4

Biological Screening of Smac Peptidomimetics

Biological screening was performed at the Department of Biochemistry, UKZN (Westville campus). All compounds tested were pure and stable at the time of analysis. A detailed description has been included in Chapter 6.

4.1 Cytotoxicity screening

4.1.1 Introduction

Cytotoxicity[xxvi] is the term coined to describe the degree to which a substance is poisonous to living cells. *In vitro* cytotoxicity assays are therefore widely used in the pharmaceutical sector for preliminary screening of potential therapeutic agents. Most commonly, anti-cancer compounds that are very selectively cytotoxic towards cancer cells are desired as potential drug leads. This technique can however also be used in many other sectors including the screening of water samples for toxins and the clinical diagnosis of food allergies.[170,171]

To date, a variety of assays have been developed to carry out cytotoxicity studies and these are based on three basic parameters, namely; cell membrane integrity, metabolic activity and cell numbers.[172] One of the most common methods employed to measure cell viability involves assessing the integrity of cell membranes using various dyes that include trypan blue and propidium iodide. The cell membrane is important in cellular structure as it forms a functional barrier around the cell and selectively allows substances across it *via* transporters, receptors and secretion pathways. The integrity of the cell membrane becomes compromised after exposure to toxic substances and hence the dye is able to "leak" across the membrane and stain intracellular components. In contrast, the dyes are unable to permeate the uncompromised membrane of healthy cells to stain intracellular components. This resulted in the term "dye exclusion" being used to describe dye-based cytotoxic assays.[173]

[xxvi] Cytotoxicity refers to the degree by which a substance is able to prevent cell proliferation and induce cell death.

Membrane integrity can also be assessed by monitoring the extracellular presence of lactate dehydrogensae (LDH)[xxvii]. This enzyme is usually present in the cytosol[xxviii] and can only be detected extracellularly if the cell membrane becomes damaged. The LDH enzyme is quantified *via* a two-step reaction.[174]

- Step one involves the catalytic conversion of lactate to pyruvate by LDH. During this reaction nicotinamide adenine dinucleotide (NAD^+)[xxix] is simultaneously reduced to dihydronicotinamide adenine dinucleotide ($NADH/H^+$).

- In step two, H/H^+ is transferred from $NADH/H^+$ to the tetrazolium salt 2-(4-iodophenyl)-3-(4-nitrophenyl)-5-phenyltetrazolium chloride (INT), which upon reduction yields a red formazan product which is solubilised and quantified spectrophotometrically.[174]

Some assays are based on the measurement of cellular metabolic activity. A reduction of the metabolic activity provides the earliest indication of cellular damage. Metabolic activity can be assessed by measuring either cellular adenosine triphosphate (ATP)[xxx] levels or mitochondrial activity *via* MTS/MTT[xxxi] reduction.[175] The first tetrazolium salt, 2,3,5-Triphenyl tetrazolium chloride (TCC) was presented by von Peachmann and Runge in 1894.[175] Since then a host of other tetrazolium-based salts have been synthesized and evaluated. The MTT assay was first described by Mosmann almost a century later in 1983 and is today a widely used and reliable technique that enables the determination of cell viability and proliferation. It is routinely employed to determine the cytotoxicity by *in vitro*

[xxvii] LDH is an enzyme which catalyses the conversion of pyruvate to lactate in the absence of oxygen and yields energy for cellular processes.

[xxviii] The cytosol is the intracellular fluid or cytoplasmic matrix found inside cells. In eukaryotes this liquid is separated by cell membranes from the contents of the organelles suspended in the cytosol. The entire contents of a eukaryotic cell, minus the contents of the cell nucleus, are referred to as the cytoplasm.

[xxix] NAD is a co-enzyme involved in the electron transport chain of cellular respiration and plays a crucial role in energy production in the cell.

[xxx] ATP is a chemical compound found in living organisms that releases energy for cellular processes.

[xxxi] MTS/MTT are tetrazolium salt based colorimetric cytotoxic assays.

testing of potential drug candidates. This assay involves the reduction of a yellow tetrazolium salt, [3-(4, 5-dimethylthiazolyl-2)-2, 5-diphenyltetrazolium bromide] (MTT) by metabolically active cells. Mitochondrial dehydrogenase enzymes generate cofactors NADH and NADPH that carry out the reduction (Figure 59). This reduction yields intracellular purple formazan crystals in healthy cells and is solubilised prior to spectrophotometric quantification.[176]

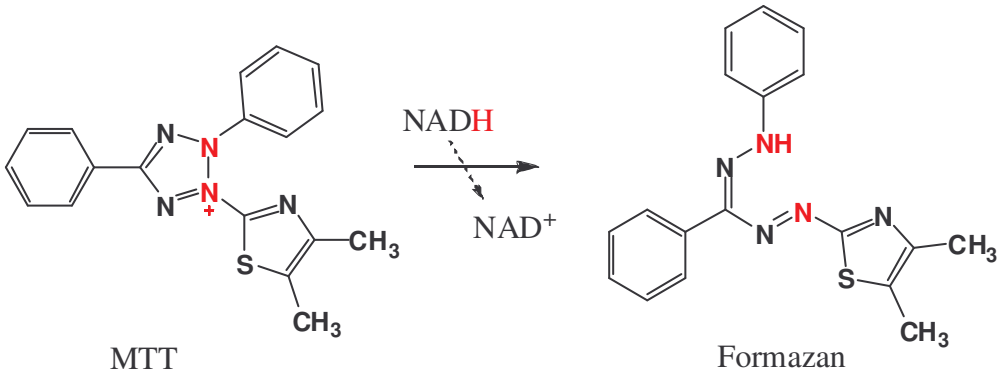

Figure 59: Reduction of MTT to formazan by NADH.

The MTS reduction assay has been previously used to determine the IC_{50} concentrations of the potential anticancer Smac mimetics by Oost *et al*. The MTT assay therefore forms an integral part of this investigation as it is essentially mechanistically similar to the MTS assay and is the in-house assay currently used in our lab.[125]

4.1.2 Cell line selection

Three mammalian cell lines were used for preliminary biological screening of the putative anticancer Smac mimetics prepared in this study. Namely, the MDBK (Madin-Darby bovine epithelial kidney), MCF-7 and MDA MB 231 cell lines. Of those, the MDBK is a healthy, non-tumoral epithelial cell line derived from a cow's kidney. The MCF-7 originates from a breast carcinoma in a 69 year old Caucasian female who underwent two mastectomies.[177] It was derived from a pleural effusion[xxxii] found after the removal of the tumours in her chest wall in 1970. MDA MB 231 is an adherent, metastatic cell line which was also initially

[xxxii] A pleural effusion is an accumulation of fluid between the layers of the membrane that lines the lungs and chest cavity.

derived from a pleural effusion of a 51 year old Caucasian female.[177-179] The MDA MB 231 cells have been found to be highly invasive, oestrogen receptor negative and to lack the p53 tumour suppressor protein.[177-179]

To determine the most appropriate cell for our current study in terms of susceptibility to novel anticancer Smac mimetics, all lines were screened against the *N*-terminal Smac tetrapeptide AVPI. The data suggests that the MDA-MB-231 cell line is the most suitable for such a purpose. This observation confirms the findings of a recent study by Tamm *et al.*[180] Thus far, most of the studies that have centred on biological screening of potential anticancer Smac mimetics have used the MDA-MB-231 cell line. It has been shown to be one of the most sensitive human cancer cell lines to the BIR3 inhibitors and contains highly over-expressed amounts of the target XIAP.[125] Given this backdrop the MDA-MB-231 cell line was selected for the present investigation. In addition, an insight into the effect of AVPI on a non-cancerous cell line is also presented in this study.

4.1.3 Results and discussion

In order to assess and compare the cytotoxicity data of putative AVPI peptidomimetics it was deemed necessary that a standardised and consistent cytotoxicity screening protocol be implemented for these measurements. To this end the following parameters were optimised:

a. The seeding cell density of individual cell lines

b. The solubilisation time of formazan crystals

An example of such an optimisation study for the MDA MB 231 cell line is presented in Figure 60. Assessing the lowest standard deviation across five replicates, the data indicates that a seeding cell density of 50 000 cells *per* well in combination with a 120 minute solubilisation time was optimal. These parameters were strictly adhered to when performing further cytotoxicity studies on the MDA MB 231 cell line. Similarly the MTT protocol was optimised for the MDBK and MCF-7 cell lines. Coincidentally identical optimal conditions to that of the MDA MB 231 cell line also prevailed for the latter two cell lines (data not shown).

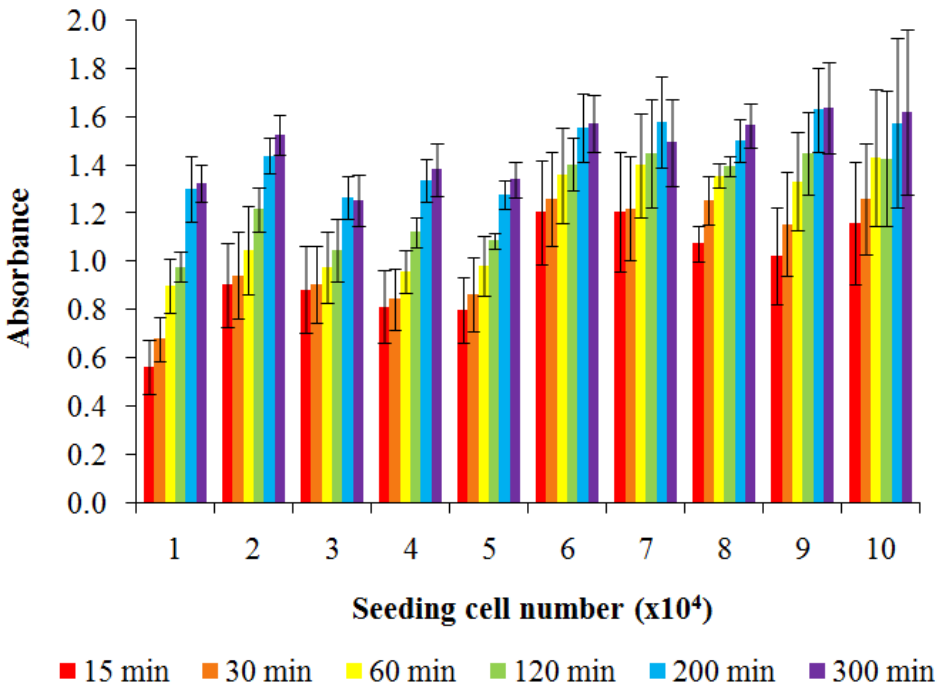

Figure 60: Optimisation of the seeding cell number and solubilisation time for MTT assay using the MDA MB 231 cell line. All standard deviations were obtained across 5 replicates.

To assess the integrity of the MTT protocol used, it was necessary to test a positive control. Since cadmium chloride ($CdCl_2$) is economical and has been shown previously to invoke a cytotoxic effect on the MDA MB 231 cell line, it was selected as the positive cytotoxic-inducing control.[181,182] All concentrations of $CdCl_2$ (Figure 61) were found to induce statistically different cytotoxicity in comparison to the negative control ($p < 0.001$) as well as each other until saturation was reached at 1.6 ppm ($p > 0.05$). The experimental IC_{50}[xxxiii] value of 1.3 parts *per* million (ppm) or 5.98 µM closely correlates to the $CdCl_2$ IC_{50} value of 5 µM that was reported by Sirchia *et al.* in 2008.[182] Statistically the variation from the reported $CdCl_2$ IC_{50} value was found to be insignificant ($p > 0.05$) and the method was therefore considered reliable.

[xxxiii] IC_{50} is the half maximal inhibitory concentration of a drug. It is a measure of the effectiveness of a compound in inhibiting a biological or biochemical function.

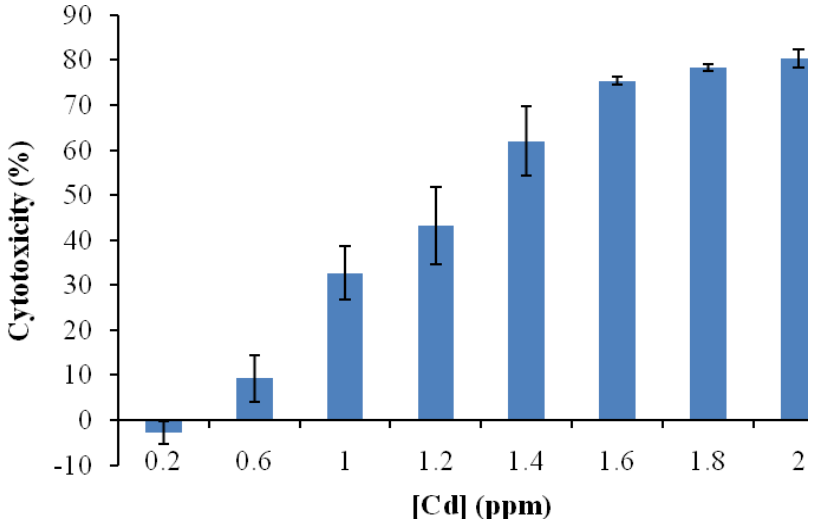

Figure 61: Cytotoxic effect of cadmium ($CdCl_2$) on MDA MB 231 cell line. All standard deviations were obtained across 5 replicates.

The MDBK cells were slightly more sensitive to cadmium induced cytotoxicity than MCF-7 cells. The half maximal inhibitory concentration of $CdCl_2$ on the MCF-7 and MDBK cell lines corresponded to IC_{50} values of 1.4 ppm and 1 ppm respectively (Figure 62). All concentrations of $CdCl_2$ were found to exhibit a cytotoxic effect on both cell lines, all of which were found to be statistically different to the negative control ($p < 0.001$).

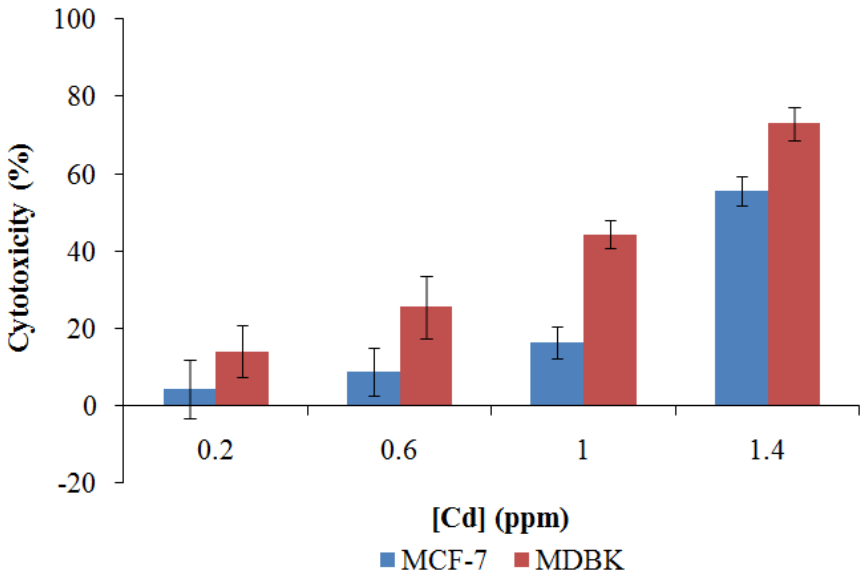

Figure 62: Cytotoxic effect of cadmium on MCF-7 and MDBK cell lines. All standard deviations were obtained across 5 replicates.

No cytotoxicity was displayed when both the MCF-7 and MDBK cell lines were exposed to the *N*-terminal Smac tetrapeptide AVPI (Figure 63). Although no such study was previously performed on the MDBK cell line, the insensitivity of the MCF-7 cell line to Smac mimetics up to 50 µM was also observed by Oost *et al.*[125] The same study also demonstrated that Smac mimetics were incapable of eliciting a cytotoxic effect on many other cell lines.[125]

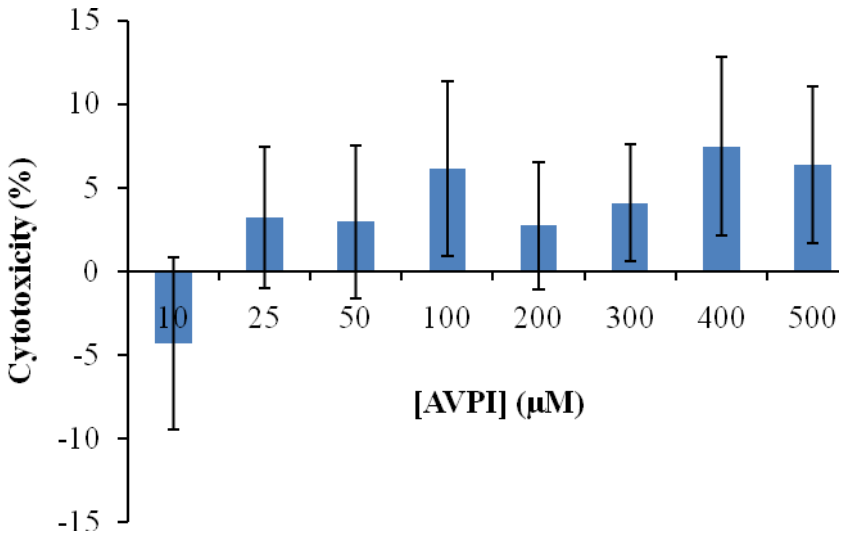

Figure 63: Assessment of the cytotoxicity of AVPI on the MCF-7 cell line. All standard deviations were obtained across 5 replicates.

The MCF-7 cell line was insensitive to AVPI up to a concentration of 500 µM (Figure 63). The cytotoxic effect of each drug concentration was not statistically different from each other or to that of the negative control ($p > 0.05$). Thus it was concluded that the MCF-7 cell line was not suitable for the purposes of this study. A similar result was obtained for the MDBK cell line (Figure 64) and it must be highlighted that this being a healthy cell line does not exhibit elevated levels of XIAP.

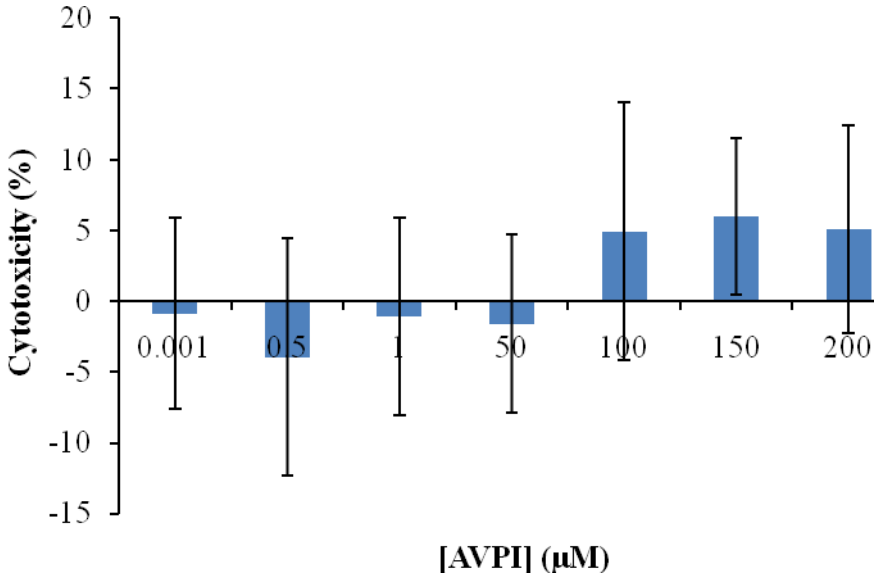

Figure 64: Assessment of the cytotoxicity of AVPI on the MDBK cell line. All standard deviations were obtained across 5 replicates.

On the contrary a cytotoxic effect was observed when the MDA MB 231 cell line was exposed for 48 hours to increasing concentrations of AVPI (Figure 65).

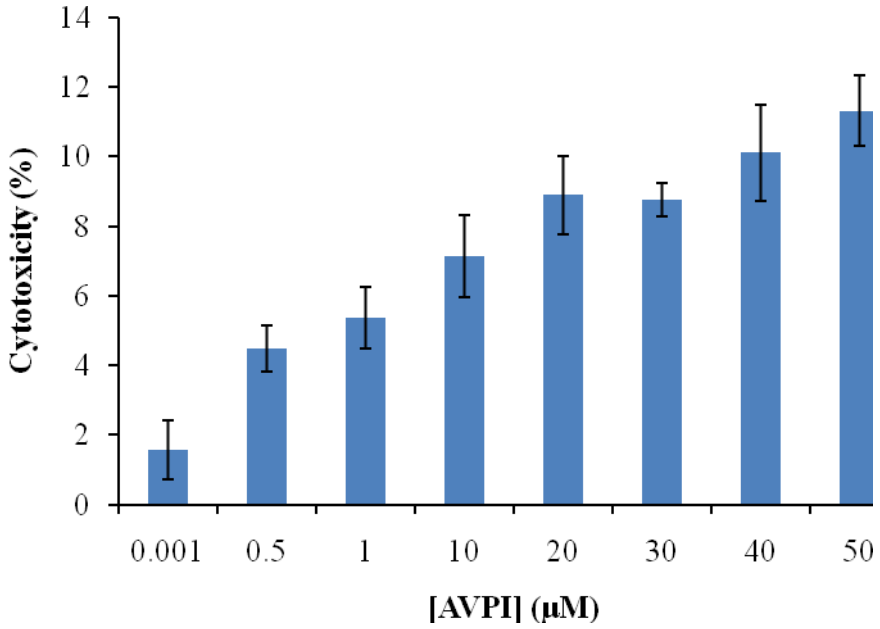

Figure 65: Assessment of the cytotoxicity of AVPI on the MDA MB 231 cell line. All standard deviations were obtained across 5 replicates.

The percentage cytotoxicity displayed at all concentrations of AVPI is statistically different to that of the negative control ($p < 0.001$). Interestingly the cytotoxicity exhibited between 0.001 μM to 20 μM are statistically different to one another ($p < 0.01$), whilst those between 20 μM and 50 μM are statistically insignificant ($p > 0.05$) thereby demonstrating saturation.

Huang *et al.* reported a maximum cell death of 20 % on exposure to 50 μM AVPI for 48 hours using ATPLite[xxxiv] assay. Moreover, the MDA MB 231 cell line was also shown to be one of the most susceptible lines to Smac mimetics, including AVPI.[125] Under similar growth and exposure conditions, the maximum cytotoxicity *via* the MTT assay was found to be 11.657 % ± 1.120 at 50 μM which is slightly lower than that reported by Huang *et al*. This discrepancy could be attributed to the different experimental assays being used and could possibly suggest that the MTT assay is slightly less sensitive to detect cytotoxicity than the ATPlite assay used by Huang.[183] Hereafter, all other putative Smac mimetics prepared in this study were assessed for their cytotoxic effect over 48 hours on the MDA MB 231 cell line and the data is summarised in Table 9.

[xxxiv] ATPlite is an adenosine triphosphate monitoring system based on luciferase. It is a luminescence assay used to quantitatively evaluate cell proliferation and cytotoxicity.

Table 9: Summary of toxicity to the MDA MB 231 cell line on exposure to novel Smac mimetics as determined by the MTT assay

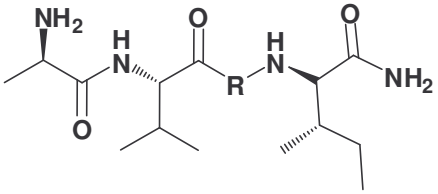

Compound	Max. Cytotoxicity (%) ± SD	Drug conc. relating to max. cytotoxicity (μM)	clogP[c]
R = 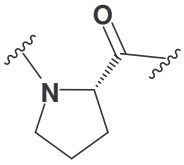	11.657 % ± 1.120	50	0.5 ± 0.71
R = 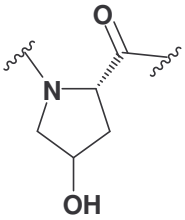	6.796 ± 3.673[a]	40	-0.77 ± 0.71
R = 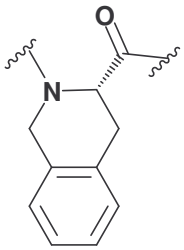	17.023 ± 1.526[a]	100	2.25 ± 0.74
R = 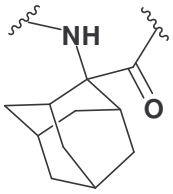	33.845 ± 2.904	200	2.11 ± 0.65
R = 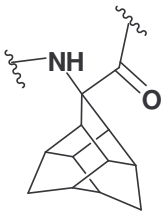	73.969 ± 3.939	400	1.26 ± 0.66

R = 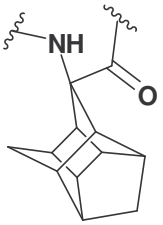	30.460 ± 1.473	400	1.26 ± 0.66
R = 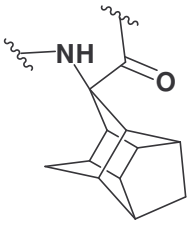	40.553 ± 1.143	200	1.26 ± 0.66
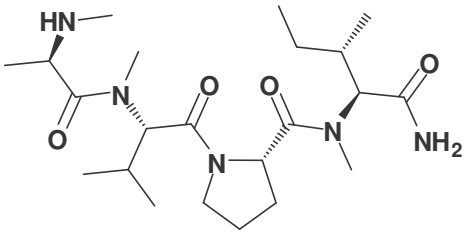	11.918 ± 1.159[a]	30	0.70 ± 0.71
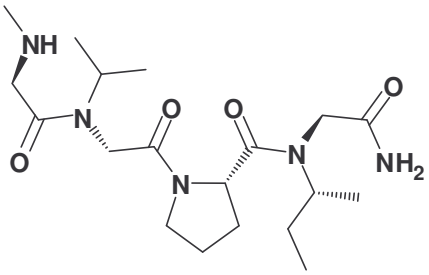	ND[b]	ND	-0.34 ± 0.71

[a] Results obtained did not follow the expected trend of increasing cytotoxicity with an increase in drug concentration and 50% decrease in cell growth could not be obtained, therefore the maximum percentage cytotoxicity and relative concentration obtained is stated.

[b] The maximum percentage kill is not statistically different from the control ($p > 0.05$) therefore result not determinable.

[c] Partition coefficients were calculated using ACD/ChemSketch (Freeware version 12.01), Advanced Chemistry Development Inc.

Interestingly, the most active compounds were found to be those including cage moieties. The trishomocubane AVPI derivative displayed the highest cytotoxicity, followed by the PCU2, adamantane and PCU1 derivatives respectively (Figure 66, Figure 67, Figure 68, and Figure 69). Thus far, the inherent poor cell permeability of Smac peptides has been identified as a major shortcoming[126] Bearing this mind, the novel Smac mimetics that were designed in this study have taken "Lipinski's rule of 5" into consideration.[124] All compounds prepared in this study possess fewer than five H-bond donors, less than ten H-bond acceptors, have a molecular weight of less than 500 g mol^{-1} and a calculated logP of less than five.[124] A

tentative explanation for the enhanced activity of the cage derivatives over our other designs, could possibly lie in their cage moieties that may significantly increase their cell permeability. This is also supported by the suggestion of Brookes *et al*. that the drug affinity for receptors could be improved if they possess a cage moiety.[150] This was later confirmed in an extensive review by Geldenhuys *et al*.[151]

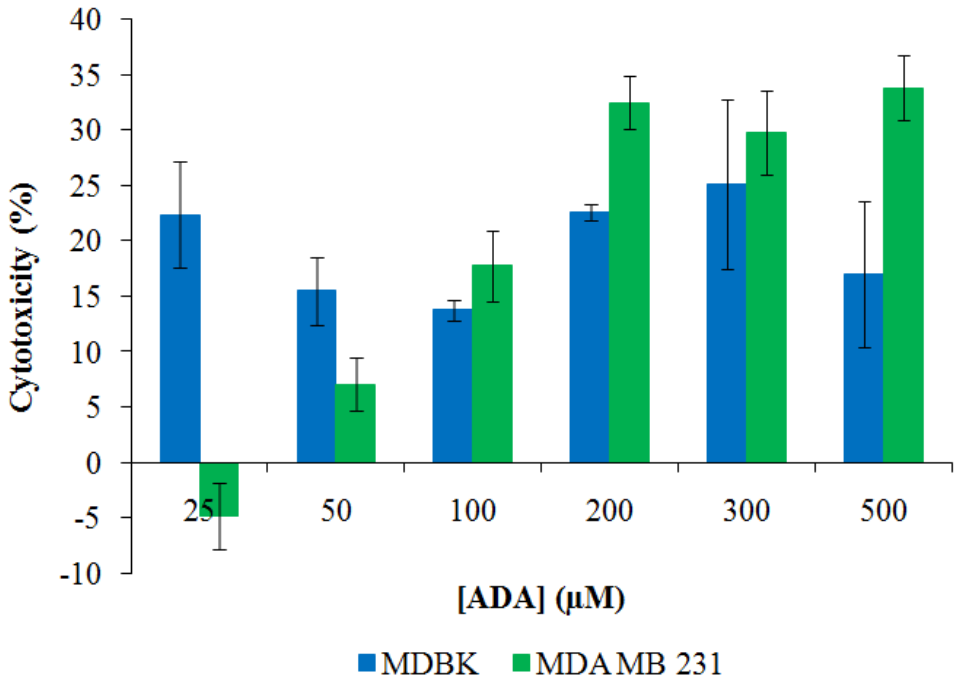

Figure 66: Assessment of the cytotoxicity of adamantane derivative on the MDBK and MDA MB 231 cell line. All standard deviations were obtained across 5 replicates.

Integration of CD data with the respective cytotoxicity of the trishomocubane derivative may explain the higher efficacy of the tris derivative in comparison to the other cage derivatives (Figure 67). The CD measurements reveal that the trishomocubane derivative has a very similar conformation to that of the AVPI tetrapeptide which could also signify higher binding affinity to the BIR2 and BIR3 domains of XIAP than the other cage derivatives. Although they fall out of the scope of the present study, further in-depth studies detailing drug cell permeability and binding affinities could provide concrete evidence to substantiate these theories.

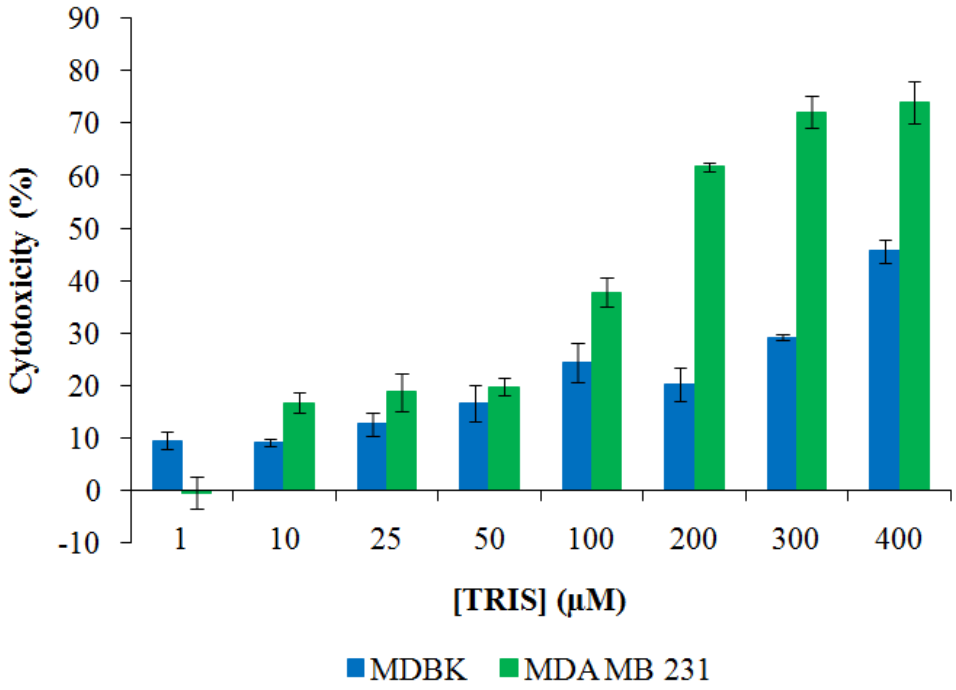

Figure 67: Assessment of the cytotoxicity of trishomocubane derivative on the MDBK and MDA MB 231 cell line. All standard deviations were obtained across 5 replicates.

Comparison of the efficacy of the two PCU diastereomers suggests that stereochemistry does play a role on the effectiveness of these compounds (Figure 68 and Figure 69). PCU2 was found to exhibit maximum cytotoxicity of 40.553 % ± 1.143 at 200 µM while PCU1 exhibited 30.460 % ± 1.473 at 400 µM. The difference could possibly be attributed to the relative pharmacophore properties of each to the target domains within XIAP. In essence PCU2 could have a more favourable conformation to fit into the XIAP binding pocket than PCU1. Once again determining the binding affinities of each would enable this hypothesis to be substantiated.

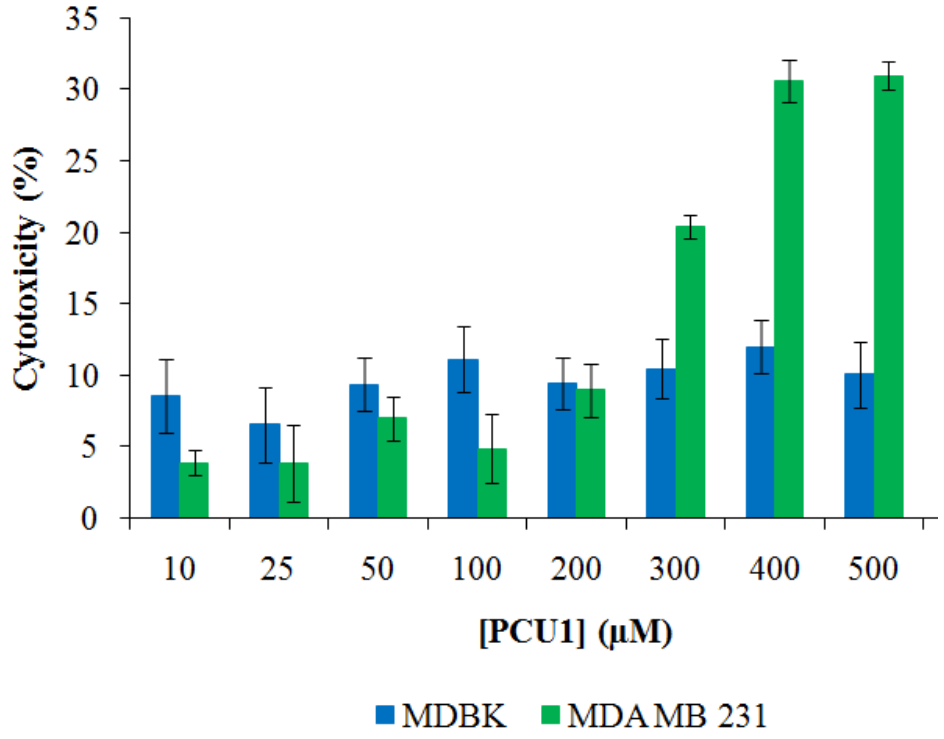

Figure 68: Assessment of the cytotoxicity of PCU1 derivative on the MDBK and MDA MB 231 cell line. All standard deviations were obtained across 5 replicates.

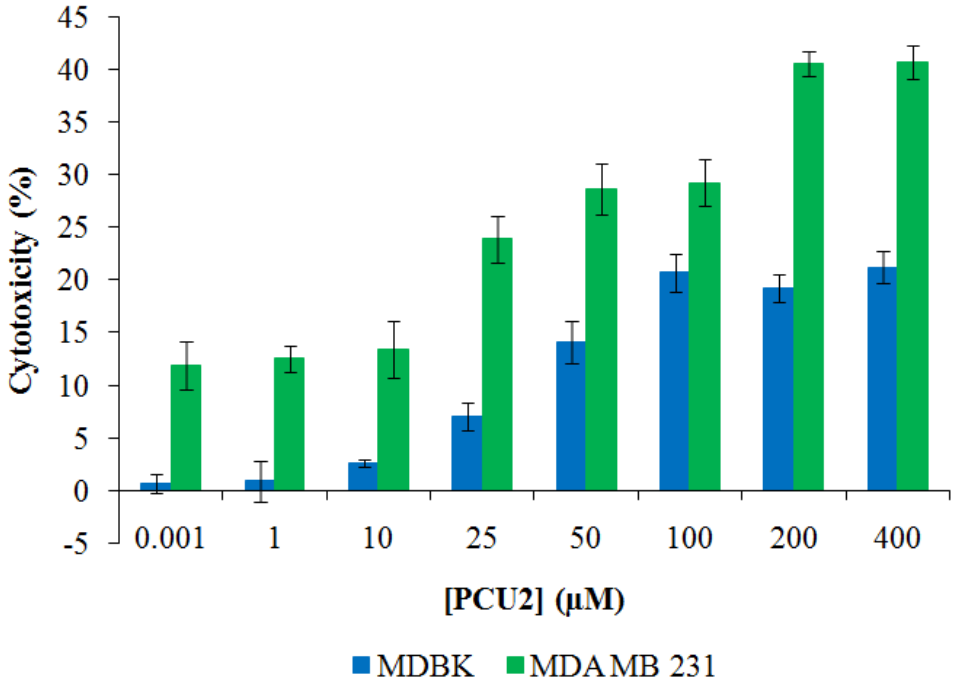

Figure 69: Assessment of the cytotoxicity of PCU2 derivative on the MDBK and MDA MB 231 cell line. All standard deviations were obtained across 5 replicates.

The most potent AVPI derivatives namely, the cage containing derivatives were thereafter assessed for their cytotoxic effects on the healthy MDBK cell line. The cytotoxic effect of the adamantane derivative on the MDBK cell line showed no real correlation between drug concentration and cytotoxicity (Figure 66). In addition, statistically insignificant differences ($p > 0.05$) between each concentration and its relative cytotoxicity were observed. An undesired property of the drug is its greater toxicity to healthy cells than cancerous cells at low concentrations (25-100 μM). However, the trishomocubane derivative (Figure 67) shows a similar trend for both cell lines with a reduced maximum cytotoxicity in the healthy line. The trishomocubane derivative showed a significant decrease in maximum cytotoxicity from 73.969 % ± 3.939 at 400 μM in the MBA MB 231 cell line to 49.584 % ± 2.033 at 500 μM in the MDBK line. This compound exhibited higher cytotoxicity against the malignant MDA MB 231 cell line. However, this desirable trend is associated with high concentrations which are undesirable for pharmaceutical applications. At low concentrations (1–10 μM) a greater cytotoxic effect is observed on the healthy line than cancer line which also seems to suggest that this compound is unsuitable for pharmaceutical application.

On comparison of the effect of the PCU1 derivative on healthy and cancer cell lines (Figure 68), it is noted that increasing drug concentrations does not correlate to an increasing cytotoxicity trend for the MDBK line. In fact the differences in the cytotoxicity observed for increasing concentrations are statistically insignificant ($p > 0.05$).

The PCU2 derivative (Figure 69) exhibited a reduction in maximum cytotoxicity from 40.553 % ± 1.143 at 200 μM on the MDA MB 231 line to 21.177 % ± 1.527 at 200 μM on the MDBK line. The most attractive character of this compound is its relatively low cytotoxic effect on the healthy cell line compared to the cancer cell line at low concentrations (0.001-25 μM). Although the maximum percent cytotoxicity of PCU2 is not as high as the trishomocubane derivative, it seems the most promising candidate from the series of potential anticancer peptides prepared in this study.

The reduction of the maximum cytotoxic effect observed in the healthy cells, seemingly suggests that PCU2 and trishomocubane derivatives are more selective towards promoting apoptosis in cancer cells rather than healthy ones. It has been shown that cancer cells possess elevated levels of XIAP[76,77] and this consequently disrupts cellular equilibrium, preventing apoptosis from occurring in malignant cells and therefore promoting proliferation of cancer

cells. When the cancer cells are exposed to these Smac mimetics, it results in the excess XIAP being antagonised and the cellular equilibrium being restored. If however a large excess of the drug is used, it results in the majority of XIAP being inhibited and therefore leads to accelerated caspase activation and consequent immediate apoptotic cell death. The acute result corresponds to a higher percentage of cell death by MTT assay.

In healthy cells, an equilibrium between Smac/DIABLO, XIAP and the caspases is established. Apoptosis without addition of the Smac mimetics will occur naturally in these cells when it is triggered. When these cells are exposed to Smac mimetics, the drug as well as Smac/DIABLO would bind to available XIAP. This results in fewer caspases being inhibited than normal. The net effect in this scenario is increased caspase activation which results in increased cytotoxicity. The differences in cytotoxicity data acquired for the healthy cell line and the malignant cell line could also be due to the variation in cell line origin, namely, bovine verses human respectively.

A limitation of the MTT assay lies in the underestimation of the extent to which apoptosis has occurred as well as discrepancies in the timing of the exact apoptotic stage. Since the initial stages of apoptosis have not been shown to compromise membrane integrity or disrupt mitochondrial activity, this assay was found to be unsuitable to detect the early stages of apoptosis.[184] It is therefore necessary to employ alternate techniques before conclusive results can be obtained. Since advances in understanding the physiological aspects of apoptosis have been made, methods have been established to identify various apoptotic parameters. Flow cytometric analysis is currently underway to confirm whether the cell death observed did in fact occur as a result of apoptosis.

On comparison of our data to other recent studies it is noted that the efficacy of this series of Smac derivatives is far lower than the current leads which exhibit nanomolar IC_{50}'s.[76,125] The high concentrations required for cell death could possibly be attributed to the lower cell permeability of the compounds. A future prospect should involve cell permeability studies and consequent modification of the compounds by linkage to a cell penetrating peptide (cpp) with an enzyme cleavable linker. One strategy could involve attachment of the HIV Tat_{49-57} protein sequence RKKRRQRRR[185,186] to the Smac mimetic by a covalent disulphide linkage with cysteine residues. Polyarginies (R5-8) have previously been directly attached to AVPI

and have shown slight improvements in efficacy.[121] However, the effect of the attachment of cpp on the active drug which may reduce its binding affinity to the XIAP binding pocket must be established in such a study. The attractiveness of the disulphide bond in drug delivery systems is its relative stability in plasma, but more importantly is its reversibility. The high redox potential difference existing between the oxidising extracellular space and reducing intracellular space of cells is very attractive.[187] This is because in oxidising environments, the covalent disulphide linkage is formed and is reversibly cleaved in the presence of reducing agents. This therefore allows controlled cleavage and release of active Smac mimetics upon cell entry.

Another important aspect to be explored would be to assess the binding affinities of this series of Smac peptidomimetics directly to the BIR2/BIR3 domain of XIAP. This will give an indication of the suitability of the drug design eliminating cell impermeability problems. This will enable conclusions to be drawn about the effectiveness of the drug conformations that would be independent of whether or not the drug penetrates the cell membrane. Thus in a more structured approach, it would be possible to optimise the drug design to best fit the binding site and thereafter attach the cpp and perform apoptotic studies.

Studies have shown that Smac mimetics can act as single agents to inhibit cell proliferation and promote apoptosis.[76] Smac mimetics have also been shown to enhance the apoptotic affect induced by chemotherapeutic agents.[121,127] They have been found to sensitize cancer cells to many anticancer agents. It may also be suggested that combination drug trials using agents such as Cisplatin and Taxol could be performed with our Smac mimetics.

Since the discovery of the Smac protein in 2000, one Smac mimetic has reached clinical development while a few other Smac mimetics are currently in advanced preclinical stages.[76] There is considerable interest in the design of Smac peptidomimetics to target XIAP. Targeting protein-protein interactions is not an easy task and it is predicted that potent, cell-permeable Smac mimetics with high *in vivo* stability may have the therapeutic potential to be developed as an entirely new class of anticancer drugs, one which overcomes the apoptotic resistance of cells.

CHAPTER 5

Conclusion

The aims of this project were successfully achieved and insight into the multidisciplinary design and development of potential anticancer drugs was gained. Six novel Smac peptidomimetics based on the *N*-terminal tetrapeptide motif AVPI were synthesized and characterized by high resolution mass spectrometry and NMR.

This involved multi-step synthesis whereby Fmoc adamantane and trishomocubane amino acids were successfully synthesized and incorporated into novel Smac tetrapeptides. Hands on experience in both manual peptide synthesis and automated microwave assisted SPPS was gained. Experience was also gained in peptide purification using semi-preparative HPLC as well as characterisation by LC/MS. Complete structural analysis of the synthetic products was also performed and experience in 2-D NMR elucidation was therefore achieved.

The potential drug candidates were thereafter assessed for anticancer properties/cytotoxic effect by the MTT assay on the MDA-MB-231 and MDBK cell lines. Experience was therefore gained in tissue culture involving growth and maintenance of cell lines, as well as testing optimisation and basic statistical calculations.

The major shortfall of the model tetrapeptide AVPI has been shown to be its low cell permeability. Our strategies which included *N*-methylation, the use of a peptoid and proline substitution by TIQ, hydroxyproline, and various "cage" amino acids attempted to increase cell permeability while maintaining the "turn" induced by proline. These modifications were carried out in accordance with information obtained from previous studies, namely, the inclusion of a rigid core and a general "U" conformation which are necessary for protein interaction.[188] It was hoped that the replacement of proline with lipophilic beta turn inducers would satisfy that both these requirements and that it would lead to a substantial increase in efficacy. From the results obtained, it can be concluded that the derivatives containing cage moieties show a greater efficacy than the other designs in this study. The PCU2 derivative also exhibited selectivity towards the cancer cell line at low concentrations (0.001 - 23 μM) and is therefore the most promising derivative from this series of Smac mimetics for potential

pharmaceutical application. It therefore appears that the position (conformational effect) of the lipophilic group on the "AVPI" peptide is of utmost importance and subsequent studies should focus on that. By doing so firm conclusions about the structural activity relationship, the cell permeability and binding affinities can be drawn and hence design modifications can be made to improve the efficacy of the potential drugs.

CHAPTER 6

Experimental

6.1 Materials and Equipment

6.1.1 Chemistry

The NMR spectra were recorded on either a Bruker AVANCE III 400 or a 600 MHz spectrometer fitted with a 5mm BBOz probe. The cage containing and *N*-methylated peptide sequences were synthesised with a Discovery CEM Liberty automated microwave peptide synthesizer. HPLC analysis was performed on an Agilent 1100 Series Liquid Chromatograph using a UV/VIS detector (190 - 210 nm) and an Ace 5 (150 x 4.6 mm) C-18 reverse phase column. High resolution mass spectra were determined with a Bruker ESI-QTOF mass spectrometer in positive mode. The final peptides were purified on a Younglin ACME 9000 instrument using a C-18 reverse phase semi-preparative HPLC column (Ace 5, 150 x 21.2 mm) with solvent A (0.1 % FA in H_2O) and solvent B (0.1 % FA in CH_3CN) as eluents. Purified compounds were lyophilized using a VirTis benchtop K freeze dryer. CD spectra were obtained using a Jasco J-810 spectropolarimeter (1 cm cell, 163 – 900 nm lamp, c = 0.1 mmol, 25 °C).

6.1.2 Biochemistry

Dulbecco's minimum essential medium (DMEM) containing 4.5 g L^{-1} glucose and L-glutamine, RPMI 1640 with 25 mM 2-[4-(2-hydroxyethyl)-1-piperazinyl] ethanesulfonic acid (HEPES) and L-glutamine, 10 000 µg mL^{-1} penicillin/streptomycin mixture, trypsin/versene mixture and phosphate buffer saline (PBS) were purchased from Lonza. Heat-inactivated foetal bovine serum (FBS) was obtained from Invitrogen. Tissue culture treated flasks (25 cm^2 and 75 cm^2) were purchased from Corning Costar. Cellstar 96-well, flat bottom tissue culture plates were purchased from Greiner Bio-one. Cryopreservation of cells was performed using a Nalgene Cryo 1 °C freezing container using 2 mL cryovials obtained from Greiner Bio-one. A Bright-Line hemacytometer from Hausser Scientific and an Olympus CKX41 microscope was used for cell counting and analysis. Cytotoxicity was assessed using the CellTiter 96 non-radioactive cell proliferation assay from Promega and absorbance

readings for the MTT assay was performed using an Automated Microplate Reader (ELx800) from Bio-Tek Instruments.

6.2 General procedure for swelling and deprotecting the rink amide resin[135]

The rink amide resin (0.17 g; 0.6 mmol g^{-1}) was pre-swollen in dry DCM for 45 minutes in a reaction vessel containing a sintered glass bottom. The resin was then washed thoroughly with DMF and treated with 20 % piperidine in DMF solution. A positive ninhydrin test was then observed. The resin was then washed with 3 x DMF followed by 3 x DCM.

6.3 The ninhydrin test[113,189]

The ninhydrin test was used to detect complete deprotection of Fmoc-protected amino acids as well as monitor the coupling of consecutive amino acids. To carry out this test three solutions were prepared.

Solution 1: A mass of 16.55 g potassium cyanide (KCN) was dissolved in 25 mL of distilled water. 1 mL of this solution was then made up to 50 mL with pyridine.

Solution 2: A mass of 1.04 g ninhydrin was dissolved in 20 mL n-butanol

Solution 3: A mass of 40.21 g phenol was dissolved in 20 mL n-butanol

Upon deprotection or coupling of amino acids, a few resin beads were placed in a pill vial and 3 drops of each solution was added. The vial was then heated in an oven for 5 minutes at 100 °C. The development of a blue/purple colour (positive result) indicated the presence of a primary amine *i.e.* complete deprotection. If no colour change was observed (negative result), it indicated the presence of a secondary amine *i.e.* complete coupling.

6.4 The chloranil test[113,189]

The chloranil test was used to detect complete deprotection of secondary amines. To carry out this test two solutions had to be prepared.

Solution 1: A volume of 1 mL acetaldehyde was made up to 50 mL with DMF.

Solution 2: A mass of 1.02 g *p*-chloranil was dissolved in 49 mL DMF.

Upon deprotection or coupling of amino acids, a few resin beads were placed in a pill vial and 3 drops of each solution was added. The vial was then left to stand at room temperature for 5 minutes. The development of a glossy blue colour (positive result) indicated the presence of a secondary amine *i.e.* complete deprotection.

6.5 Synthesis of Fmoc-L-hydroxyproline-OH[190]

Sodium bicarbonate (0.96 g, 11.44 mmol) was added to a solution composed of double distilled water (20 mL) and dioxane (22 mL) (pH 9). The mixture was allowed to stir in a 100 mL round bottom flask (RBF) at room temperature (RT). L-hydroxyproline (0.75 g, 5.72 mmol) was added to the RBF. The mixture was cooled in an ice bath and left to stir. Fmoc-Cl (2.96 g, 11.44 mmol) was dissolved in dioxane (15 mL). The Fmoc-Cl solution was added drop wise to the stirring solution. After the addition the mixture was left to stir at RT over night. Work up involved acidifying the pale yellow mixture to pH 2 with concentrated HCl. Double distilled water (200 mL) was added in order to precipitate out a white product. An extraction with ethyl acetate was carried out and the organic layer was removed *in vacu* yielding yellow oil. The oil was dissolved in ethyl acetate and left to crystallise out the Fmoc-L-hydroxyproline-OH as a fine white powder (1.83 g, 90%). ^{1}H-NMR and LC/MS showed that no further purification was necessary. ^{1}H NMR [$(CD_3)_2SO_2$, 600 MHz] : δ_H 1.95 (m, H), δ_H 2.04 (m, H), δ_H 2.16 (t, H), δ_H 2.27 (t, H), δ_H 3.45 (d, H), δ_H 3.51 (d, H), δ_H 4.16 (m, 2H), δ_H 4.22 (m, 2H), δ_H 4.42 (t, H), δ_H 5.16 (s, H), δ_H 7.34 (m, 3H), δ_H 7.43 (m, 3H), δ_H 7.67 (t, 3H), δ_H 7.90 (t, 3H), δ_H 12.71 (s, 1H deuterium exchangeable). ^{13}C NMR [$(CD_3)_2SO_2$, 150 MHz]: δ_C 38.45 (s), 47.14 (d), 54.94 (s), 55.53 (s), 57.94 (s), 58.32 (s), 67.11 (s), 67.62 (s), 68.24 (s), 120.61 (t), 125.61 (d), 127.60 (t), 128.20 (d), 141.11 (d), 144.10 (d), 154.55 (d), 174.01 (s), 174.51 (s). MS (+H) = 375.9 g mol^{-1}.

6.6 General SPPS procedure[135]

Note: This method was used for the synthesis of peptides 1, 3 and 4

6.6.1 General procedure for coupling of amino acids to primary amines[135]

Fmoc-AA-OH (0.4 mmol) and HBTU (0.4 mmol) was dissolved in DMF and added to the swollen resin. DIEA (0.5 mmol) was then added to the solution and the resin was left to stir by bubbling with nitrogen gas for 2 hours. After this period of time a negative ninhydrin test was observed. A solution of 20 % piperidine in DMF was then added to the resin and left to stir for 20 minutes until a positive ninhydrin test was observed.

6.6.2 General procedure for coupling of amino acid to secondary amines[135]

The resin was washed with 3 x DMF and 3 x DCM. Fmoc-AA-OH (0.4 mmol) and HBTU (0.4 mmol) was dissolved in DMF until clear and added to the resin. DIEA (0.4 mmol) was then added to the solution and the resin was left to stir for 2 hours until a negative Chloranil test was observed. Deprotection was carried out with 20 % piperidine in DMF for 20 minutes.

6.6.3 General procedure for cleavage of the peptide from the resin[135]

The resin containing the complete deprotected peptide chain was washed 10 times with DCM prior to cleavage in order to remove residual DMF and dried under vacuum. The peptides were cleaved from the resin with 95 % TFA solution in DCM (5 mL) for 35 minutes. The cleavage mixture was vacuum filtered into a flask containing 10 mL double distilled water. This solution was then quantitatively transferred into a polypropylene vial and made up to 25mL with double distilled water. The TFA and DCM was removed from the solution by bubbling with compressed air. The solution was then lyophilized.

6.7 Peptoid synthesis[164]

Rink amide resin (0.17 g, 0.6 mmol g^{-1}) was pre-swollen in DCM for 45 minutes by bubbling with nitrogen gas. The resin was washed with 3 x DMF and 3 x DCM. A 20 % piperidine in DMF solution was added and stirred for 20 minutes until a positive Ninhydrin test was observed. The resin was washed with 3 x DMF and 3 x DCM after each step. Bromoacetic acid solution in DMF (1.5 mL, 1.2 M) and neat *N,N*-diisopropylcarbodiimide (DIC) (340 µL) was added to the resin and stirred for 20 minutes. After washing, a sec-butylamine solution

in DMF (2 mL, 1 M) was added and the reaction mixture was agitated for 20 minutes. Fmoc-Pro-OH (0.14 g, 0.4 mmol) and 1-[bis-(dimethyl-amino)methyliumyl]-1H-1,2,3-triazolo[4,5-b]pyridine-3-oxide hexaflurophosphate (HATU) (0.16 g, 0.4 mmol) was dissolved in DMF and added to the resin. DIEA (72 μL, 0.4 mmol) was added to the solution and allowed to stir for 2 hours. The resin was washed with 3 x DMF and 3 x DCM prior to deprotection with 50 % piperidine with very rapid bubbling for 5 minutes. After washing, the bromoacetylation step was carried out followed by a monomer amine displacement with isopropylamine. These steps were repeated with methylamine to yield the desired AVPI peptoid. Final deprotection with 20 % piperidine in DMF for 20 minutes was carried out prior to cleavage from the resin.

6.8 Cleavage of peptoid from the resin[135]

The resin was washed 10 times with DCM prior to cleavage in order to remove residual DMF. The Ala-Val-Pro-Ile peptoid was cleaved from the resin with 95 % TFA solution in water (7 mL) for 10 minutes. The cleavage mixture was filtered into a flask containing 10mL double distilled water. This solution was then quantitatively transferred into a polypropylene vial and made up to 25 mL with double distilled water. The TFA was removed from the solution by bubbling with compressed air. The solution was then lyophilized.

6.9 Synthesis of adamantane hydantoin[153,158]

A mixture of 2-adamantanone (1.0 g, 6.60 x 10^{-2} mmol), sodium cyanide (NaCN) (1.0 g, 2.04 x 10^{-2} moles) and $(NH_4)_2CO_3$ (2.0 g, 20.8 mmol) were added to a solution of ethanol (10 mL) and NH_4OH (15 mL) and sealed in a glass pressure tube. The tube was placed in an oil bath and allowed to stir at 60 °C for 2 hours, 100 °C for 2 hours and 120 °C overnight. The reaction mixture was allowed to cool, vacuum filtered and washed with ethanol to yield a sand coloured solid which was recrystallised from isopropanol to yield white crystals (1.3 g, 89%). ^{1}H NMR [$(CD_3)_2SO_2$, 400 MHz] : δ_H 1.54 (m, 4H), δ_H 1.67 (s, 2H), δ_H 1.76 (m, 2H), δ_H 2.0 (d, 2H), δ_H 8.38 (s, 1H deuterium exchangeable), δ_H 10.48 (s, 1H deuterium exchangeable). ^{13}C NMR [$(CD_3)_2SO_2$, 100 MHz]: δ_C 25.6 (d), 26.2 (d), 31.5 (t), 32.8 (t), 34.6 (d), 37.3 (t), 65.5 (s), 155.8 (s), 177.2(s). MS (+H) = 221.3 g mol^{-1}.

6.10 Synthesis of adamantane amino acid[153]

Crude hydantoin (1.7 g, 7.72 mmol) was placed in a metal pressure vessel containing a 1.25 M NaOH solution (100 mL). The pressure vessel was placed in an oil bath and left to stir at 175 °C overnight. The solution was acidified to pH 9 with concentrated HCl. The amino acid precipitated out and yielded a pearly suspension in a pale yellow solution. The amino acid was filtered under vacuum and washed with water (1.32 g, 88 %). MS (+H) = 195.2 g mol^{-1}.

6.11 Synthesis of Fmoc-adamantane amino acid[190]

Sodium hydrogen carbonate (0.43 g, 5.12 mmol) was added to a solution composed of double distilled water (20 mL) and 1.4-dioxane (22 mL) (pH 9). The mixture was allowed to stir in a RBF at RT. A mass of adamantane amino acid (0.5 g; 2.56 mmol) was added to the RBF. The mixture was cooled in an ice bath and left to stir. Fmoc-Osu (1.21 g; 3.58 mmol) was dissolved in dioxane (15 mL). The Fmoc-Osu solution was added drop wise to the stirring solution. After the addition the mixture was left to stir at RT over night. Work up involved acidifying the pale yellow mixture to pH 2 with 10 % HCl. Approximately 50 mL water was added in order to precipitate out a white product. An extraction with ethyl acetate was carried out and the organic layer was dried over sodium sulphate and vacced down yielding yellow oil. The oil was dissolved in ethyl acetate and left to crystallise out the Fmoc-adamantane-OH as a fine white powder (0.80 g, 75 %). ^{1}HNMR and LC/MS showed that no further purification was necessary. ^{1}H NMR [$(CD_3)_2SO_2$, 600 MHz] δ_H 1.2-1.4 (m, 4H), 1.92-2.20 (m, 8H), 2.5 (m, 2H), 4.2 (m, H), 4.4 (m, 2H), 7.3-7.9 (m, 8H), 8.0 (s, H), 12.18 (s, H). ^{13}C NMR [$(CD_3)_2SO_2$, 150 MHz]: δ_C 26.2 (d), 31.3 (s), 33.6 (s), 34.1 (s), 36.4 (s), 46.7 (s), 62.6 (s), 65.2 (s), 120.1 (s), 125.1 (s), 127.0 (s), 127.6 (s), 140.7 (d), 143.8 (d), 155.9 (s), 172.7 (d). MS (+Na) = 450 g mol^{-1}.

6.12 Synthesis of trishomocubane hydantoin[168,190]

A mixture of the monoketone (1.0 g, 6.30 mmol), sodium cyanide (NaCN) (1.0 g, 22.4 mmol) and $(NH_4)_2CO_3$ (2.0 g, 20.8 mmol) were added to a solution of ethanol (10 mL) and NH_4OH (15 mL) and sealed in a glass pressure tube. The tube was placed in an oil bath and allowed to stir at 60 °C for 2 hours, 100 °C for 2 hours and 120 °C overnight. The reaction mixture

was allowed to cool and diluted with water. The solution was filtered to yield the crude hydantoin. The crude product was washed with water, acetone and diethyl ether and recrystallised from THF to yield a white solid (1.32 g, 92 %). ^{1}HNMR and LC/MS showed that no further purification was necessary. ^{1}H NMR [$(CD_3)_2SO_2$, 400 MHz] : δ_H 1.18-1.38 (m, 4H), δ_H 1.89-2.09 (m, 2H), δ_H 2.45 (s, 1H), δ_H 2.84 (s, 1H), δ_H 7.86 (s, 1H), δ_H 10.53 (s, 1H). ^{13}C NMR [$(CD_3)_2SO_2$, 100MHz]: δ_C 32.23 (d), 32.83 (d), 41.51 (d), 42.07 (d), 43.02 (d), 44.96 (d), 45.95 (d), 46.45 (d), 54.12 (d) 54.98 (d), 72.85 (s), 156.62 (s), 176.92 (s). MS (+H) = 231.3 g mol^{-1}.

6.13 Synthesis of trishomocubane amino acid[190]

A mass of the crude hydantoin (1.32 g, 5.742 mmol) was placed in a metal pressure vessel containing a 1.25 M NaOH solution (50 mL). The pressure vessel was placed in an oil bath and left to stir at 170 °C overnight. This yielded a brown solution which was acidified to pH 9 with concentrated HCl. This resulted in precipitation of the trishomocubane amino acid which was filtered and washed with water and diethyl ether (0.76 g, 84 %).

6.14 Synthesis of Fmoc trishomocubane amino acid[190]

A solution of the amino acid (0.76 g, 3.65 mmol) in dioxane (15 mL) and 10 % v/v Na_2CO_3 (50 mL) was cooled in an ice bath and left to stir. Fmoc-Cl (2.50 g; 7.3 mmol) was dissolved in 15 mL dioxane. The Fmoc-Cl solution was added drop wise to the stirring solution. After the addition the mixture was left to stir at RT over night. Work up involved acidifying the pale yellow mixture to pH 2 with 10 % HCl. Water (50 mL) was added in order to precipitate out a white product. An extraction with ethyl acetate was carried out and the organic layer was dried over sodium sulphate and vacced down yielding yellow oil. The oil was dissolved in ethyl acetate and left to crystallise out the Fmoc-trishomocubane-OH as a fine white powder (0.81 g, 78 %). ^{1}HNMR and LC/MS showed that no further purification was necessary. ^{1}H NMR [$CDCl_3$, 400 MHz]: δ_H1.11–1.40 (m, 4H), 1.90–2.30 (m, 7H), 2.30–2.40 (m, 1H), 3.35 (s, 1H, D_2O exchangeable), 4.10–4.43 (m, 3H), 7.22–8.08 (m, 8H), 12.19 (s, 1H, D_2O exchangeable). APT NMR [$CDCl_3$, 100 MHz]: δ_C 31.7 (t), 32.7 (t), 42.5 (d), 42.6 (d), 42.8 (d), 43.8 (d), 46.1 (d), 46.4 (d), 46.7 (d), 52.8 (d), 53.3 (d), 65.1 (s), 68.6 (t), 120.0 (d), 125.1 (d), 125.2 (d), 126.9 (d), 127.9 (d), 140.6 (s), 140.7 (s), 143.7 (s), 143.8 (s), 155.3 (s), 174.0 (s). MS (+Na) = 440 g mol^{-1}.

6.15 Synthesis of peptide 2 (*N*-methylated Ala-Val-Pro-Ile)

After numerous unsuccessful attempts to manually synthesize this peptide, it was finally obtained by automated microwave assisted SPP synthesizer (Liberty).

6.16 General procedure for the synthesis of peptides using microwave power (peptides 2, 5, 6, 8 and 9)

Solutions of amino acids (0.2 mM), *N,N*-diisopropylethylamine (DIPEA) (1 mM) and 2-(1H-Benzotriazole-1-yl)-1,1,3,3-tetramethyluronium-hexafluorophosphate (HBTU) (2 mM) or 1-[bis-(dimethyl-amino)methyliumyl]-1H-1,2,3-triazolo[4,5-b]pyridine-3-oxide hexaflurophosphate (HATU) were made up with DMF and transferred into the reagent bottles on the automated peptide synthesizer. All peptides were synthesized on a 0.1 mmol scale using microwave power. The details of the microwave conditions are given in Table 5.

Table 10: Microwave conditions for automated peptide synthesis

Method	Microwave power (W)	Time (s)	Temperature (°C)
Arginine coupling	0	1500	156.1
	25	300	156.1
Normal coupling	25	300	71
Deprotection	60	180	71

An arginine coupling method was used for coupling the PCU, Trishomocubane and Adamantane amino acids (*i*) to each of (*i*-1) and (*i*+1)[xxxv] The normal coupling method was used for subsequent couplings and for Fmoc deprotection, the deprotection method was used as indicated in table.

[xxxv] (*i*-1) and (*i*+1) are Val and Ile respectively in case of Ala-Val-Tris/Ada/PCU-Ile.

6.17 Cleavage from resin

The resin was washed 10 times with DCM prior to cleavage in order to remove residual DMF and dried under vacuum. The *N*-methylated Ala-Val-Pro-Ile peptide was cleaved from the Sieber amide resin with 2 % TFA solution in DCM (5 mL) for 15 minutes. The cage containing sequences were cleaved using TFA: H_2O: TIS (95:2.5:2.5) for one hour. The cleavage mixture was filtered into a flask containing double distilled water (10 mL). The resin was washed with 5 x DCM and 5 x MeOH. This solution was then quantitatively transferred into a polypropylene vial and made up with double distilled water (25 mL). The TFA and DCM was removed from the solution by bubbling with compressed air. The solution was then lyophilized.

6.18 General procedure for purification of all peptides

The crude peptide samples obtained from lyophilisation was re-dissolved in a water/ acetonitrile mixture (5 mL) and purified by semi-prep HPLC through an ACE C-18 column using varying solvent gradients and a wavelength of 190 nm.

Table 11: Summary of solvent systems used to purify peptides

Compound	Observed mass (+H) ($g\ mol^{-1}$)	Solvent system (% CH_3CN)	Run time (min)	Elution time (min)
1-AVPI	398.2753	5 – 95	20	5.7
2-*N*-meth	440.3224	10 – 35	20	9.9
3-TIQ	460.2904	15 – 70	40	10
4-HP	414.2696	5 – 50	80	8
5-Ada	478.3381	25 – 50	60	8
6-Tris	488.3224	10 – 60	30	13
7-Peptoid	398.2751	5 – 35	20	9
8-PCU1	488.3213	5 – 60	30	27.7
9-PCU2	488.3260	5 – 60	20	29.2

6.19 Growth and maintenance of cell lines[191]

Note: Aseptic techniques were used when working with all cell lines.

6.19.1 Preparation of growth media

Reconstituted Dulbecco's minimal essential medium (DMEM) was prepared by the addition of 2.5 M HEPES, to yield a final concentration of 25 mM, and penicillin/streptomycin to give a final concentration of 0.1 mg mL^{-1}. Reconstituted RPMI 1640 already containing 25 mM HEPES was also supplemented with penicillin/streptomycin to give a final concentration of 0.1 mg mL^{-1}. 10 % (v/v) heat-inactivated foetal calf serum (FCS) was used for the MDA-MB-231 and MCF-7 cell lines, while a 5 % (v/v) concentration of FCS was used for growth of the MDBK cell line. The fully constituted DMEM was used for the growth of MCF-7 and MDBK cell lines while the fully constituted RPMI 1640 was used for the MDA-MB-231 cell line.

6.19.2 Removal of cells from cryopreservation

Cryovials of cells were removed from storage under liquid nitrogen and allowed to rapidly thaw in a water bath preheated to 37 °C. After disinfecting the vials with 70 % (v/v) ethanol in distilled water, the contents were transferred to a sterile 12 mL centrifuge tube. Cells were centrifuged at 1000 rpm for 3 minutes until a pellet had formed. The supernatant was removed and freshly prepared growth media (5 mL) was added to loosen the pellet. After gentle mixing by pipette, aliquots of the cell suspension was added to 75 cm^2 flasks containing fresh media (10 mL) and incubated at 37 °C.

6.19.3 General procedure for sub-culturing cells

Once the cells had reached approximately 80 % confluence, the culture medium was removed by pipette. Cell monolayers were washed with 10 mL 1 x PBS which was removed prior to trypsinization[xxxvi]. A volume of 1.5 mL 0.25 % (w/v) trypsin/versene was added to the 75 cm^2 flasks to cover the entire monolayer. Cells were monitored under microscope and once

[xxxvi] Trypsinization involves the removal of cells adhered to the flask by use of a trypsin/versene mixture.

they began to round up the trypsin solution was removed. The flask was gently tapped against the palm of the hand to dislodge cells and 10 mL of fully constituted culture medium was added to wash down cells and inhibit the action of trypsin. Once the cells were evenly distributed in the culture media, 5 mL of the cell suspension was added to each of two 75 cm^2 flasks already containing 10 mL culture medium. The cells were distributed evenly by pipetting and allowed to incubate at 37 °C.

6.19.4 Cryopreservation of cells

Different passages of each cell line were cryopreserved using 70-80 % confluent cultures. Cells were washed with 10 mL 1 x PBS, trypsinized and dislodged as described above. The dislodged cells were evenly distributed in 1.9 mL fully constituted DMEM and transferred to a 2 mL cryogenic vial. Dimethylsulfoxide (DMSO) was used as a cryoprotectant and (10 % v/v) was added and the cryogenic vials were immediately subjected to cooling at a steady rate of 1 °C per minute to approximately -70 °C. Vials were finally stored in liquid nitrogen at -196 °C.

6.20 MTT assay

Fully constituted RPMI 1640 was prepared by adding a penicillin/streptomycin mixture to yield a final concentration of 0.1 mg mL^{-1} as well as 10 % (v/v) FCS. Cells were trypsinized as described above and resuspended in RPMI 1640.

A cell count was carried out on the cell suspension using a haemocytometer. The optimum cell number was found to be 50 000 cells *per* well and was hence used for this assay. Since 100 µL of the cell solution was to be transferred to each well an appropriate dilution was carried out using fully constituted RPMI 1640. The plates were then incubated at the 37 °C for either six or 24 hours to allow the cells to attach to the wells. The culture media was then removed and 60 µL of fresh RPMI 1640 was added to each well. 40 µL of the prepared samples were added and the plates were then incubated at 37°C for 48 hours.

After the incubation period, cell viability was assessed using the CellTiter 96 non-radioactive cell proliferation assay (Promega) as per manufacturer's instructions. 15 µL of the dye solution was added to each well and the plate incubated at 37°C for three hours.

Solubilization solution (100 µL) was then added to each well and the plate incubated at 30°C with gentle agitation (120 rpm).

The absorbance maximum for formazan is 570 nm. A wavelength of 690 nm was also used to cancel the effects of background absorbance. The plate reader was programmed to give a final reading derived by subtraction of an optical density (OD) reading at 570 nm from the reading at 690 nm.

Cytotoxicity was thereafter calculated as follows:

MTT reduction = (OD of sample / OD of control) × 100%

Percent cytotoxicity = 100 – MTT reduction

To ensure that the protocol established was efficient, the sensitivity of the cells to cadmium was determined. Cadmium chloride samples (40 µL) at various concentrations (0 ppm – 3 ppm) were prepared in sterile water and RPMI 1640 media and added to cell cultures from which media was removed and fresh media added. Plates were sealed and incubated for 48 hours at 37°C. Cell viability was then assessed as described above.

Various concentrations of each synthesised peptide were prepared using water and RPMI 1640 and 40 µL of each used to determine the cytotoxic effect of each peptide on the MDA MB 231 cell line. The optimum concentration range for each was determined as well as the maximum percentage cytotoxicity exhibited. Cell preparation and test protocol were as described above.

All assays were performed with a minimum of 5 replicates and repeated twice. Statistical analysis was carried out with Graphpad Instat using the One-way analysis of variance (ANOVA) and the Tukey-Kramer multiple comparisons test.

REFERENCES

1. Bergman, P. J. *Veterinary Clinics of North America: Small Animal Practice* **1997**, *27*, 47-57.

2. Story, M. *Frontiers in Bioscience* **1998**, *3*, 367-375.

3. Dean, E. J.; Ranson, M.; Blackhall, F.; Holt, S. V.; Dive, C. *Cancer Treatment Reviews* **2007**, *33*, 203-212.

4. Foster, I. *Radiography* **2007**, *14*, 144-149

5. Heron, M.; Hoyert, D. L.; Murphy, S. L.; Xu, J.; Kochanek, K. D.; Tejada-Vera, B. *CDC National Vital Statistics Reports* **2009**, *57*, 1-80.

6. World Health Organisation, *Cancer WHO cancer controls programme* **2006**, http://www.who.int/cancer/en/. (Date accessed: 12-08-08)

7. www.health-e.org.za. (Date accessed: 15-06-10)

8. www.herkules.oulu.fi/isbn9514266676/html/i267388.html. (Date accessed: 08-10-08)

9. Robertson, J. D.; Orrenius, S. *Critical Reviews in Toxicology* **2000**, *30*, 609-627.

10. Nachmias, B.; Ashhab, Y.; Ben-Yehuda, D. *Seminars in Cancer Biology* **2004**, *14*, 231-243.

11. Hanahan, D.; Weinberg, R. A. *Cell* **2000**, *100*, 57-70.

12. Abbott, R. G.; Forrest, S.; Pienta, K. J. *Journal of Artificial. Life* **2006**, *12*, 617-634.

13. Hayflick, L. *Biochemistry* **1997**, *62*, 1180-1190.

14. Kelland, L. *Clinical Cancer Research* **2007**, *13*, 4960-4963.

15. Alpin, A. E.; Howe, A.; Alahari, S. K.; Juliano, R. L. *Pharmacological Reviews* **1998**, *50*, 197-263.

16. Weinberg, R. A. *Cell* **1995**, *81*, 323-330.

17. Becker *The World of the Cell*; Pearson Education Inc.: Boston, 2003.

18. Ferreira, C. G.; Epping, M.; Kruyt, F. A. E.; Giaccone, G. *Clinical Cancer Research* **2002**, *8*, 2024-2034.

19. Kerr, J. F. *British Journal of Cancer* **1972**, *26*, 239-257.

20. Shi, Y. *Nature Structural Biology* **2001**, *8*, 394-401.

21. Danial, N. N.; Korsmeyer, S. J. *Cell* **2004**, *116*, 205-219.

22. Lowe, S. W.; Lin, A. W. *Carcinogenesis* **2000**, *21*, 485-495.

23. Solary, E. *European Respiratory Journal* **1996**, *9*, 1293-1305.

24. Zimmermann, K. C.; Bonzon, C.; Green, D. R. *Pharmacology and Therapeutics* **2001**, *92*, 57-70.

25. Reed, J. C. *American Journal of Pathology* **2000**, *157*, 1415-1430.

26. Hengartner, M. O. *Nature* **2000**, *40*, 770-776.

27. Wyllie, A. H. *International Review of Cytology* **1980**, *68*, 251-306.

28. http://www.bioscience.org/2009/v14/af/3509/fig2.jpg. (Date accessed: 13-05-09)

29. Fei, G. *Blood* **2002**, *99*, 3419-3426.

30. Finucane, D. M.; Bossy-Wetzel, E.; Waterhouse, N. J.; Cotter, T. G.; Green, D. R. *Journal of Biological Chemistry* **1999**, *274*, 2225-2233.

31. Crompton, M.; Virji, S.; Ward, J. M. *European Journal of Biochemistry* **1998**, *258*, 729-735.

32. Green, D. R.; Kroemer, G. *Science* **2004**, *5684*, 626-629.

33. Yang, J. C.; Cortopassi, G. A. *Free Radical Biology and Medicine* **1998**, *24*, 624-631.

34. Zou, H.; Yuchen, L.; Xuesing, L.; Wang, X. *Journal of Biological Chemistry* **1999**, *274*, 11549-11556.

35. Susin, S. A.; Lorenzo, H. K.; Zamzami, N.; Marzo, I.; Snow, B. E.; Brothers, G. M.; Mangion, J.; Jacotot, E.; Costantini, P.; Loeffler, M.; Larochette, N.; Goodlett, D. R.; Aebersold, R.; Sideovski, D. P.; Penninger, J. M.; Kroemer, G. *Nature* **1999**, *6718*, 387-389.

36. Du, C.; Fang, M.; Li, Y.; Li, L.; Wang, X. *Cell* **2000**, *102*, 22-42.

37. Wei, M. C.; Lindsten, T.; Mootha, V. K.; Weiler, S.; Gross, A.; Aishiya, M.; Thompson, C. B.; Korsmeyer, S. J. *Genes and Development* **2000**, *14*, 2060-2071.

38. Letai, A.; Bassik, M. C.; Walensky, L. D.; Sorcinelli, M. D.; Weiler, S.; Korsmeyer, S. J. *Cancer Cell* **2002**, *2*, 183-192.

39. Korsmeyer, S. J.; Wei, M. C.; Saito, M.; Weiler, S.; Oh, K. J.; Schlesinger, P. H. *Cell Death Differentiation* **2000**, *12*, 1166-1173.

40. Nechustan, A.; Smith, C. L.; Yoon, I. L. H.; Youle, R. J. *Journal of Cell Biology* **2001**, *153*, 1265-1276.

41. Kuwana, T.; Mackay, M. R.; Perkins, G.; Ellisman, M. H.; Letterich, M.; Schneiter, R.; Green, D. R.; Newmeyer, D. D. *Cell* **2002**, *111*, 331-342.

42. Aggarwal, B. B.; Shishadia, S. *Resveratrol in Health and Disease*; CRC: Texas, **2005**.

43. www.cafemom.com. (Date accessed: 01-12-09)

44. www.london-nano.com. (Date accessed: 01-12-09)

45. www.ccs.k12.in.us. (Date accessed: 01-12-09)

46. https://eapbiofield.wikispaces.com/FRF+PR7. (Date accessed: 12-09-09)

47. Foster, I. *Radiography* **2007**, *14*, 144-149.

48. Barisic, K. *Acta Pharmaceutica* **2003**, *53*, 151-164.

49. www.rsc.org/ej/NP/2001/A909080K/. (Date accessed: 26-02-09)

50. Cryns, V. L.; Bergeron, L.; Zhu, H.; Li, H.; Yuan, J. *Journal of Biological Chemistry* **1996**, *271*, 31277-31282.

51. Kothakota, S.; Azuma, T.; Reinhard, C.; Klippel, A.; Tang, J.; Chu, K.; McGarry, T. J.; Kirschner, M. W.; Koths, K.; Kwiatkowski, D. J.; Williams, L. T. *Science* **1997**, *5336*, 294-298.

52. Lazebnik, Y. A.; Kaufmann, S. H.; Desnoyers, S.; Poirier, G. G.; Earnshaw, W. C. *Nature* **1994**, *6495*, 346-347.

53. Lazebnik, Y. A.; Takahashi, A.; Moir, R. D.; Goldman, R. D.; Poirier, G. G.; Kaufmann, S. H.; Earnshaw, W. C. *Proceedings of the National Academy of Science U.S.A.* **1995**, *92*, 9042-9046.

54. Mashima, T.; Naito, M.; Fujita, N.; Noguchi, K.; Tsutuo, T. *Biochemical and Biophysical Research Communications* **1995**, *217*, 1185-1192.

55. Los, M.; Burek, C. J.; Stroh, C.; Benedyk, K.; Hug, H.; Mackiewicz, A. *Drug Discovery Today* **2003**, *8*, 67-77.

56. Thompson, C. B. *Science* **1995**, *267*, 1456-1462.

57. Yuan, J. *Nature* **2000**, *407*, 802-809.

58. Shi, Y. *Cell Death and Differentiation* **2002**, *9*, 93-95.

59. Crook, N. E.; Clem, R. J.; Miller, L. K. *Journal of Virology* **1993**, *67*, 2168.

60. Kipp, R. A.; Case, M. A.; Wist, A. D.; Cresson, C. M.; Carrell, M.; Griner, E.; Wiita, A.; Albiniak, P. A.; Chai, J.; Shi, Y.; Semmelhack, M. F.; Mclendon, G. L. *Biochemistry* **2002**, *41*, 7344-7349.

61. Schimmer, A. D.; Dalili, S.; Batey, R. A.; Riedl, S. J. *Cell Death and Differentiation* **2006**, *13*, 179-188.

62. Arnt, C. R.; Chiorean, M. V.; Heldebrant, M. P.; Gores, G. J.; Kaufmann, S. H. *The Journal of Biological Chemistry* **2002**, *277*, 44236-44243.

63. Rothe, M.; Pan, M. G.; Henzel, W. J.; Ayres, T. M.; Goeddel, D. V. *Cell* **1995**, *83*, 1243-1252.

64. Duckett, C. S.; Nava, V. E.; Gedrich, R. W.; Clem, R. J.; Dongen, J. L. V.; Gilfillan, M. C.; Shiels, H.; Hardwick, J. M.; Thompson, C. B. The *EMBO Journal* **1996**, *15*, 2685-2694.

65. Liston, P.; Roy, N.; Tamal, K.; Lefebvre, C.; Baird, S.; Cherton-Horvat, G.; Farahani, R.; McLean, M.; Ikeda, J. E.; MacKenzie, A.; Korneluk, R. G. *Nature* **1996**, *379*, 349-353.

66. Ambrosini, G. *Nature Medicine* **1997**, *3*, 917-921.

67. Deveraux, Q. L.; Takahashi, R.; Salvesen, G. S.; Reed, J. C. *Nature* **1997**, *388*, 300-304.

68. Hauser, H. P.; Bardroff, M.; Pyrowolakis, G.; Jentsch, S. *Journal of Cell Biology* **1998**, *141*, 1415-1422.

69. Vucic, D. *Current Biology* **2000**, 1359-1366.

70. Deveraux, Q. L.; Reed, J. C. *Genes and Development* **1999**, *13*, 239-252.

71. Fesik, S. W. *Cell* **2000**, *103*, 273-282.

72. Huang, Y.; Rich, R. L.; Myszka, D. G.; Wu, H. *The Journal of Biological Chemistry* **2003**, *278*, 49517-49522.

73. Chai, J.; Shiozaki, E.; Srinivasula, S. M.; Wu, Q.; Dataa, P.; Alnemri, E. S.; Shi, Y. *Cell* **2001**, *104*, 769-780.

74. Riedl, S. J.; Renatus, M.; Schwarzenbacher, R.; Zhou, Q.; Sun, C.; Fesik, S. W.; Liddington, R. C.; Salvesen, G. S. *Cell* **2001**, *104*, 791-800.

75. Huang, Y.; Park, Y. C.; Rich, R. L.; Segal, D.; Myszka, D. G.; Wu, H. *Cell* **2001**, *104*, 781.

76. Sun, H.; Nikolovska-Coleska, Z.; Yang, C. Y.; Qian, D.; Lu, J.; Qiu, S.; Bai, L.; Peng, Y.; Cai, Q.; Wang, S. *Accounts of Chemical Research* **2008**, *41*, 1264-1277.

77. Mastrangelo, E.; Cossu, F.; Milani, M.; Sorrentino, G.; Lecis, D.; Delia, D.; Manzoni, L.; Drago, C.; Seneci, P.; Scolastico, C.; Rizzo, V.; Bolognesi, M. *Journal of Molecular Biology* **2008**, *384*, 673-689.

78. Korsmeyer, S. J. *Annual Review of Immunology* **1992**, *10*, 785-807.

79. Mcdonnell, T. J.; Stanley, J. *Nature* **1991**, *349*, 254-256.

80. Strasser, A. *Nature* **1990**, *348*, 331-333.

81. Vaux, D. L. *Nature* **1988**, *355*, 440-442.

82. Symonds, H. *Cell* **1994**, *78*, 703-711.

83. Harris, C. C. *Carcinogenesis* **1996**, *17*, 1187-1198.

84. Sun, H.; Nikolovska-Coleska, Z.; Lu, J.; Qiu, S.; Yang, C. Y.; Gao, W.; Meagher, J.; Stuckey, J.; Wang, S. *Journal of Medicinal Chemistry* **2006**, *49*, 7916.

85. Sun, H. *Journal of American Chemical Society* **2007**, *129*, 15279-15294.

86. Wu, G.; Chai, J.; Suber, T. L.; Wu, J. W.; Du, C.; Wang, X.; Shi, Y. *Nature* **2000**, *408*, 1008-1012.

87. Wu, G. *Nature* **2000**, *408*, 1008-1012.

88. Liu, Z.; Sun, C.; Olenjniczak, E. T.; Meadows, R. P.; Betz, S. F.; Oost, T.; Herrmann, J.; Wu, J. C.; Fesik, S. W. *Nature* **2000**, *408*, 1004-1008.

89. Scott, F. L.; Denault, J. B.; Riedel, S. J.; Shin, H.; Renatus, M.; Salvesen, G. S. *The EMBO Journal* **2005**, *24*, 645-655.

90. Petersen, S. *Cancer Cell* **2007**, *12*, 445-456.

91. Vince, J. E.; Wong, W. W. L.; Khan, N.; Feltham, R.; Chau, D.; Ahmed, A. U.; Benetatos, C. A.; Chunduru, S. K.; Condon, S. M.; McKinlay, M.; Brink, R.; Leverkus, M.; Tergaonkar, V.; Schneider, P.; Callus, B. A.; Koentgen, F.; Vaux, D. L.; Silke, J. *Cell* **2007**, *131*, 682-693.

92. Varfolomeev, E.; Blankenship, J. W.; Wayson, S. M.; Fedorova, A. V.; Kayagaki, N.; Garg, P.; Zobel, K.; Dynek, J. N.; Elliot, L. O.; Wallweber, H. J. A.; Flygare, J. A.; Fairbrother, W. J.; Deshayes, K.; Dixit, V. M.; Vucic, D. *Cell* **2007**, *131*, 669-681.

93. Wang, L.; Du, F.; Wang, X. *Cell* **2008**, *133*, 693-703.

94. Bertrand, M. J. *Molecular Cell* **2008**, *30*, 689-700.

95. Bhutia, S. K.; Maiti, T. K. *Trends in Biotechnology* **2007**, *26*, 210-217.

96. Ponder, B. A. J. *Nature* **2001**, *411*, 336-341.

97. Nicholson, D. W. *Nature* **2000**, *407*, 810-816.

98. www.chemocare.com/bio. (Date accessed: 12-04-09)

99. Sewald, N.; Jakubke, H. D. *Peptides: Chemistry and Biology*; Wiley-VCH: Germany, 2002.

100. Murray, R. K. *Harpers Illustrated Biochemistry*, 26 th ed.; McGraw-Hill Beirut, 2003.

101. Chou, K. C. *Analytical Biochemistry* **2000**, *286*, 1-16.

102. Albericio, F.; Arvidson, P. I.; Bisetty, K.; Giralt, E.; Govender, T.; Jail, S.; Kongsaeree, P.; Kruger, H. G.; Prabpai, S. *Chemical Biology Drug Design.* **2008**, *71*, 125-130.

103. Henrickson, J. B.; Cram, D. J.; Hammond, G. S. *Organic Chemistry*; McGraw-Hill: New York, 1970; Vol. 3.

104. Venkatachalam, C. M. *Biopolymers* **1968**, *6*, 1425-1436.

105. Levitt, M. *Journal of Molecular Biology* **1976**, *104*, 59-107.

106. Lewis, P. N.; Momany, F. A.; Scheraga, H. A. *Biocheica Biophysica Acta* **1973**, *303*, 211-229.

107. Chalmers, D. K.; Marshall, G. R. *Journal of American Chemical Society* **1995**, *117*, 5927-5937.

108. Enholm, E.; Bharadwaj, A. *Bioorganic and Medicinal Chemistry Letters* **2005**, *15*, 3470-3471.

109. Somu, R. V.; Johnson, R. L. *Journal of Organic Chemistry* **2005**, *70*, 5954-5963.

110. Merrifiled, R. B. *Journal of American Chemical Society* **1963**, *85*, 2149-2154.

111. Borgia, J. A.; Fields, G. B. *TIBTECH* **2000**, *18*, 243-251.

112. Williams, P. L.; Albericio, F.; Giralt, E. *Tetrahedron* **1993**, *49*, 11065-11133.

113. Atherton, E. *Solid Phase Peptide Synthesis: A Practical Approach*; Oxford University Press, 1989.

114. Gisin, B. F.; Merrifield, R. B. *Journal of American Chemical Society* **1972**, *94*, 3102-3106.

115. Montalbetti, C. A. G. N.; Falque, V. *Tetrahedron* **2005**, *61*, 10827-10852.

116. Albericio, F.; Carpino, L. A. *Enzymology: SPPS* **1997**.

117. Kaiser, E.; Colescott, R.; Bossiriger, C.; Cook, P. *Analytical Biochemistry* **1970**, *34*.

118. Yu, H. M.; Chen, S. T.; Wang, K. T. *Journal of Organic Chemistry* **1992**, *57*, 4781-4785.

119. Grieco, P. *Chemistry Today* **2004**, 18-20.

120. Fulda, S.; Wick, W.; Weller, M.; Debatin, K. M. *Nature Medicine* **2002**, *8*, 808-815.

121. Yang, L.; Mashima, T.; Sato, S.; Mochizuki, M.; Sakamoto, H.; Yamori, T.; Oh-hara, T.; Tsuruo, T. *Cancer Research* **2003**, *63*, 831-837.

122. Lipinski, C. A. *Drug Discovery Today: Technologies* **2004**, *1*, 337-341.

123. Lipinski, C. A.; Lombardo, F.; Dominy, B. W.; Feeney, P. J. *Advanced Drug Delivery Reviews* **2001**, *46*, 3-26.

124. Lipinski, C. A.; Lombarod, F.; Dominy, B. W.; Feeney, P. J. *Advanced Drug Delivery Reviews* **1997**, *23*, 1-3.

125. Oost, T. K.; Sun, C.; Armstrong, R. C.; Al-Assaas, A. S.; Betz, S. F.; Deckwerth, T. L.; Ding, H.; Elmore, S. W.; Meadows, R. P.; Olejniczak, E. T.; Oleksijew, A.; Oltersdorf, T.; Rosenberg, S. H.; Shoemaker, A. R.; Tomaselli, K. J.; Zou, H.; Fesik, S. W. *Journal of Medicinal Chemistry* **2004**, *47*, 4417-4426.

126. Sun, H.; Nikolovska-Coleska, Z.; Yang, C. Y.; Xu, L.; Liu, M.; Tomita, Y.; Pan, H.; Yoshioka, Y.; Krajewski, K.; Roller, P. P.; Wang, S. *Journal of Medicinal Chemistry* **2004**, *47*, 4147-4150.

127. Sun, H.; Nikolovska-Coleska, Z.; Chen, J.; Yang, C. Y.; Tomita, Y.; Pan, H.; Yoshioka, Y.; Krajewski, K.; Roller, P. P.; Wang, S. *Bioorganic and Medicinal Chemistry Letters* **2005**, *15*, 793-797.

128. Park, C. M.; Sun, C.; Olejniczak, E. T.; Wilson, A. E.; Meadows, R. P.; Betz, S. F.; Elmore, S. W.; Fesik, S. W. *Bioorganic and Medicinal Chemistry Letters* **2005**, *15*, 771-775.

129. Zobel, K.; Wang, L.; Varfolomeev, E.; Franklin, M. C.; Elliot, L. O.; Wallweber, H. J. A.; Okawa, D. C.; Flygare, J. A.; Vucic, D.; Fairbrother, W. J.; Deshayes, K. *ACS Chemical Biology* **2006**, *1*, 525-533.

130. Thomas, L. L. *Science* **2004**, *305*, 1471-1474.

131. Nikolovska-Coleska, Z. *Analytical Biochemistry* **2008**, *374*, 87-98.

132. Wang, Z.; Zhang, Q. *International Journal of Pharmaceutics* **2004**, *269*, 451-456.

133. Huang, J. W. *Journal of Medicinal Chemistry* **2008**, *51*, 7111-7118.

134. Chatterjee, J.; Gilon, C.; Hoffman, A.; Kessler, H. *Accounts of Chemical Research* **2008**.

135. Teixido, M.; Albericio, F.; Giralt, E. *Journal of Peptide Research* **2005**, *65*, 153-166.

136. Doig, A. J.; Hughes, E.; Burke, R. M.; Su, T. J.; Heenan, R. K.; Lu, J. *Biochemical Society Transactions* **2002**, *20*, 537-542.

137. Ben-Ishai, D. *Journal of American Chemical Society* **1957**, *79*, 5736-5738.

138. Carpino, L.; Han, G. *Journal of Organic Chemistry* **1972**, *37*, 3404-3409.

139. Freidinger, R. M.; Hinkle, J. S.; Perlow, D. S.; Arison, B. H. *Journal of Organic Chemistry* **1983**, *48*, 77-81.

140. Zhang, S.; Govender, T.; Arvidsson, P. I. *Journal of Organic Chemistry* **2005**, *70*, 6918-6920.

141. Urban, J.; Vaisar, T.; Shen, R.; Lee, M. S. *International Journal of Peptide and Protein Research* **2009**, *47*, 182-189.

142. Carpino, L. A. *Journal of American Chemical Society* **1993**, *115*, 4397-4398.

143. Koepler, O.; Laschat, S.; Baro, A.; Fischer, P.; Miehlich, B.; Hotfilder, M.; Viseur, C. l. *European Journal of Organic Chemistry* **2004**, 3611.

144. Spengler, J.; Schedel, H.; Sieler, J.; Quaedflieg, P. J. L. M.; Broxterman, Q. B.; Duchateau, A. L. L.; Burger, K. *Synthesis* **2001**, *10*, 1513-1518.

145. Guerrini, R.; Capasso, A.; Marastoni, M.; Bryant, S. D.; Cooper, P. S.; Lazarus, L. H.; Temussi, P. A.; Salvadori, S. *Bioorganic and Medicinal Chemistry* **1998**, *6*, 57-62.

146. Bisetty, K.; Carcho, F. J.; Canto, J.; Kruger, H. G.; Perez, J. J. *Journal of Peptide Science* **2006**, *12*, 92-105.

147. Bisetty, K.; Gomez-Catalan, J.; Aleman, C.; Giralt, E.; Kruger, H. G.; Perez, J. J. *Journal of Peptide Science* **2004**, *10*, 274-284.

148. James, B.; Rath, N. P.; Suresh, E.; Nair, M. S. *Tetrahedron Letters* **2006**, *47*, 5775-5779.

149. Zah, J.; Terre'Blanche, G.; Erasmus, E.; Malan, S. F. *Bioorganic and Medicinal Chemistry* **2003**, 11.

150. Brookes, K. B.; Hickmott, P. W.; Jutle, K. K.; Schreyer, C. A. *South African Journal of Chemistry* **1992**, *45*, 8-11.

151. Geldenhuys, W. J.; Malan, S. F.; Bloomquist, J. R.; Marchand, A. P.; Schyf, C. J. V. D. *Medicinal Research Reviews* **2005**, *25*, 21-48.

152. Nagasawa, H. T.; Elberling, J. A.; Shirota, F. N. *Journal of Medicinal Chemistry* **1975**, *18*, 826-830.

153. Nagasawa, H. T.; Elberling, J. A.; Shirota, F. N. *Journal of Medicinal Chemistry* **1973**, *16*, 823-826.

154. Oliver, D. W.; Dekker, T. G.; Snyckers, F. O.; Fourie, T. G. *Journal of Medicinal Chemistry* **1991**, *34*, 851-854.

155. Oliver, D. W.; Dekker, T. G.; Snyckers, F. O. *Journal of Medicinal Chemistry* **1991**, *26*, 375-379.

156. Govender, T.; Hariprakasha, H. K.; Kruger, H. G.; Raasch, T. *South African Journal of Chemistry* **2005**, *58*, 37-40.

157. Ware, E. *Chemical Reviews* **1950**, *46*, 403-406.

158. Saadaldin, M. A., *MSc Thesis* **2008**, University of Kwazulu-Natal

159. Zuckermann, R. N. *Journal of American Chemical Society* **1992**, *114*, 10646-10647.

160. Horn, T.; Lee, B. C.; Dill, K. A.; Zuckermann, R. N. *Bioconjugate Chemistry* **2004**, *15*, 428-435.

161. Wu, C. W.; Sanborn, T. J.; Zuckermann, R. N.; Barron, A. E. *Journal of American Chemical Society* **2001**, *123*, 6778-6784.

162. Maayan, G.; Yoo, B.; Kirshenbaum, K. *Tetrahedron Letters* **2008**, *49*, 335-338.

163. Chan, W. C.; White, P. D., Eds. *Fmoc solid phase synthesis, A practical approach*; Oxford university press.

164. Holub, J.; Jang, H.; Kirshenbaum, K. *Organic and Biomolecular Chemistry* **2006**, *4*, 1497-1502.

165. Kelly, S. M.; Jess, T. J.; Price, N. C. *Biochimica et Biophysica Acta* **2005**, *1751*, 119-139.

166. Scrocchi, L. A.; Chen, Y.; Waschuk, S.; Wang, F.; Cheung, S.; Darabie, A. A.; McLaurin, J.; Fraser, P. E. *Journal of Inorganic Biochemistry* **2002**, *318*, 697-706.

167. Hickmott, P. W.; Wood, S.; Murray-Rust, P. *Journal of Chemical Society Perkin Transactions I* **1985**, 2033-2038.

168. Govender, T.; Kruger, H. G.; Raasch, T. *Structural Chemistry* **2005**, *16*, 129-134.

169. Fourie, L.; Govender, T.; Hariprakasha, H. K.; Humcha, K.; Kruger, H. G.; Raasch, T. *Magnetic Resonance in Chemistry* **2004**, *47*, 617-623.

170. Whitcutt, J. M. *South African Journal of Chemistry* **2005**, *101*, 383-388.

171. Terr, A. I. *The Western Journal of Medicine* **1983**, *139*, 702-703.

172. Crouch, S. P. M.; Slater, K. J. *DDT* **2001**, *6*, 48-53.

173. Weyermann, J.; Lochmann, D.; Zimmer, A. *International Journal of Pharmaceutics* **2005**, *288*, 369-376.

174. Roche *Apoptosis, Cell Death and Cell Proliferation*, 3 ed.: Mannhein, 2006.

175. Smith, F. E. *Science* **1951**, *113*, 751-754.

176. Berridge, M. V.; Tan, A. S.; Mccoy, K. D.; Wang, R. *Biochemica* **1996**, *4*, 14-19.

177. Shao, C.; Folkard, M.; Held, K. D.; Prise, K. M. *BMC Cancer* **2008**, *8*, 1-9.

178. Kim, J. H.; Kim, B. G. *Journal of Korean Cancer Association* **1999**, *31*, 1151-1158.

179. Belkacemi, L.; Lam, E.; Caldwell, J. D.; Siemens, D. R.; Graham, C. H. *Experimental Cell Research* **2006**, *312*, 1685-1692.

180. Tamm, I.; Kornblau, S. M.; Segall, H.; Krajewski, S.; Welsh, K.; Kitada, S.; Scudiero, D. A.; Tudor, G.; Qui, Y. H.; Monks, A.; Andreeff, M.; Reed, J. C. *Clinical Cancer Research* **2000**, *6*, 1796-1803.

181. Cannino, G.; Ferruggia, E.; Luparello, C.; Rinaldi, A. M. *Journal of Inorganic Biochemistry* **2008**, *102*, 1668-1676.

182. Sirchia, R.; Longo, A.; Luparello, C. *Biochimie* **2008**, *90*, 1578-1590.

183. Ulukaya, E.; Ozdikicioglu, F.; Oral, A. Y.; Demirci, M. *Toxicology in Vitro* **2008**, *22*, 232-239.

184. McKeague, A. L.; Wilson, D. J.; Nelson, J. *British Journal of Cancer* **2003**, *88*, 125-131.

185. Brookes, H.; Lebleu, B.; Vives, E. *Advanced Drug Delivery Reviews* **2005**, *57*, 559-577.

186. Futaki, S. *Advanced Drug Delivery Reviews* **2005**, *57*, 547-558.

187. Saito, G.; Swanson, J. A.; Lee, K. *Advanced Drug Delivery Reviews* **2002**, *55*, 199-215.

188. Crisostomo, F. R. P.; Feng, Y.; Zhu, X.; Welsh, K.; An, J.; Reed, J. C.; Huang, Z. *Bioorganic and Medicinal Chemistry* **2009**, *19*, 6413-6418.

189. AdvancedChemtech *Handbook of Combinatorial, Organic and Peptide Chemistry*, 2003-2004.

190. Raasch, T. *MSc Thesis* **2003**, University of Natal.

191. Govender, P. *MSc Thesis* **1995**, University of Durban Westville.